Design and synthesis of multifunctional microtubule targeting agents endowed with dual pro-apoptotic and anti-autophagic efficacy

Journal Pre-proof

Design and synthesis of multifunctional microtubule targeting agents endowed with dual pro-apoptotic and anti-autophagic efficacy

Giuseppe Campiani, Tuhina Khan, Cristina Ulivieri, Leopoldo Staiano, Chiara Papulino, Stefania Magnano, Seema Nathwani, Anna Ramunno, Daniel Lucena-Agell, Nicola Relitti, Stefano Federico, Luca Pozzetti, Gabriele Carullo, Alice Casagni, Simone Brogi, Francesca Vanni, Paola Galatello, Magda Ghanim, Niamh McCabe, Stefania Lamponi, Massimo Valoti, Ola Ibrahim, Jeffrey O'Sullivan, Richard Turkington, Vincent P. Kelly, Ruben VanWemmel, J. Fernando Díaz, Sandra Gemma, Daniela Zisterer, Lucia Altucci, Antonella De Matteis, Stefania Butini, Rosaria Benedetti

PII: S0223-5234(22)00176-3

DOI: https://doi.org/10.1016/j.ejmech.2022.114274

Reference: EJMECH 114274

To appear in: *European Journal of Medicinal Chemistry*

Received Date: 19 January 2022

Revised Date: 28 February 2022

Accepted Date: 8 March 2022

Please cite this article as: G. Campiani, T. Khan, C. Ulivieri, L. Staiano, C. Papulino, S. Magnano, S. Nathwani, A. Ramunno, D. Lucena-Agell, N. Relitti, S. Federico, L. Pozzetti, G. Carullo, A. Casagni, S. Brogi, F. Vanni, P. Galatello, M. Ghanim, N. McCabe, S. Lamponi, M. Valoti, O. Ibrahim, J. O'Sullivan, R. Turkington, V.P. Kelly, R. VanWemmel, J.F. Díaz, S. Gemma, D. Zisterer, L. Altucci, A. De Matteis, S. Butini, R. Benedetti, Design and synthesis of multifunctional microtubule targeting agents endowed with dual pro-apoptotic and anti-autophagic efficacy, *European Journal of Medicinal Chemistry* (2022), doi: https://doi.org/10.1016/j.ejmech.2022.114274.

during the production process, errors may be discovered which could affect the content, and all legal disclaimers that apply to the journal pertain.

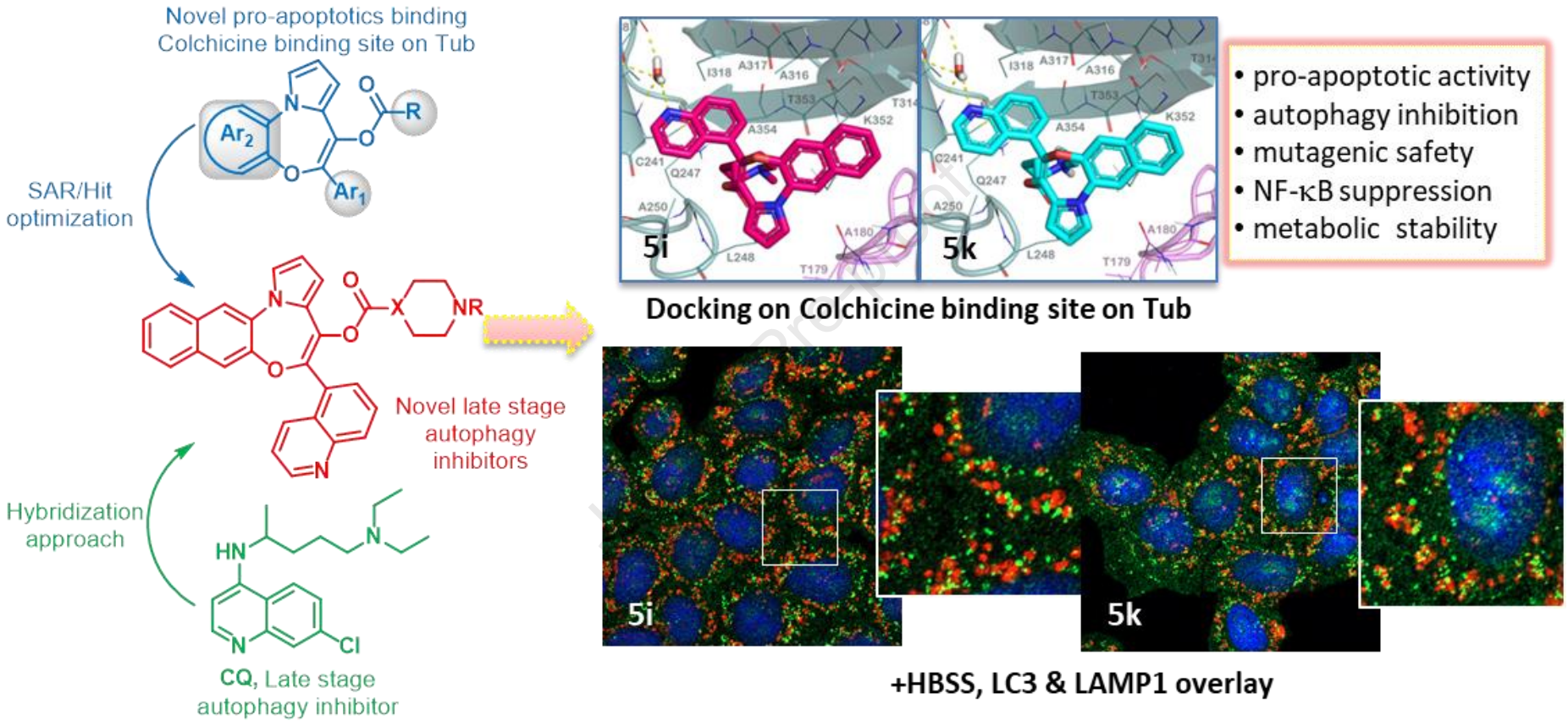
Novel pro-apoptotics binding
Colchicine binding site on Tub
SAR/Hit
optimization
Novel late stage
autophagy
inhibitors
Hybridization
approach
CQ, Late stage
autophagy inhibitor
5i
5k
• pro-apoptotic activity
• autophagy inhibition
• mutagenic safety
• NF-κB suppression
• metabolic stability
Docking on Colchicine binding site on Tub
5i
5k
+HBSS, LC3 & LAMP1 overlay

Design and Synthesis of Multifunctional Microtubule Targeting Agents endowed with Dual Pro-apoptotic and Anti-autophagic Efficacy

Giuseppe Campiani,[1,*] Tuhina Khan,[1] Cristina Ulivieri,[2,3] Leopoldo Staiano,[4,5] Chiara Papulino,[6] Stefania Magnano,[7] Seema Nathwani,[7] Anna Ramunno,[8] Daniel Lucena-Agell,[9] Nicola Relitti,[10] Stefano Federico,[1] Luca Pozzetti,[1] Gabriele Carullo,[1] Alice Casagni,[1] Simone Brogi,[11] Francesca Vanni,[2] Paola Galatello,[8] Magda Ghanim,[7] Niamh McCabe,[12] Stefania Lamponi,[1] Massimo Valoti,[2] Ola Ibrahim,[13] Jeffrey O'Sullivan,[13] Richard Turkington,[12] Vincent P. Kelly,[7] Ruben VanWemmel,[9] J. Fernando Díaz,[9] Sandra Gemma,[1] Daniela Zisterer,[7] Lucia Altucci,[6,14] Antonella De Matteis,[4,+] Stefania Butini,[1,3,*,+] Rosaria Benedetti[6,+]

[1]Department of Biotechnology, Chemistry and Pharmacy, DoE Department of Excellence 2018-2022, University of Siena, via Aldo Moro 2, 53100, Siena, Italy;

[2]Department of Life Sciences, University of Siena, via Aldo Moro 2, 53100, Siena, Italy,

[3]Istituto Toscano Tumori, University of Siena, via Aldo Moro 2, I-53100, Siena, Italy;

[4]Cell Biology and Disease Mechanisms, Telethon Institute of Genetics and Medicine, Via Campi Flegrei, 34, 80078 Pozzuoli Naples, Italy;

[5]Institute for Genetic and Biomedical Research, National Research Council (CNR), via Fratelli Cervi 93, 20054 Segrate, Milan, Italy.

[6]Department of Precision Medicine, University of Campania Luigi Vanvitelli, Vico L. De Crecchio 7 80138 Naples, IT.

[7]School of Biochemistry and Immunology, Trinity Biomedical Sciences Institute, Trinity College Dublin, 152-160 Pearse Street, Dublin 2, Ireland;

[8]Department of Pharmacy, University of Salerno, via G. Paolo II 132, 84084 Fisciano (SA), Italy;

[9]Centro de Investigaciones Biologicas Margarita Salas, Consejo Superior de Investigaciones Cientificas, Ramiro de Maeztu 9, 28040 Madrid, Spain

[10]IRBM Science Park, Via Pontina km 30,600, 00071 Pomezia, Rome, Italy;

[11]Department of Pharmacy, University of Pisa, 56126 Pisa, Italy;

[12]School of Medicine, Dentistry and Biomedical Sciences, Queen's University Belfast, 97 Lisburn Road, Health Sciences Building, BT9 7BL, Belfast, United Kingdom;

[13]School of Dental Science, Trinity College Dublin, Lincoln Place, Dublin 2, Ireland;

[14]Biogem Institute of Molecular Biology and Genetics, Via Camporeale, 83031, Ariano Irpino, Italy.

[*]Corresponding authors. giuseppe.campiani@unisi.it (G.C.), butini3@unisi.it (S.B.)

[+]Co-last authors

Abstract

Autophagy is a lysosome dependent cell survival mechanism and is central to the maintenance of organismal homeostasis in both physiological and pathological situations. Targeting autophagy in cancer therapy attracted considerable attention in the past as stress-induced autophagy has been demonstrated to contribute to both drug resistance and malignant progression and recently interest in this area has re-emerged. Unlocking the therapeutic potential of autophagy modulation could be a valuable strategy for designing innovative tools for cancer treatment. Microtubule-targeting agents (MTAs) are some of the most successful anti-cancer drugs used in the clinic to date. Scaling up our efforts to develop new anti-cancer agents, we rationally designed multifunctional agents **5a-l** with improved potency and safety that combine tubulin depolymerising efficacy with autophagic flux inhibitory activity. Through a combination of computational, biological, biochemical, pharmacokinetic-safety, metabolic studies and SAR analyses we identified the hits **5i,k.** These MTAs are characterised as potent pro-apoptotic agents and also demonstrate autophagy inhibition efficacy. To measure their efficacy at inhibiting autophagy, we investigated their effects on basal and starvation-mediated autophagic flux by quantifying the expression of LC3II/LC3I

and p62 proteins in oral squamous cell carcinoma and human leukaemia through western blotting and by immunofluorescence study of LC3 and LAMP1 in a cervical carcinoma cell line. Analogues **5i** and **5k**, endowed with pro-apoptotic activity on a range of hematological cancer cells (including *ex-vivo* chronic lymphocytic leukemia (CLL) cells) and several solid tumor cell lines, also behaved as late-stage autophagy inhibitors by impairing autophagosome-lysosome fusion.

Keywords

Autophagy, autophagy inhibitors, apoptosis, microtubule-targeting agents, cancer, *ex vivo*.

1. Introduction

Autophagy is a lysosome-dependent catabolic degradation process that controls eukaryotic cellular organelle and protein turnover to maintain cellular homeostasis. It is frequently stimulated in response to stress (e.g. chemotherapy exposure or nutrient deprivation) to offer an alternative metabolic fuel source for cell survival when regular energy-generating pathways are compromised [1]. Mechanistically, it includes several major steps including induction, nucleation, autophagolysosome formation, and degradation (Figure 1) [2–7].

Over the last decade, stress-induced autophagy has been demonstrated to contribute to drug resistance and malignant progression in preclinical and clinical studies.[8] Furthermore, genetic knockdown or pharmacological impairment of autophagy has produced therapeutic benefits [9]. The signalling and regulatory pathways involved in autophagy induction have been characterised by several biomarkers and pharmacological targets (see Figure 1 for details) [10]. Often, due to the compensatory nature of these pathways, autophagic flux is still maintained even when one specific regulatory pathway is targeted. Interestingly, all the

pathways leading to autophagy flux eventually converge on the lysosome. In the last decade, clinical research focused on the repositioning of lysosomotropic agents, such as the cheap antimalarials **1a**,**b** (Figure 2). These antimalarial agents **1a,b** are the foremost autophagy inhibitors in use despite toxicity and the high dose regimens required in clinical trials [8,11–13]. These molecules have been recently used in combination with target-specific drugs to successfully treat cancers [14], even when all approved treatment options were exhausted. Furthermore, other trials recently demonstrated the benefits of combinations of **1b** with other anti-cancer agents. Although the potency of these drugs is limited, clinicians found that these quinolines may enhance responsiveness and/or decrease resistance to anti-cancer agents through targeting specific cellular pathways such as MAP kinase pathways [14–16]. Taken together, these data highlight that targeting autophagy in cancer still holds promise and warrants further efforts to identify new autophagy inhibitors.

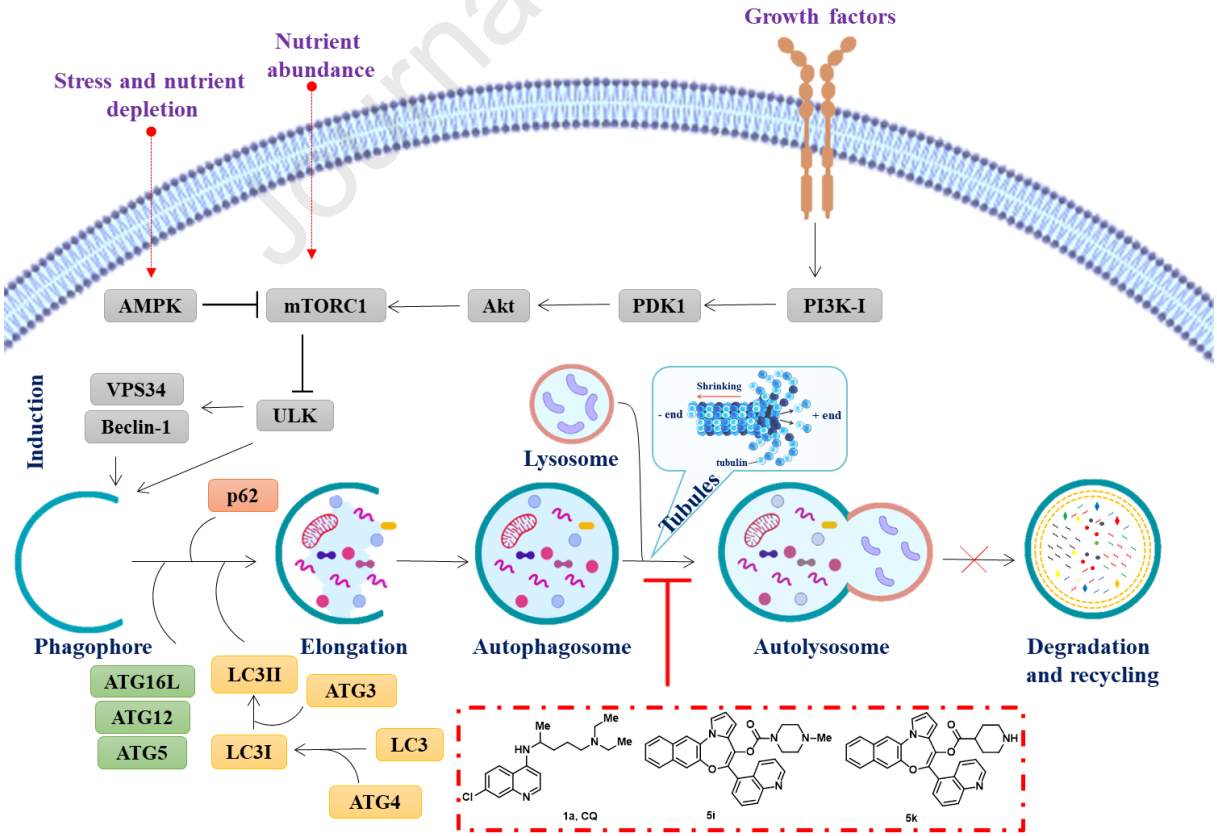

Figure 1. Autophagy regulatory pathways link to microtubules and late-stage autophagy

inhibition by CQ and the new hits **5i** and **5k**. Akt, protein kinase B; AMPK, 5′-adenosine monophosphate-activated protein kinase; ATG, autophagy-related genes; CQ, chloroquine; LC3, protein light chain 3; mTORC1, mammalian target of rapamycin complex 1; PDK1, pyruvate dehydrogenase kinase 1; p62, p62/sequestosome 1; PI3K, phosphoinositide 3-kinase; ULK, unc-51 like autophagy-activating kinase; VPS34, vacuolar protein sorting-34 complex.[7]

The microtubule (MT) network, a major cytoskeletal component, is involved in several cellular signalling pathways and processes including apoptosis and autophagy [17–20]. Current understanding of the relationship between autophagy and MTs indicates the importance of MT dynamics, tubulin post-translational modifications, and MT motors in autophagic flux [21]. Although MTs are not involved in autophagolysosome formation, they may serve as local suppliers of early-stage autophagy proteins such as Beclin1 [22] and may orchestrate the signaling, trafficking, and motility of autophagosomes [18]. Indeed, MTs exert a critical role in mediating autophagic flux, and in lysosomal fusion [4]. They act as the main tracks through which the cellular vesicles move and are associated with key proteins of the autophagic machinery [5,6]. Indeed, tubulin from stable MTs may undergo post-translational modifications like detyrosination and/or acetylation that may regulate the recruitment of molecular motors and MT-bound proteins. Acetylated tubulin (by recruiting dynein) drives and supports the dynein-mediated movements of the autophagosome and the eventual fusion of autophagosomes with the lysosomes. Because Histone Deacetylases (HDACs) control the acetylation status of tubulin, there is an additional level of crosstalk between epigenetics and autophagy. Thus, MT dynamics greatly influence autophagic processes. Microtubule-Targeting Agents (MTAs) represent one of the most effective anti-cancer agents to date even though their clinical efficacy is often hampered by the acquisition of resistance. MTAs induce apoptotic cell death, through the involvement of different cellular MAP kinases ERK and JNK. The cytotoxic effect of the MT-stabiliser taxol (**2**) is partially dependent upon its ability to block autophagosome maturation [23] while the MT-destabiliser

colchicine (**3,** Figure 1) has been proposed to be administered at a clinically permissible dose along with autophagy inhibitors in lung cancer [24]. Furthermore, the novel colchicine analogue (**4**), as demonstrated in colon cancer cells, combines a microtubule depolymerising effect and autophagy induction [25]. Other tubulin-binding drugs, e.g., vinblastine, naphtharazin, and 2-methoxyestradiol may stimulate autophagy to contribute to the anti-cancer activity [18,20]. Also, paclitaxel and nocodazole can efficiently stimulate and reduce the autophagosome clustering, respectively, under hypertonic stress in a DYNC/dynein-dependent manner [26].

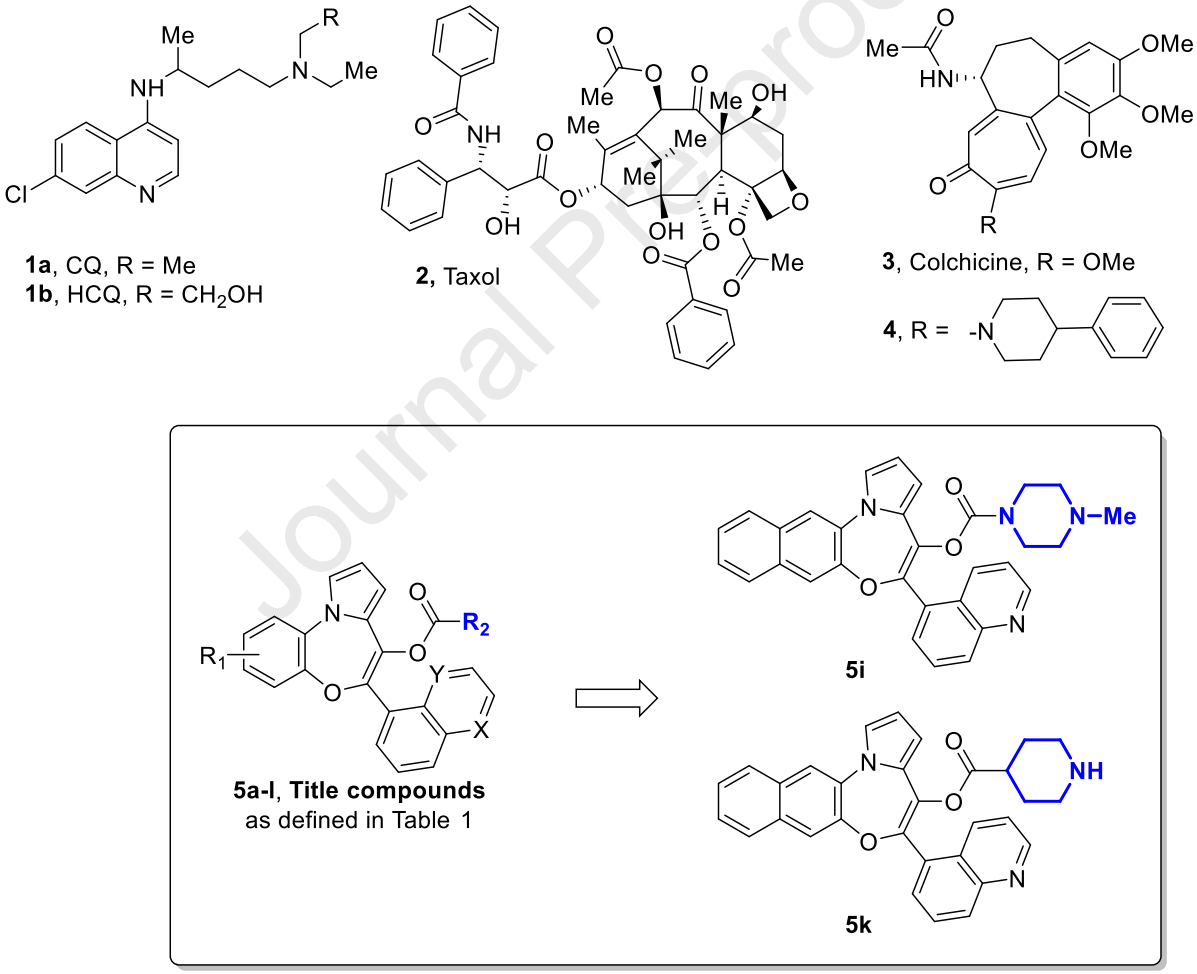

Figure 2. Autophagy inhibitors (**1a**,**b**) microtubule targeting agents (**2-4**), and title compounds (**5a-l**).

We have been involved in the development of novel MTAs and in the past, we characterised several pro-apoptotic benzoxazepines with efficacy on a wide range of cancer cells.[27–29]

In particular, in 2013, we demonstrated how PBOX-6 was able to induce apoptosis in colon cancer cells and to activate autophagic flux as a survival mechanism. Blocking autophagy in the late stages by BAF-A1 was a valuable strategy to synergistically enhance the apoptotic potential of PBOX-6 [30]. The results highlighted that: *i)* prolonged exposure of cancer cells to PBOX-6, activated autophagy as a cytoprotective mechanism against PBOX compounds, reducing their efficacy, *ii)* the original benzoxazepines were not able to inhibit autophagic flux and *iii)* the use of autophagy inhibitors was able to reverse resistance of colon cancer cells to PBOXs. The benzoxazepine scaffold of PBOX was further investigated and, in 2019, we confirmed this class of molecules as novel MTAs that binds to the colchicine binding site of tubulin [31]. Based on these findings, in the present study, we embarked on the challenging task of developing multifunctional agents that combine tubulin depolymerising efficacy with autophagic flux inhibitory activity. To this end, we applied a hybridization strategy through the introduction of protonatable groups (aliphatic, as in CQ **1a**, or heteroaromatic) into the pyrroloxazepine core and we developed the hybrids **5a-l** (Figure 2, and Table 1) characterised by microtubule targeting pro-apoptotic efficacy and potent autophagy inhibition properties (**5i**, and **5k**). The present manuscript focuses on the characterisation of the biological hybrid profile, in terms of microtubule targeting and autophagy inhibition, of the novel heterocycles (**5a-l**). A structure-activity relationship (SAR) analysis was also performed, and molecules were tested on a panel of cancer cells. The new pharmacological tools herein described (**5**) were characterized in a wide range of tumor cell lines, including those derived from both hematological (e.g. chronic lymphocytic leukemia (CLL), and solid tumors (e.g. oral squamous cell carcinoma (OSCC) and also in non-tumor cells to assess their toxicity profiles. In the panel, we included oral and haematological cancers since they belong to the leading type of malignancies worldwide with high incidence rates and mortality [32]. For both these tumor types, the currently available therapies (e.g.,

chemotherapy, radiotherapy, immunotherapy, and stem cell transplantation) face numerous drawbacks such as high dose administration, development of drug resistance, and adverse side effects in clinical trials [33–35]. *Ex vivo* pro-apoptotic activity was ascertained for compounds **5g**, **5i**, **5k**, **5l**, which were characterised as promising pro-apoptotic agents in splenocytes obtained from the Eμ-TCL1 mouse model of CLL. *In vitro* metabolic stability, pharmacokinetic properties, and *in vitro* effects on the NF-κB transcription factor were evaluated for the best performing compounds. Additionally, we demonstrated the efficacy of the novel hybrids on modulating autophagic flux. These studies delivered crucial insight into the autophagic activity and the mechanism of action of the new pyrroloxazepines. These integrated and complementary studies contributed to the identification of hybrids **5i** and **5k** as autophagy inhibitors with a clear-cut pro-apoptotic activity in a range of cancerous cell lines.

2. Results and discussion

2.1. Chemistry

The retrosynthetic scheme for the synthesis of the new anticancer agents **5a-l** (Figure 2 and Table 1) is represented in Figure 3. The synthesis of the key cyclic ketones **6a-g** was conceived by cyclization of the appropriate acids **7a-g**, which could be obtained by treatment of the corresponding pyrrolylphenol derivatives **10a-g** either by an alkylation pathway (**7a-e**) with an α-bromoester **8a**,**b** (reacted with **10a-e**) or by a Jocic-Reeve reaction pathway (**7f**,**g**) [36] with commercially available aldehydes **9a**,**b** (reacted with **10f**,**g**).

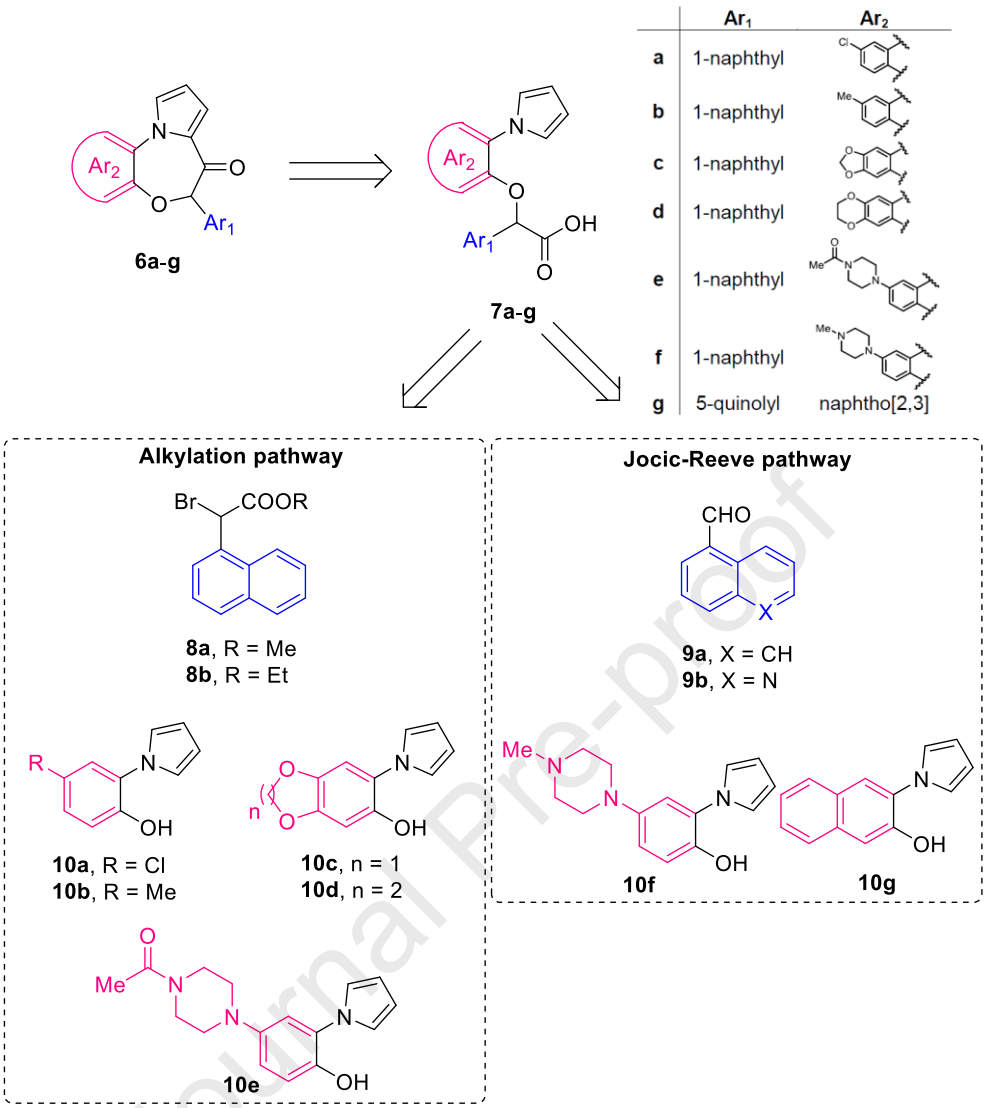

Figure 3. Retrosynthetic pathway of the key cyclic ketones **6a-g**.

The synthetic approach for the pyrrolyl-derivatives **10a-g** is described in Schemes 1 and 2. Commercially available aminophen(naphth)oles **11a-c** were converted to **10a**,**b**,**g**[37–39] following a Clauson-Kaas protocol in the presence of aqueous acetic acid and 2,5-dimethoxytetrahydrofuran (Scheme 1, A). Otherwise, a multistep approach was performed for the synthesis of **10c-f** (Scheme 1, B and Scheme 2).

Scheme 1. Synthesis of pyrrolyphenol intermediates **10a-d**,**g**[a]

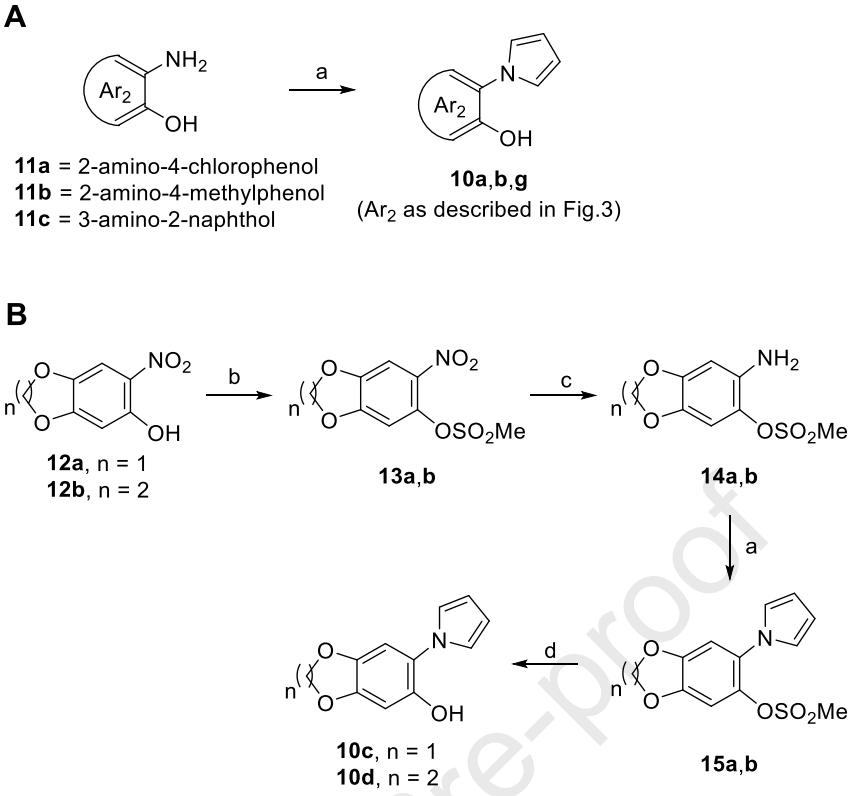

[a]Reagents and conditions: (a) AcOH, 2,5-dimethoxytetrahydrofuran, 100 °C, 30 min, 50-90%; (b) MsCl, dry TEA, dry DCM, 25 °C, 16 h, 88% (for **13a**) and 78% (for **13b**); (c) $SnCl_2$, EtOH, 80 °C, 12 h, 70% for **14a**, 78% for **14b**; (d) KOH, MeOH, 70 °C, 2 h, 70% for **10c**, 82% for **10d**.

The nitrophenol **12a**[40] and the 6-nitrobenzo[*d*][1,3]dioxol-5-ol **12b**[41–43], obtained as previously reported, were used to synthesise the compounds **10c** and **10d**, respectively, in four steps. First, the phenol group in **12a**,**b** was protected by using methanesulfonyl chloride (**13a**,**b**) and by a reduction operated with stannous chloride, the amino derivatives **14a**,**b** were obtained. The anilines **14a**,**b** underwent a Clauson-Kaas reaction to afford **15a**,**b** followed by a mesyl deprotection to achieve compounds **10c**,**d**.

Scheme 2. Synthesis of pyrrolylphenol intermediates **10e**,**f**[a]

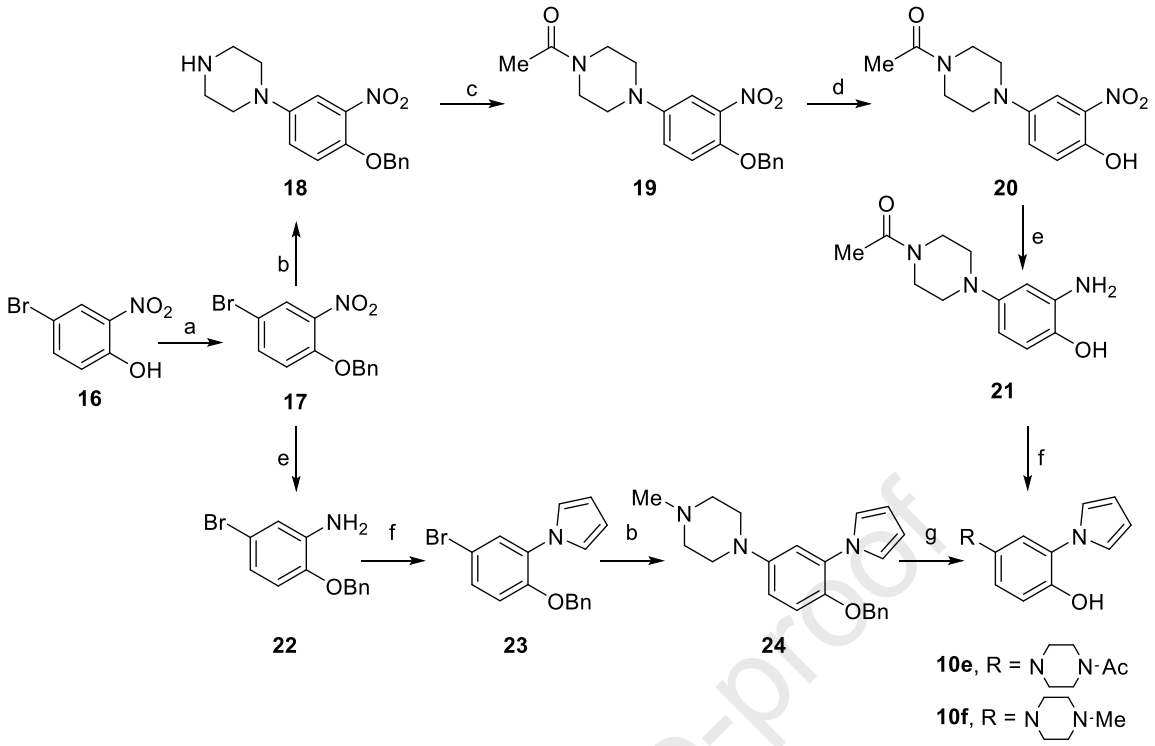

[a]Reagents and conditions: (a) $PhCH_2Br$, K_2CO_3, dry DMF, 85 °C, 12 h, 100%; (b) piperazine (for **18**) or *N*-methylpiperazine (for **24**), $Pd(OAc)_2$, (±)-BINAP, Cs_2CO_3, 1,4-dioxane, sealed tube, 100 °C, 12 h, 71%; (c) TEA, Ac_2O, 25 °C, 12 h, 100%; (d) TFA, toluene, thioanisole, 70 °C, 12 h, 85%; (e) Fe, $CaCl_2$, $EtOH/H_2O$, 90 °C, 30 min, 60% for **21** and 54% for **22**; (f) 2,5-dimethoxytetrahydrofuran, AcOH, H_2O, 100 °C, 1 h, 50% for **10e** or 2,5-dimethoxytetrahydrofuran, 1,4-dioxane, 6N aq. HCl, (100 °C, 10 min, 88% for **23**; (g) Pd/C, H_2, MeOH, 25 °C, 2 h, 100% for **10f.**

In Scheme 2, the synthesis of pyrrolylphenols containing the piperazine moiety (**10e**,**f**) is reported. Benzylation of the 4-bromo-2-nitrophenol **16** afforded derivative **17** that was submitted to a Pd-catalysed Buchwald-Hartwig cross-coupling reaction in the presence of piperazine,[44] to obtain **18** which underwent acetylation (**19**), by reaction with acetic anhydride and triethylamine (TEA). The acetyl derivative **19** was deprotected with trifluoroacetic acid and thioanisole [45] to furnish the nitrophenol **20.** The reduction of the nitrophenol **20**, performed with iron and calcium chloride, furnished the corresponding amine **21**, which was subjected to a Clauson-Kaas protocol to synthesize compound **10e**. For the synthesis of **10f**, the nitro-compound **17** was reduced to amine **22**, which was used in a Clauson-Kaas reaction protocol performed in hydrochloric acid and water medium [46] to

generate the pyrrolyl compound **23**. This latter underwent, in the presence of *N*-methylpiperazine, a Buchwald-Hartwig cross-coupling reaction to synthesize the intermediate **24** that furnished compound **10f** after removal of the benzyl group by catalytic hydrogenation.

Scheme 3 reports the final steps of the synthesis of compounds (**5a-l**). Arylpyrrolylphenols **10a-e** were submitted to an alkylation reaction with the appropriate α-bromoesters **8a**,**b** [38] either with potassium carbonate or sodium hydride to produce the ester intermediates **25a-e**. These esters were hydrolyzed into the corresponding acids **7a-e** in an alkaline medium. The acid intermediates **7f**,**g** were obtained through a Jocic-Reeve-based straightforward approach recently developed by us [36]. The ketones **6a-g** were obtained from the corresponding acids after treatment with phosphorus pentachloride towards an intramolecular Friedel-Crafts cyclization. The cyclization for **6a-e** was performed by heating the *in situ* acyl chloride in dry DCM at reflux temperature. Conversely, the ketones **6f**,**g** were synthesized by following the same approach but using dry DCE as solvent at 85 °C. The final compounds, **5a-d**,**f**,**j**,**l** were synthesized by reacting the appropriate acyl chlorides with the enolate salt of the cyclic ketones **6a-d**,**f**,**g**. Treatment of **5j** with trifluoroacetic acid generated the compound **5k**. Compound **5e** was synthesized from **6e** by reacting triethylamine, 4-dimethylamino pyridine, and acetic anhydride. Synthesis of the carbamate-based compounds, **5g-i** was accomplished by activating the sodium enolates of **6f**,**g** generated *in situ* into a carbonate system in the presence of 4-nitrophenyl chloroformate, that were successively reacted with the appropriate amines [47].

Scheme 3. Synthesis of the compounds **5a-l**.[a]

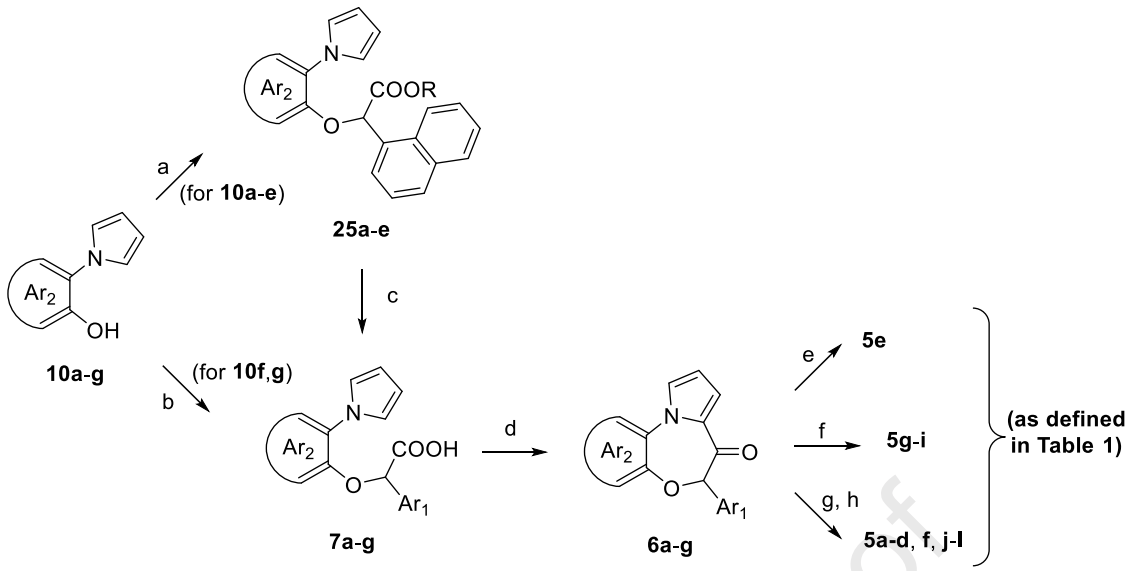

[a]Reagents and conditions: (a) **8a**, K_2CO_3, dry DMF, 25 °C, 12 h, 80-92% for **25a-d** or **8b**, NaH, dry THF, 25 °C, 12 h, 100% for **25e**; (b) NaOH, $CHBr_3$, dry THF, 0 °C (1 h) to 25 °C (12 h), 39% for **7f**, 37% for **7g**; (c) 5% NaOH (aq), THF, MeOH, 25°C, 2 h, 93-98% for **7a-e**; (d) PCl_5, [Bmim]Br, dry DCM, reflux, 12 h, 60-90% for **6a-d** or PCl_5, dry DCM, reflux, 12 h, 20% for **6e** or PCl_5, dry DCE, 85 °C, 12 h, 42% for **6f**,**g**; (e) dry TEA, DMAP, Ac_2O, dry DCM, 0 °C to 25 °C, 12 h, 30% for **5e**; (f) NaHMDS, 4-nitrophenyl chloroformate, diethylamine (for **5g**), or *N*,*N*-diethylpentane-1,4-diamine (for **5h**) or *N*-methylpiperazine (for **5i**) -78 °C (1 h) to 25 °C (4 h), 33% for **5g**, 30% for **5h**, and 56% for **5i**; (g) KH, dry THF, dimethyl carbamoyl chloride, 25 °C, 12 h, 71% for **5a** or KH, dry THF, AcCl, 25 °C, 12 h, 38-50% for **5b-d** or NaHMDS, CH_3COCl, -78 °C (3 h) to 25 °C, (12 h), 23% for **5f** or NaHMDS, 4-nitrophenyl choroformate, 4-(*tert*-butoxycarbonyl)piperazine-1-carboxylic acid, -78 °C (3 h) to 25 °C (12 h), 64% for **5j** or NaHMDS, nicotinoyl chloride, -78 °C (3 h) to 25 °C, (12 h), 31% for **5l**; (h) **5j**, TFA, dry DCM, 0 °C to 25 °C 30 min, 96% for **5k**.

2.2. Molecular Docking and SAR of the compounds

To gain more information about the binding mode of the developed compounds (**5a-l**, Table 1), a comprehensive SAR study was performed to investigate the behaviour of the novel series of molecules within the colchicine binding site of tubulin. A molecular docking calculation was performed employing Glide software implemented in the Maestro suite (Schrödinger Release 2015-4: Glide, Schrödinger, LLC, New York, NY, 2015) [48]. Starting from the PDB structure 6GJ4, a crystal structure of α/β tubulin in complex with compound **26** and to assess the validity of our computational protocol, the crystallized compound was re-docked into the protein binding site, showing a slight difference in its binding mode as

confirmed by the very low value of RMSD: 0.2744 (Figure S3). All the new compounds could be accommodated within the active site similar to compound **26** (Figure 4A) except for compounds **5e** and **5f**. For compound **5g**, due to the combination of bulky substituents both in R_1 and R_2 position (Table 1), it was not possible to retrieve a proper accommodation within the binding site. For the other compounds, the same pattern of interaction was found. The main contacts established by this series of molecules are represented by: a cation-π stacking established between K352 and the pyrrole ring of the core scaffold, along with some hydrophobic interactions within the binding cavity with residues T179, A180 and V181 (α subunit), C241, L248, A250, L255, A316, I318 and K352 (β subunit) (Figures 4 and 5). Interestingly, all the compounds that hold a 5-quinoline substituent interacted, through water-mediated contacts, with the backbone of G237 and C241 as well as with the sidechain of C241 (Figure 4). Specifically, **5a** (Figure 4A), with dimethylamine as R_2 substituent, establishes additional nonpolar contacts with A354 and Q247. An additional H-bond with K352 was detected with the oxygen atom of the carbonyl in most of the conformation of the two methyl chains, while the chlorine atom provides additional contacts of minor relevance such as the hydrophobic interactions with the α-subunit amino acids T179, A180, and V181. Also in the presence of a methyl group (**5b**, Figure 4B) the compound accommodates similarly to **5a**, except for the acetyl group of the ester moiety that lacks the polar contact with K352, due to the higher distance between the carbonyl and the lysine lateral chain. The benzodioxole and benzodioxine analogues **5c** and **5d** easily accommodate in the hydrophobic cavity of the binding site (Figure 4C, D) targeting, besides the same hydrophobic residues listed above, also T314 and A316. The compounds **5e**,**f** with acetyl- or a methyl-piperazine in R_1 displayed a different accommodation in the binding site. For **5e** (Figure 4E) the tricyclic core turns to project the OCOMe toward the hydrophobic cavity and the acetylpiperazine towards the opening of the binding site. This allows **5e** to reach the R221 belonging to the α-

subunit by establishing double H-bonds. For compound **5f** (Figure 4F) the substitution of the acetyl with a methyl group, exposes the piperazine moiety to the solvent and does not establish any relevant polar contact with the cavity residues.

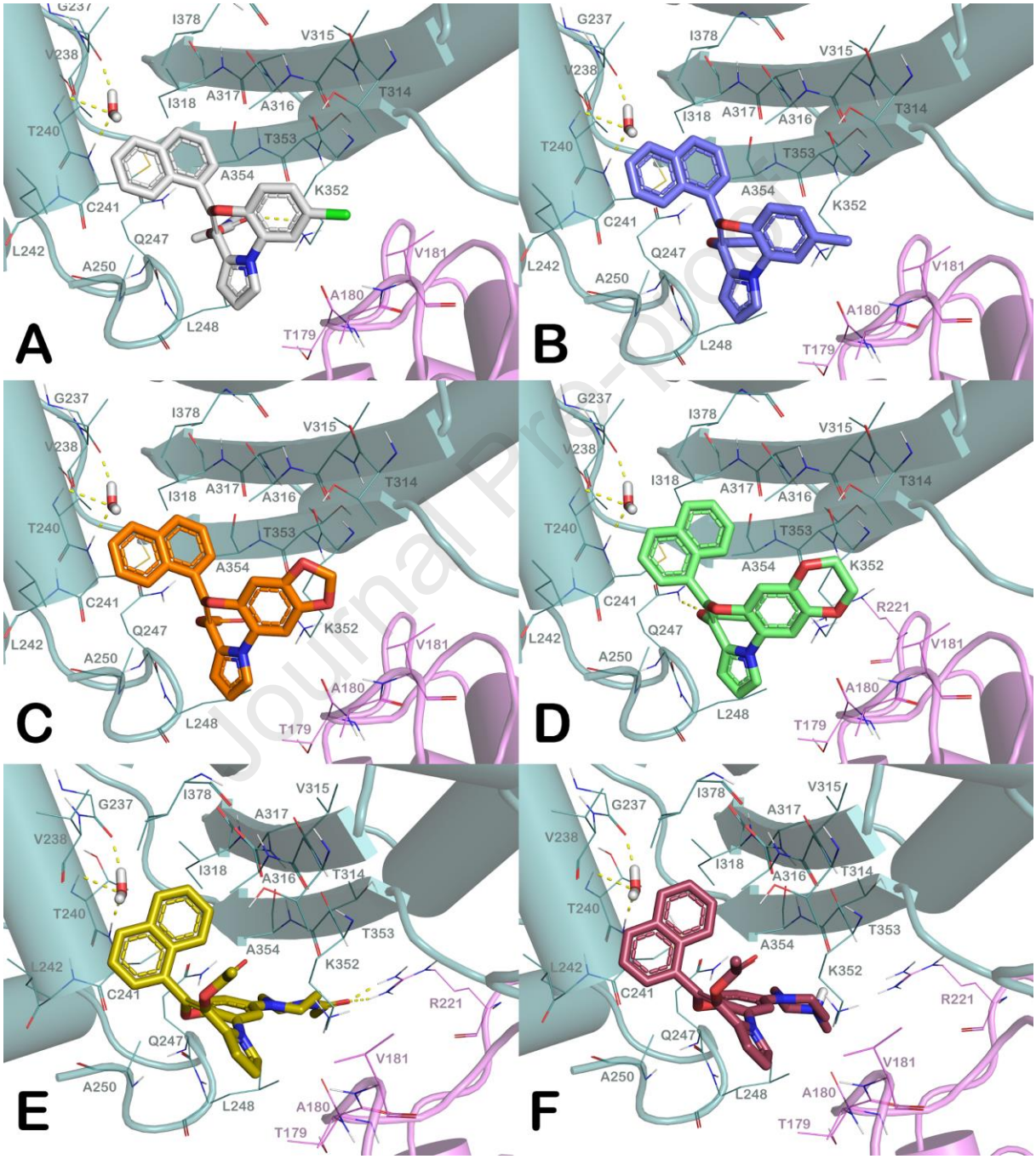

Figure 4. Complexes of compounds **5a-f** (represented as sticks in different colours, panels A-F respectively) with tubulin (α-tubulin is represented in pink cartoon, β-tubulin is represented in teal, PDB ID: 6GJ4) as found by molecular docking calculation.

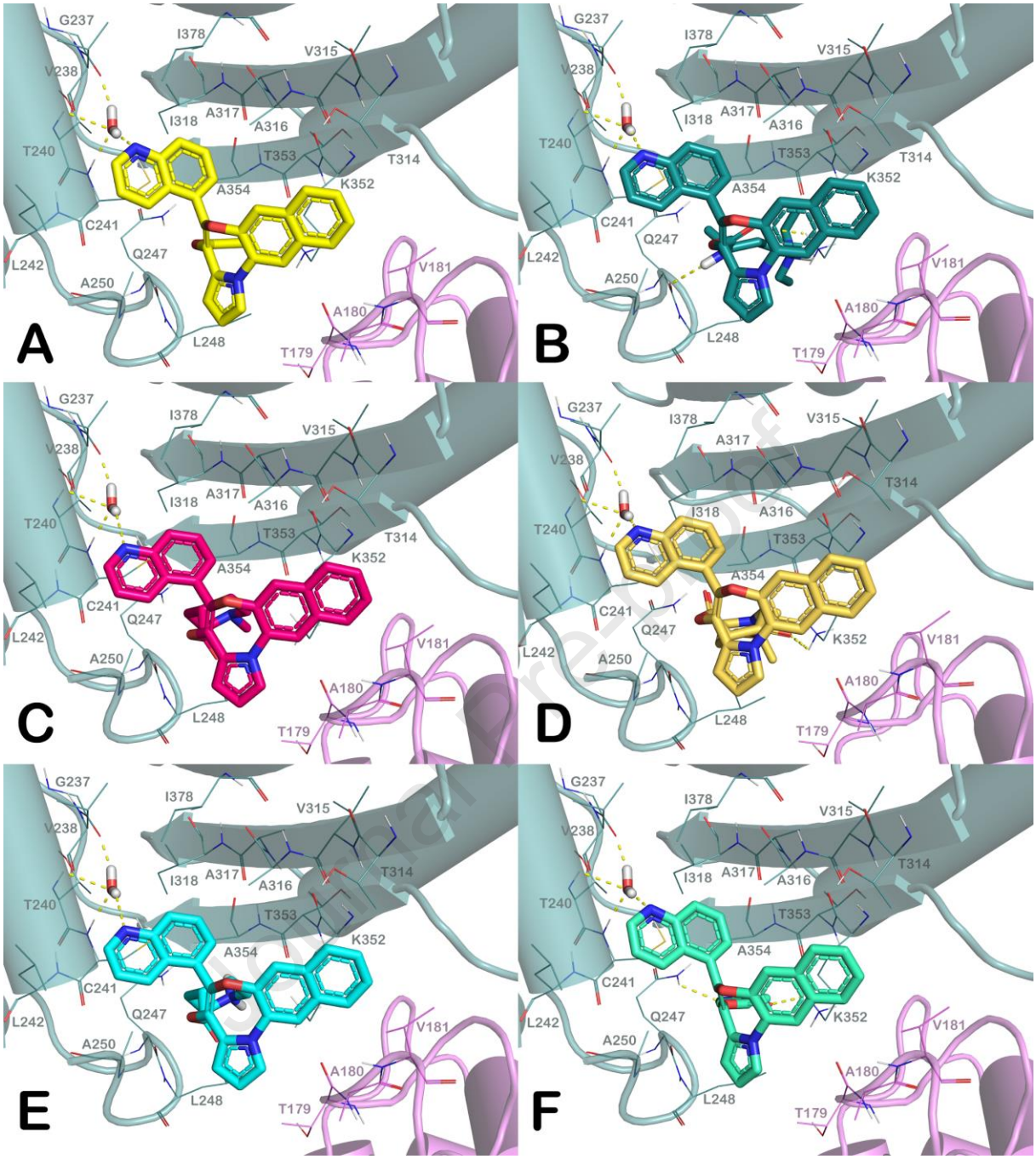

Figure 5. Complexes of compound **26** panel A, and compounds **5h-l** (represented as sticks in different colours, panels B-F respectively) with tubulin (α-tubulin is represented in pink cartoon, β-tubulin is represented in teal, PDB ID: 6GJ4) as found by molecular docking calculation.

Interestingly, the introduction of a 5-quinolyl (compounds **5h-l**, Table 1 and Figure 5) allows the formation of water-mediated H-bonds with G237, V238, and T240. The modification of the R_2 lateral chain modified the pattern of interaction at the entrance of the binding site. In particular, **5h** (Figure 5B), by the *N*,*N*-diethylaminopentan-2-yl carbamate chain can interact

through two H-bonds with Q247 (backbone) and K352 (side chain). In **5i** (Figure 5C) the *N*-methylpiperazine hampers the establishment of H-bonds, thus the compound is less solvent-exposed and better accommodates within the binding cavity by targeting the hydrophobic residues L248 and A354. Moreover, the central region of the molecule is involved in a double π-π stacking with K352. The bulky lateral chain of compound **5j** (Figure 5D) establishes an additional H-bond through the carbonyl oxygen with K352 along with the discussed hydrophobic contacts. The piperidine-containing analogue **5k** (Figure 5E) mainly targets T179, A180 and V181 (α subunit), C241, L248, A250, L255, A316, I318, K352 and A354 (β subunit). The substitution of the piperidine with a pyridine-3-yl system (**5l**, Figure 5F) allows an H-bond with Q247 through the nitrogen atom of the pyridine, while maintaining the other contacts.

2.3. Biological Assays

The characterisation of the pro-apoptotic potential of the new hybrid title compounds **5a-l** was measured in oral and esophageal squamous carcinoma cell lines, in promyelocytic leukaemia cells and in a cervical carcinoma cell line. Moreover, compounds were also tested in splenocytes from a Eμ-TCL1 mouse model of human CLL. As reference molecules, we used the heterocyclic compounds **26-29** (Table 1) previously identified as pro-apoptotic agents in multidrug-resistant leukaemic cancer cell lines [27,28]. We also performed an investigation to characterise the novel molecules as MTAs, since their design was based on the crystallographic data of **26** in complex with tubulin showing that its binding site (and that of the title compounds) partially overlap with that of colchicine [27]. The success of our hybridisation strategy was determined through the analysis of the effect of selected hybrid compounds (**5h,i,k,l**) on autophagic flux. Their profile was compared to precursors **26** and **28**, whose effect on autophagic processes was never investigated before. For selected hybrid

molecules we also investigated physico-chemical and preliminary pharmacokinetic properties, including toxicity.

Table 1. Structural details and overall pro-apoptotic effects on the human promyelocytic leukaemia HL-60 cell line of title compounds (**5a-l**) and reference pro-apoptotic compounds (**26-29**).

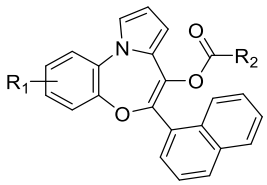

5a-g, and **27**

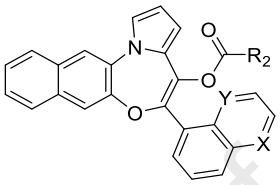

5h-l, and **26, 28, 29**

Cmpds	X	Y	R_1	R_2	48h incub time	24h incub time	
					10 µM	10 µM	25 µM
5a	-	-	2-Cl	NMe_2	NT	++	++
5b	-	-	2-Me	Me	NT	-	++
5c	-	-	[1,3]dioxolo[2,3]	Me	NT	++	++
5d	-	-	[1,4]dioxino[2,3]	Me	NT	++	++
5e	-	-	2-(4-acetylpiperazine)	Me	- 20µM +++ 50µM	NT	
5f	-	-	2-(4-methylpiperazine)	Me	-	NT	
5g	-	-	2-(4-methylpiperazine)	NEt_2	-	NT	
5h	N	CH	-	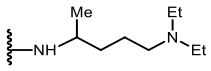	+++	NT	
5i	N	CH	-	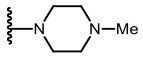	+++	NT	
5j	N	CH	-	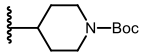	+	NT	
5k	N	CH	-	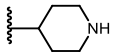	+++	NT	
5l	N	CH	-		+++	NT	
26[49]	N	CH	-	Me	+++	NT	
PBOX6 **27**[50]	-	-	-	NMe_2	+++	NT	
PBOX15 **28**[49]	CH	CH	-	Me	+++	++	NT
29[49]	CH	N	-	Me	+++	NT	

+++: ≥ 70%, very potent; ++: ≥ 50%, potent; +: ≥ 30%, poor; -: < 30%, poorly effective; NT: not tested.

*2.4. Determination of the pro-apoptotic potential of compounds **5a-l** on haematological cancer cells*

*2.4.1. Cell-based assays of compounds **5a-l** on HL-60 cell line*

As a primary screening approach, the pro-apoptotic potential of all the synthesised analogues was evaluated in the HL-60 cell line. For the first set of analogues (**5a-e**, Table 1) HL-60 cells were incubated with two different concentrations of each compound for 24 h (**5a-d**) or 48 h (**5e**). Quantification of the % apoptosis by flow cytometric analysis of propidium iodide-stained cells (sub G0/G1) revealed that, in general, these analogues could somewhat challenge the profile of the compounds **27** and **28** (Table 1, and Figures S1 and S2 of the Supplementary Information (SI)) when tested at 10 and 25 μM for 24 h. Only compound **5e** could induce apoptotic cell death above 75%, when tested at a concentration of 50 μM for 48 h (Table 1, and Figure S2).

With this data in mind, we decided to insert one or two basic moieties into the molecules thus generating the second set of compounds (**5f-l**, Table 1 and Figure 6). We measured the dissipation of the mitochondrial membrane potential in tetramethylrhodamine methyl ester (TMRM) loaded cells following treatment with the compounds **5f-l** and reference compounds, **26** and **28** previously developed as pro-apoptotic agents [30] but ineffective as autophagic inhibitors. After treating HL-60 cells with a 10 μM concentration of each compound for 48 h (Table 1 and Figure 6), all the compounds, except for **5f**,**g**, potently promoted apoptosis. This indicated a notable pro-apoptotic potential for the whole new series of structurally related analogues (**5a-l**). In general, this data provided evidence that the pro-apoptotic efficacy of compounds **5a-l** is greatly influenced by the nature and the position of the substituents in the polycyclic core scaffold (low potency analogues **5a**,**b** and **5c**,**d**). The presence of an acetylpiperazine (**5e**), as well as the presence of a piperazine system embedded with the fused benzo ring in the Ar_2 portion (as in **5f**,**g**), negatively influenced the pro-apoptotic activity.

The structural pro-apoptotic features of the hit **26** (a pro-apoptotic agent previously identified [30] were combined with the key moieties of **1a**, applying a hybridisation concept to develop multifunctional tools. In this context, we pursued the synthesis of compounds bearing both aliphatic and heterocyclic basic moieties by hybridising the key pharmacophoric elements of **1a**. This approach initially resulted in compound **5h** which demonstrated very promising pro-apoptotic potential. As a next step, and in response to the results of our SAR study, we decided to remove the chiral centre present in the basic lateral chain on the right-end of our compounds thus generating analogues **5i-l**. In these compounds, a piperazine, a piperidine and a pyridine system were inserted. All the compounds demonstrated excellent pro-apoptotic effects that challenged those of **26** and **28**. Notably, in line with our expectations, the masking of the basic piperidine nitrogen (**5j**) was deleterious for the apoptotic effect. These results were used to select those for advancement as the most promising candidates for further testing.

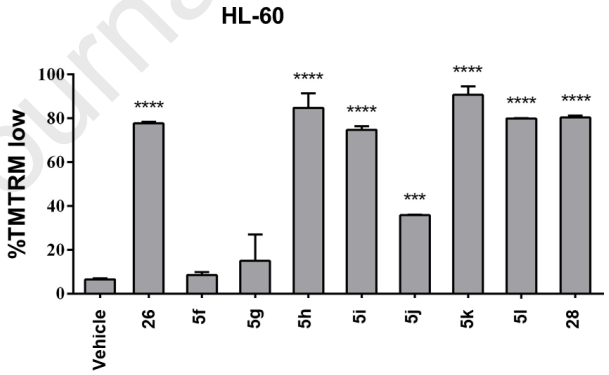

Figure 6. Flow cytometric analysis of mitochondrial membrane depolarisation in HL-60 cells treated with **5f-l** compounds, compounds **26**, **28** (10 μM) or DMSO (vehicle) for 48 h. Cells were treated with the indicated compounds and loaded with TMRM. The bar graph shows the percentage of apoptotic cells (TMRM low cells). Data are presented as mean values ± SD (n = 2). One way ANOVA ****p≤0.0001, ***p≤0.001 *vs*. Vehicle.

2.4.2. Cell-based assays of selected compounds in ex-vivo CLL cells

The most promising analogues were further tested in CLL cells. Interestingly, **5g**, **5i**, **5k**, and **5l** were able to induce apoptosis in splenocytes obtained from the Eμ-TCL1 mouse model of

CLL characterised by an expansion of leukaemic B cells dependent, at least in part, on defective apoptosis. Of note, reference compounds, **26** and **28**, were also effective in inducing apoptosis in these cells (Figure 7).

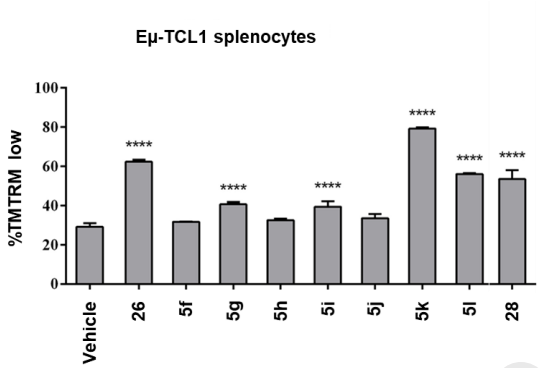

Figure 7. Flow cytometric analysis of mitochondrial membrane depolarization in Eμ-TCL1 splenocytes treated with **5f-l** compounds, compounds **26**, **28** (10 μM) or DMSO (vehicle) for 48 h and loaded with TMRM. The bar graph shows the percentage of apoptotic cells (TMRM low cells). Data are presented as mean values ± SD (n = 3). One way ANOVA ****p≤0.0001 *vs*. vehicle.

2.5. Cell-based assays on solid tumour cell lines

To explore and expand the potential applicability of these newly identified pro-apoptotic agents, the cytotoxic and pro-apoptotic potential of some analogues (**5f**, **5h**, **5i**, and **5k**) was further investigated in various solid tumour cell lines such as oral and esophageal cancerous cell lines.

2.5.1. Effect of selected compounds on oral squamous cell carcinoma (OSCC) cell lines

The selected compounds **5f**, **5h**, **5i** and **5k** were tested on a panel of three different OSCC cell lines, SCC4, Ca9.22, and TR146. As a preliminary assessment, the AlamarBlue assay was performed to investigate the effect of compounds **5f**, **5h**, **5i**, and **5k** along with the reference compounds **26**, **27** and **29** on cell viability in SCC4 cells for 48 h. IC_{50} values (defined as the concentration of the drug which reduces the cell viability by half) were calculated using Graphpad Prism to estimate the variation in cell sensitivity (Table 2). Interestingly, three

compounds (**5h**, **5i**, **5k)** and the reference one **29** were able to decrease the cell viability in a dose-dependent manner and exhibited IC_{50} values in the nanomolar range (908, 539, and 849 nM, respectively), while no effect was detected after treatment with **5f**. The three most promising analogues were further tested in the Ca9.22 (p53 mutated) and TR146 cell lines. Compound **5i** stood out as an extremely potent cytotoxic agent for both the cell lines (Ca9.22, IC_{50} ~ 130 nM; TR146, IC_{50} ~ 880 nM, Table 2), while **5h** and **5k** were active in the micromolar range (**5h**: IC_{50}: Ca9.22 ~ 2 μM, TR146 ~ 1.5 μM; **5k**: IC_{50}: Ca9.22 ~ 2 μM, TR146 ~ 4.5 μM, Table 2).

Table 2. Reduction in OSCC cell viability by selected analogues and determination of IC_{50} values

Cmpds	**IC_{50} (μM)**[a]		
	SCC4	**CA9.22**	**TR146**
26	0.22 ± 0.07	13.4 ± 0.09	NT[b]
5h	0.91 ± 0.06	2 ± 0.5	1.5 ± 0.25
5i	0.54 ± 0.15	0.13 ± 0.01	0.88 ± 0.06
5k	0.85 ± 0.12	2 ± 0.2	4.5 ± 1.2
27	0.16 ± 0.02	0.17 ± 0.01	NT[b]
29	0.13 ± 0.01	NT[b]	NT[b]

[a]IC_{50} values were determined on SCC4, Ca9.22, and TR-146 cell lines; cells were treated with increasing concentrations (at least 8) of each compound for 48 h. Data represent the mean ± SD of at least three independent experiments; [b]NT not tested.

Following these encouraging results, we decided to investigate the pro-apoptotic potential of selected compounds in SCC4 (Figure 8, A and B), Ca9.22 (Figure 8, C), and TR146 (Figure 8, D) cell lines. Apoptosis induction was evaluated using the Annexin V/Propidium iodide (PI) dual staining assay, which can distinguish between the early and late-stage apoptosis. The cells were treated with the compounds at both 0.5 or 2 μM of concentrations for 48 h. **5h**,

5i and **29** induced apoptosis in SCC4 cells at both concentrations, while no apoptosis was observed following the treatment with **5f** at those concentrations (results not shown, Figure S1). **5k** was not able to induce apoptosis at 0.5 μM concentration but produced a positive result following treatment of cells with 2 μM. In addition, the compounds were evaluated for their pro-apoptotic efficacy in Ca9.22 and TR146 cell lines at a concentration of 0.5 μM for 48 h. As expected, **5i** produced the best outcome. In general, all these results are in line with the results obtained from the AlamarBlue viability assay.

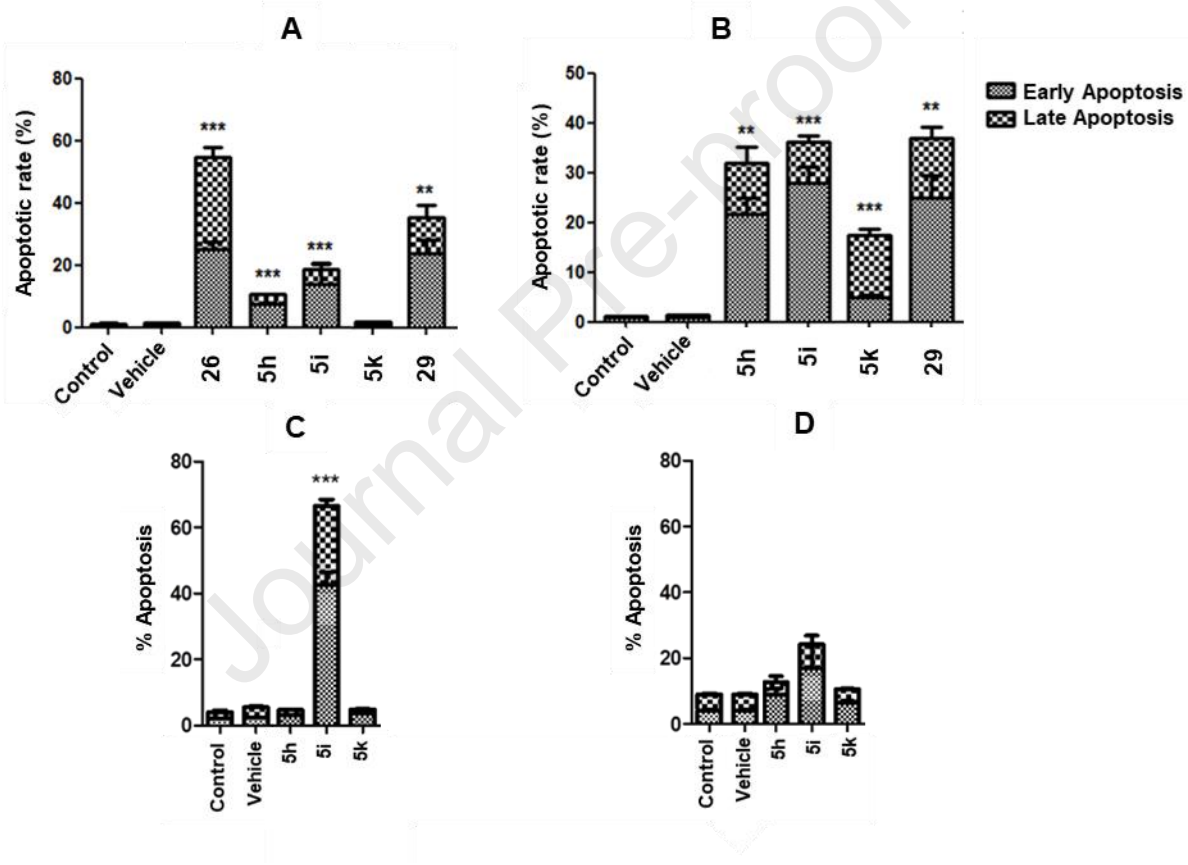

Figure 8. (A) compound concentration of 0.5 μM and (B) compound concentration of 2 μM. Annexin V/PI assay of the compounds on the OSCC cell line, SCC4. Values represent the mean ± S.E.M of three independent experiments (n = 3). Statistical analysis was performed using an unpaired one-tailed student t-test to compare mean values between vehicle and treated cells ***$p < 0.001$, **$p < 0.01$. (C) Ca9.22 cells were seeded at a density of 30 X 10^4 cells/mL and were left untreated (control) or treated with either vehicle (1% EtOH (v/v)) or 500 nM of the compound for 48 h. (D) TR146 cells were seeded at a density of 30 X 10^4 cells/mL and were treated with either vehicle control (1% EtOH (v/v)) or 500 nM of the compound for 48 h. After incubation cells were harvested and stained with Annexin V/ PI and were analyzed by flow cytometry using BD FACs Accuri software. 10,000 cells were

gated on vehicle-treated cells. Values represent the mean ± S.E.M of three independent experiments (n = 3). Statistical analysis was performed using a student t-test. **p = 0.001".

2.5.2. Effect of selected compounds on esophageal squamous cell carcinoma (ESCC) cell lines

The selected compounds **5h**, **5i**, and **5k** along with compound **26** were further characterised in KYSE-520 cells, a multidrug-resistant ESCC cell line. It has been reported that KYSE 520 cells have elevated levels of expression of cyclooxygenase-2 (COX-2) [51], which might be responsible for playing a role in carcinogenesis, cancer progression, and multidrug resistance [52–54]. COX-2 has been shown to induce the expression of the multidrug resistance 1 gene encoding Pgp, *via* phosphorylation of c-Jun at Ser63/73, resulting in the efflux of chemotherapeutic agents in colorectal cancer [55,56]. An AlamarBlue assay was performed to investigate the effects of the compounds on cell viability of KYSE-520 (Table 3). All the compounds exhibited effects on viability in a time-dependent manner.

Table 3. Cytotoxic activity, as IC_{50} (μM), of the selected analogues (**26**, **5h**, **5i**, and **5k**) on the growth of KYSE-520 and EAC cell lines.

Cmpds	IC_{50} (μM)[a]						
	KYSE-520 48 h	KYSE-520 72 h	OE-33 72 h	OE-19 72 h	FLO-1 72 h	MFD-1 72 h	SKGT4 72 h
26	n.d[b]	138.30 ± 0.1	0.32 ± 0.08	0.73 ± 0.13	0.28 ± 0.08	1.09 ± 0.28	0.51 ± 0.12
5h	n.d[b]	41.94 ± 0.06	1.38 ± 0.58	n.d[b]	n.d[b]	n.d[b]	n.d[b]
5i	3.60 ± 0.1	1.68 ± 0.04	0.40 ± 0.11	0.73 ± 0.16	0.40 ± 0.31	1.21 ± 0.38	0.55 ± 0.15
5k	1.68 ± 0.1	0.89 ± 0.02	1.93 ± 0.50	n.d[b]	n.d[b]	n.d[b]	n.d[b]

[a]IC_{50} values were determined on KYSE-520, OE-33, OE-19, FLO-1, MFD-1, and SKGT4 cell lines; cells were treated with increasing concentrations (at least 8) of each compound for 72 h (72 h and 48 h in the case of KYSE-520 cell line). Data represent the mean ± SD of at least three independent experiments; [b]n.d. - not determined.

The compounds **26** and **5h** were not able to affect the cell viability when incubated for 48 h even at 500 μM, but, when incubated for 72 h, displayed activity with IC_{50} values in the high μM range (138.30 and 41.94 μM, respectively, Table 3). Interestingly, both **5i** and **5k** were able to inhibit the cell growth within the two-time frames (IC_{50}: 3.60 μM at 48 h, 1.68 μM at 72 h and 1.68 μM at 48 h, 0.89 μM at 72 h, respectively) with **5k** being the most active compound on KYSE-520 cells at 72 h.

Driven by the promising cell viability results, the pro-apoptotic effects of the compounds were analysed, following treatment of cells at 3 and 10 μM for 72 h, by flow cytometric analysis of Annexin V/PI dual stained cells (Figure 9). All the compounds were able to induce apoptosis (from > 20% to < 60%) at both concentrations. **26**, **5k** and **5i** displayed a concentration-dependent apoptosis induction profile in line with the results found from the AlamarBlue viability assay.

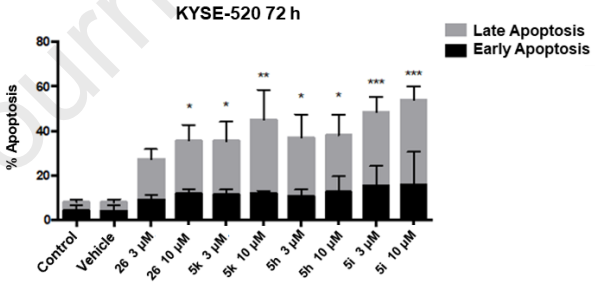

Figure 9. Annexin V/PI assay for the compounds **26**, **5h**, **5i**, and **5k** on KYSE-520 cells at 3 and 10 μM concentrations; incubation time 72 h.

2.5.3. Effect of selected compounds on human esophageal adenocarcinoma (EAC) cell lines

The compounds **26**, **5h**, **5i**, and **5k** were then characterised in a panel of EAC cell lines (Table 3) [57–59]. As a first step, an MTT viability assay was performed to investigate the effects of the compounds on the viability of OE-33 cells at 72 h. As evidenced in Table 3, **26** and **5i** were able to affect the cell growth in the nanomolar range with IC_{50} values of 296 nM and

391 nM, respectively. **5h** and **5k** displayed IC_{50} values of 1.40 μM and 1.32 μM, respectively. The best performing compound **5i**, along with the reference compound **26**, were then tested on additional EAC cell lines. Both the compounds exhibited an inhibitory effect on cell viability in the nanomolar concentration range in OE-19 (**26** and **5i**, IC_{50} = 730 nM), FLO-1 (**26**, IC_{50} = 280 nM; **5i**, IC_{50} = 400 nM) and SKGT4 cells (**26**, IC_{50} = 510 nM; **5i**, IC_{50} = 550 nM), and in the low micromolar range for MFD-1 cells (**26**, IC_{50} = 1.10 μM; **5i**, IC_{50} = 1.20 μM).

2.6. Effect of selected compounds on tubulin dynamics

Previous studies have confirmed that compounds **26-29** act as microtubule disrupting, colchicine-binding agents [49]. Tubulin polymerisation results in large structures (microtubules and microtubule bundles) that make the solution turbid, therefore turbidity is a good marker to monitor the tubulin assembly reaction. Therefore, we evaluated the microtubule depolymerising effects of the most potent pro-apoptotic agents active on a wide range of tumour cell lines (**5h**, **5i**, and **5k**). An assembly time-course experiment of 25 μM of tubulin at 37°C in the presence of 27.5 μM of the compounds was performed monitoring the absorbance at 350 nm (Figure 10).

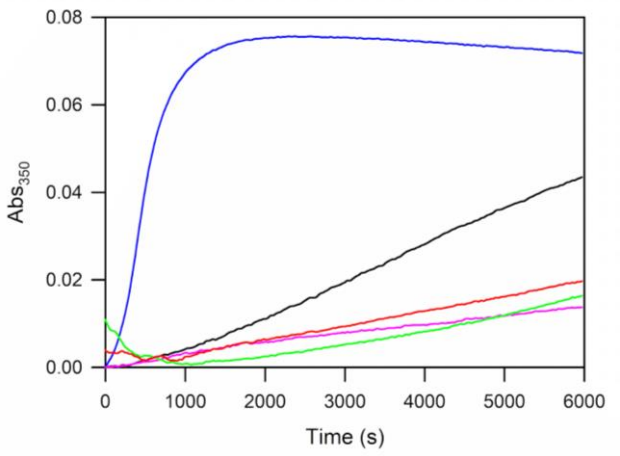

Figure 10. Time course of 25 μM tubulin polymerisation (GAB buffer) in the presence of DMSO (compound vehicle; blue line) or 27.5 μM of compounds **5h** (black line), **5i** (pink

line) or **5k** (green line). 27.5 μM of Podophyllotoxin (red line) was used as a control destabiliser.

Podophyllotoxin, a well-known colchicine site binding compound, was used as a positive control. As shown in Figure 10, at time 0 the temperature is raised from 4º to 37º degrees, in the absence of polymerization inhibitors the absorbance rapidly increases indicating the formation of microtubules, on the other hand the increase of absorbance is inhibited in the presence of all the compounds indicating that as podophyllotoxin they inhibit microtubule polymerization. Though the compound 5h is not as good as the other two compounds inhibiting polymerization, it still showcased a negative effect on the microtubule assembly. However, the lower decrease of absorbance observed in the presence of 5h could also be attributed to the formation of tubulin aggregates.

2.6.1. Biochemical characterization of compound **5i**

Compound **5i** was further biochemically characterised. Firstly, the evaluation of stoichiometry needed to inhibit the polymerisation dynamics was determined (Figure 11A) (the y-axis of the plot represents the increase of absorbance of the solution upon polymerization as described in figure 10). As it can be seen 5 μM **5i** fully inhibited 20 μM tubulin assembly, indicating a substoychiometric mode of action, very similar to our previously characterised compounds [49]. Following on from this, we used fluorescence to characterise the binding of **5i** to tubulin. We examined the intrinsic fluorescence of **5i** and possible changes upon binding to tubulin. To do this, we carried out an UV/vis absorbance spectrum of **5i** and noted the absorption in the 340-400 nm range (Figure 11B). We found that the excitation of **5i** at 350 nm produced a fluorescence peak around 460 nm, which was greatly enhanced in the presence of 10 μM tubulin (Figure 11C). We took advantage of this feature (high fluorescence while bound to tubulin and weak fluorescence while free) to

investigate the binding site and binding constant of **5i** to tubulin. To this end, we performed saturation experiments to obtain the binding site and binding constant and competition experiments using podophyllotoxin as the competitor. Surprisingly, podophyllotoxin was unable to displace **5i** from tubulin (no decrease of fluorescence indicating release of the compound from tubulin was observed) (Figure 11D) even at molar ratios up to 250:1 (data not shown). This observation indicated that the **5i** fluorescence observed upon interaction with tubulin is either due to binding to a different site from that of colchicine (the site where podophyllotoxin binds) or that the observed fluorescence arises from a non-specific interaction with the protein. To test this hypothesis, we performed a saturation experiment using increasing concentrations of cross-linked microtubules (MTX) instead of tubulin. Since the colchicine binding site is not accessible in the microtubule lattice, no increase of fluorescence upon interaction with tubulin should be observed [48]. Despite the binding site being occluded, an increment of **5i** fluorescence was observed upon increasing MTX concentration (Figure 11E), indicating that most probably the compound binds microtubules non-specifically. To confirm this, we tested **5i** binding to bovine serum albumin (BSA). Following non-specific binding to proteins, an increase in **5i** fluorescence was observed with increasing concentrations of BSA (Figure 11F), precluding the determination of the binding constant and binding site of **5i** utilising our biochemical approaches. At present, we cannot exclude specific binding to the colchicine site, but we also cannot discriminate between specific and non-specific binding.

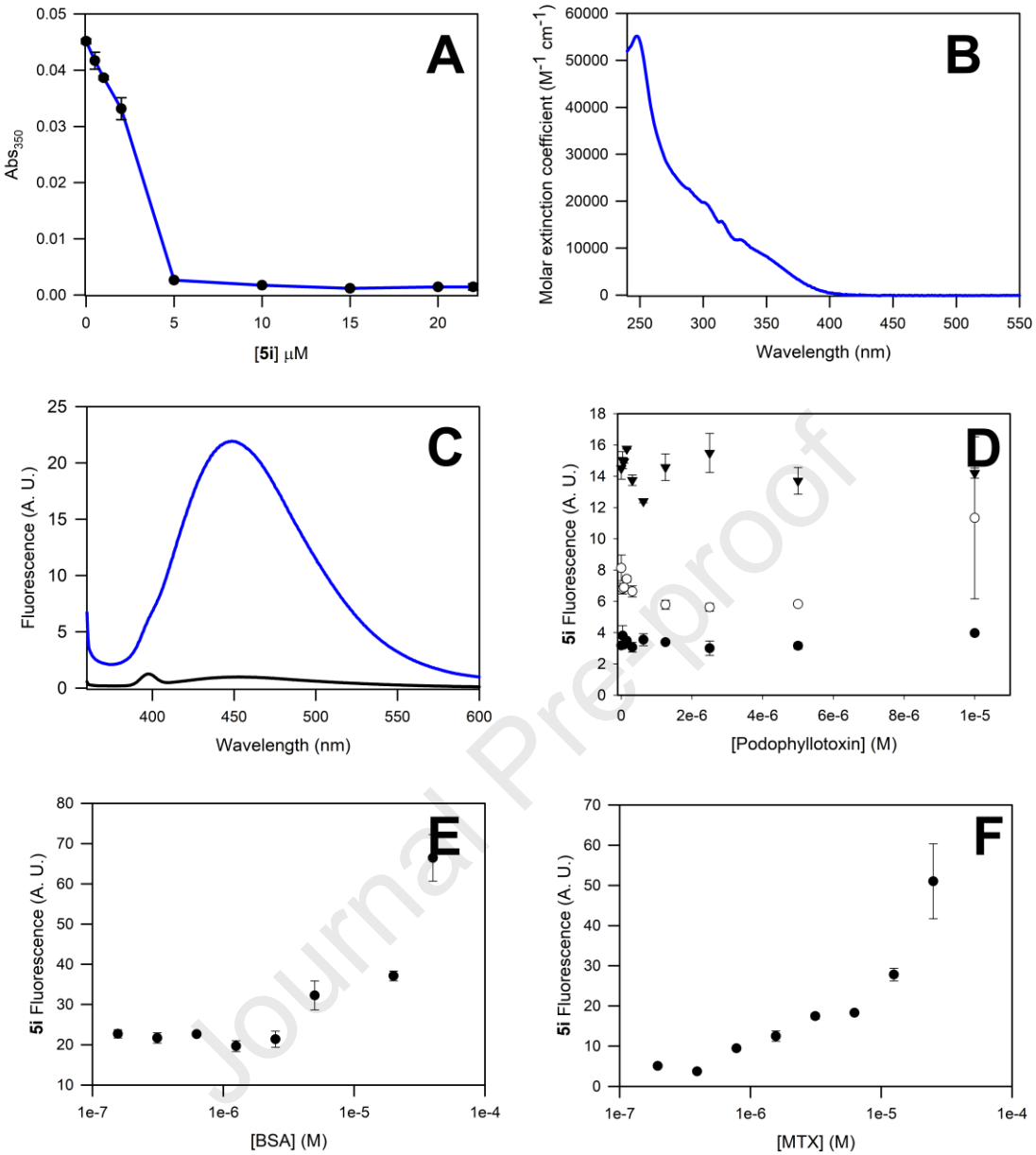

Figure 11. (A) Stoichiometry of the tubulin depolymerization in the presence of **5i**. A range of different concentrations of **5i** up to 22 µM was added to 20 µM of tubulin in polymerizing conditions. Polymerization was carried out as described in the experimental conditions. Plotted values of Abs350 represent the last value obtained from the plateau phase from every polymerization curve. (B) Absorbance spectrum of 20 µM **5i**. (C) Fluorescence emission spectrum of 10 µM **5i** alone (dark line and inset) or in presence of 10 µM tubulin (blue line) (D) Competition assay between **5i** and podophyllotoxin, a range of podophyllotoxin concentrations up to 10 µM was used to displace three different concentrations of **5i** and tubulin (0.1 µM of both, blue symbols; 0.5 µM of both, white symbols; 1 µM of both, red symbols). **5i** was excited at 350 nm and the fluorescence emission was recorded at 450 nm in a Varioskan (ThermoFisher) plate reader. (E) and (F) Saturation assays carried out in the presence of bovine serum albumine BSA (E) or cross-linked microtubules MTX (F). A fixed concentration of 1 µM was incubated with increasing amounts of the corresponding proteins. **5i** was excited at 350 nm and the fluorescence emission was recorded at 450 nm in a Varioskan (ThermoFisher) plate reader.

2.7. Toxicity evaluation

The newly synthesised analogues, along with the compounds **26** or **28** were next characterised in a range of non-tumorous (e.g., murine fibroblast, human oral epithelial primary cells) and additional tumour cell lines.

2.7.1. Effect of selected analogues on non-tumorous and additional tumour cell lines

The effects of the compounds (**5b-d**, **5f-l**) on mouse fibroblast non-cancerous NIH3T3 cells were investigated by measuring the percentage of viable cells at a concentration range of 0.1 to 120 μM (Table 4). It has previously been reported that the IC_{50} values of **2**, **3**, **26**, and **28** against mouse fibroblast NIH3T3 are in the nanomolar range of 25 ± 3, 25 ± 4, 126 ± 4, and 42 ± 9, respectively [49]. The new analogues **5b-d**, exhibited a similar cytotoxic profile (IC_{50}) with values in the low nanomolar concentration range, while the other three analogues required a relatively higher concentration range (**5f** ~ 45 μM; **5g** ~ 5 μM) for the 50% inhibitory effect. On the other hand, all the analogues displayed higher IC_{50} values than those of compounds **26** and **28**.

Table 4. Cytotoxicity assessment and (EC_{50} μM) evaluation of the compounds on the growth of mouse fibroblast NIH3T3 cells and human oral epithelial primary cells.

Cmpds	EC_{50} (μM)	
	NIH3T3 cells	Human Primary Oral Epithelial Cells[a]
5b	0.3	NT
5c	0.15	NT
5d	0.1	NT
5f	45	NT
5g	5	NT
5h	6	45
5i	0.45	45
5j	6	NT
5k	0.6	45
5l	6	NT

[a]Cell viability was measured by the Neutral Red Uptake (NRU) test; all compounds were tested at increasing concentrations ranging from 0.1 to 120 μM; SD, < 5%; NT, Not Tested.

Additionally, the cytotoxic effects of three selected compounds (**5h**, **5i**, and **5k**) were investigated on the growth of human primary oral epithelial cells. All the compounds produced promising results with IC_{50} values of 45 μM. Of note, these three compounds were also tested on the keratinising buccal mucosa tumour cell line TR146, and they all produced considerably lower IC_{50} values in comparison with the primary cells of the buccal mucosa (Table 2, TR146: **5h** = 1.5 μM, 30-fold; **5i** = 0.88 μM, 51-fold; **5k** = 4.5 μM, 10-fold), thus indicating quite a wide safety window.

Table 5. Cytotoxicity assessment and IC_{50} (nM) value determination of the compounds on the growth of a non-small lung tumour cell line (A549), two ovarian tumour cell lines (A2780 and A2780AD) and two cervical tumour cell lines (HeLa and HeLaβ3).

Cmpd	**IC_{50} (nM)**[a]						
	A549	**A2780**	**A2780AD**	**R/S**	**HeLa**	**HeLaβ3**	**R/S**
Podophyllotoxin	12 ± 1	15 ± 2	20 ± 2	1.33	17 ± 1	14 ± 1	0.82
5h	1380 ± 472	1031 ± 71	1213 ± 81	1.18	921 ± 265	661 ± 54	0.72
5i	774 ± 251	600 ± 115	399 ± 50	0.67	469 ± 64	331 ± 104	0.71
5k	6147 ± 305						

[a]IC_{50} values were determined utilizing the MTT assay on A549, A2780 and its P-gp overexpressing counterpart A2780AD, HeLa and HeLaβ3 cell lines (overexpressing the tubulin β3 isotype, which is related to a specific mechanism of resistance for some microtubule-targeting agents). Cells were treated with increasing concentrations of each compound for 48 h. Data represent the mean ± SD of three independent experiments. R/S is the ratio between a resistant or a mutated cell line.

We also tested an additional panel of cell lines (ovarian and HeLa), some of them carrying general (i.e. Pgp overexpression) or specific (i.e. β3 tubulin isotype overexpression) mechanisms of resistance compared to their wild-type counterparts (Table 5). As observed from the IC_{50} values, the compounds are as potent as the reference ligand, podophyllotoxin, with compound **5i**, deemed the most potent from this series. On the other hand, **5h**, as well as

5i, can bypass the specific βIII tubulin resistance. Moreover, **5i** is not a substrate of Pgp as the IC_{50} values obtained in the A2780 cell line was similar to those in the A2780AD cell line which over expresses this pump. We can therefore hypothesise that **5i** is not affected by this mechanism of resistance in cancer cells.

2.7.2. Mutagenic effects of the selected compounds

As an additional profiling step, we determined the mutagenic effects of two of the best performing compounds (**5i** and **5k**) in the *Salmonella typhimurium* strains, TA98 and TA100. The Ames test is performed to detect any potential mutagenicity risks at the early stages of drug development. Although the assay can be executed with/without the rat liver fraction, S9, the latter condition is a more in-depth analysis to assess the potential mutagenicity risks resulting from the metabolites of the compounds. Interestingly, after applying both the experimental conditions, no mutagenic effects were observed for both the compounds over the tested concentration range (0.3-60 μM).

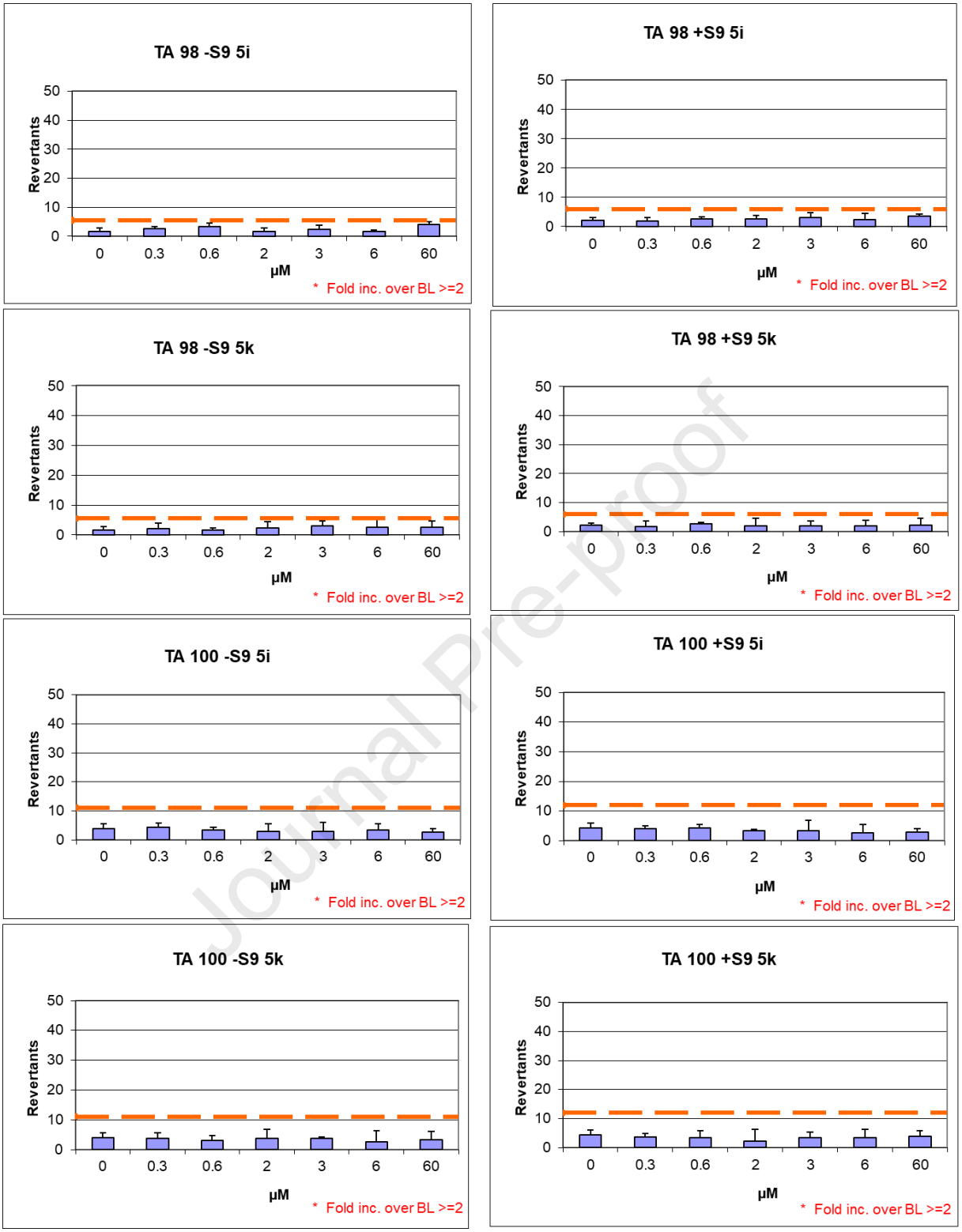

Figure 12. Ames tests performed on *S. Typhimurium* TA98 and TA100 strains for compounds **5i** and **5k**.

2.8. Autophagy studies of the selected compounds on SCC4, HL-60, and HeLa cell lines

To gain insights into the autophagy modulation profile exerted by the most potent pro-apoptotic analogues, and due to a dynamic nature and complex mechanism of autophagy, we carried out a series of independent assays in different cell lines before drawing any conclusions. Autophagic flux is frequently monitored through the conversion of LC3I to LC3II by immunoblotting, accumulation of p62 and fluorescence microscopy [2,60]. We used different approaches to determine the autophagy inhibitory potential of our lead compounds in solid and haematological tumour cell lines.

Furthermore, since **5i** and **5k** compounds were designed as MTAs, acetylated-tubulin levels were also measured, and the strongest reduction was observed with compound **5i**. Interestingly, the acetylation of tubulin is required for autophagosome formation and is correlated to the movement with dynein before fusion with lysosomes [5]. Its reduction blocks the autophagosome/lysosome assembly, an early (and necessary) event in autophagic flux.

Five compounds (**5h**, **5i**, **5k, 26** and **29**) were firstly tested on the OSCC cell line SCC4 to evaluate their activity as autophagy modulators (Figure 13). Their effects on both basal and starvation-induced autophagy were characterised. For starvation-induced autophagy, cells were treated with Earle's Balanced Salts (EBSS) medium for 30 minutes before treating the cells with a 10 μM concentration of each compound [61]. **1a** (CQ) at 10 μM was used as a positive control for autophagy inhibition and GAPDH served as a loading control [2,7,62]. Cells were treated for 3 h and the expression levels of LC3I/II were evaluated by Western Blot analysis. GAPDH served as the loading control. As expected, a significant increase in the LC3II/LC3I ratio was observed in cells treated with **1a** (CQ) in the presence/absence of EBSS due to the inhibition of autophagic flux at the very late stage, thereby resulting in the block of LC3II turnover [60]. Interestingly, a significant increase in the LC3II/LC3I ratio was also observed in cells treated with the compounds **5k** and **5i** under basal conditions and a

further elevation was found under the starved conditions. This comparable profile of **1a** (CQ) with **5i** and **5k** suggests the potent autophagy flux inhibitory nature of these two new analogues. However, compounds **26**, **5h** and **29** also elicited an increase in the levels of LC3II/LC3I in both basal and starved conditions but to a minor extent (Figure 13, B).

Taken together these results suggest that the five compounds enhance the expression of LC3II protein in SCC4 cells, indicating that they exhibit autophagy modulatory properties. Moreover, a similar profile of autophagic protein expression in cells treated with the compounds **5k** and **5i** compared to **1a** (CQ) indicate that these two novel compounds could behave as potent autophagic flux inhibitors. To further investigate the inhibition of the autophagic flux induced by **5i** or **5k**, SCC4 cells were then treated, under basal conditions, with both compounds at 10 μM for 24 h. As reported in Figure 13, **5i** and **5k** decrease Ulk1 protein levels and induce Ulk1 phosphorylation on Ser757, thus supporting the conclusion that these compounds inhibit the autophagy process [63,64]. Furthermore, since ATG7 and ATG3 account for lipid modification of LC3, switching inactive LC3I to active LC3II, the upregulation of ATG7, accompanied with the increase in the ratio of LC3II/LC3I, is again suggestive of a block of the autophagic flux [65]. The p62 protein binds to ubiquitinated proteins, delivering them via membrane-bound LC3 to the phagophore for subsequent degradation, and then p62 is degraded through autolysosomes. Conventionally p62 accumulation has been identified as a general marker of reduced autophagic flux. Noticeably, the levels of p62 are increased by treatment with **5i** and **5k** [66]. The block in autophagic flux is probably an early event, as suggested by the observed reduction of acetylation of tubulin (Figure 3, C). Tubulin acetylation increases both in labile and stable microtubules and it is required to allow the autophagy process [67]. Treatment with **5i** and **5k** induced a reduction of acetylated-tubulin levels, leading to the impairment of autophagy. This observation is also in line with the MT-destabilising effect of these compounds.

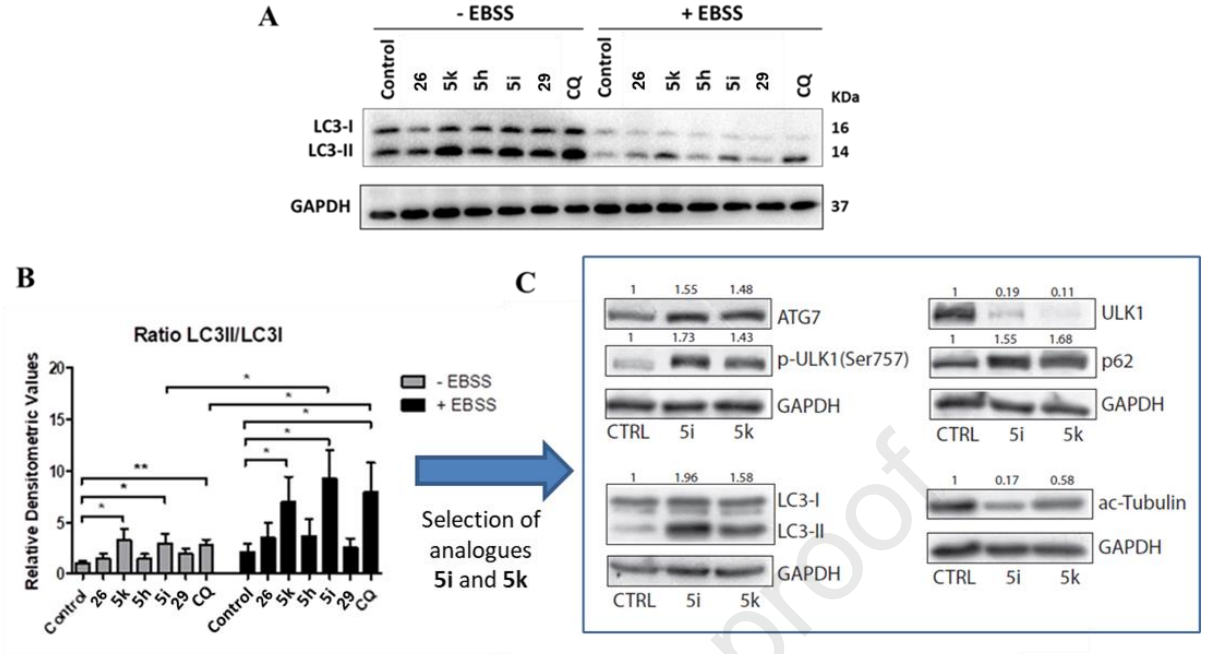

Figure 13. Immunoblot analysis of key proteins of the autophagic machinery in SCC4 cells to determine the autophagy modulatory activity of compounds **26**, **5k**, **5h**, **5i**, **29**. (**A**) Cells were pre-incubated with or without EBSS (Earle's Balanced Salts) medium for 30 min before adding the compounds (10 μM). CQ (10 μM) was used as a positive control for autophagy inhibition. Cells were harvested after 3 h and the expression levels of LC3I/II were assessed by Western Blot analysis. GAPDH served as the loading control. (**B**) Densitometric analysis of LC3I and LC3II bands was performed using ImageLab software and values represent the mean ± S.E.M. of four independent experiments. Statistical analysis was performed using an unpaired one-tailed t-test. $^{**}p \leq 0.01$, $^{*}p \leq 0.05$. (**C**) The expression level of autophagy-related proteins in SCC4 cell line treated with **5i** and **5k** for 24 h. Densitometric analyses are reported as normalized ratio/CTRL (vehicle) values and were calculated with ImageLab software.

To further expand the applicability of this new class of compounds, their ability to modulate autophagic flux was investigated in a representative leukaemic HL-60 cell line by comparing the amount of LC3II both in the presence and in absence of **1a** (Figure 14) [66]. HL-60 cells were treated in full medium with the selected compounds (**5h**, **5i**, **5k**, **5l** and **26** and **28**) and accumulation of LC3II was measured by immunoblot. Treatment with the tested compounds resulted in an increase in LC3II compared to basal conditions, with higher levels observed when the compounds were used in combination with **1a**. These data suggest that the tested compounds also induce the accumulation of autophagosomes in HL-60 cells. Accordingly,

levels of p62 were significantly increased in HL-60 cells treated with the test compounds compared with vehicle-treated cells confirming that these compounds are responsible for autophagosome accumulation. Since both the accumulation of p62 and LC3II occur when autophagy is inhibited,[60] these results further support that **5k** and **5i** likely act as potent autophagy inhibitors.

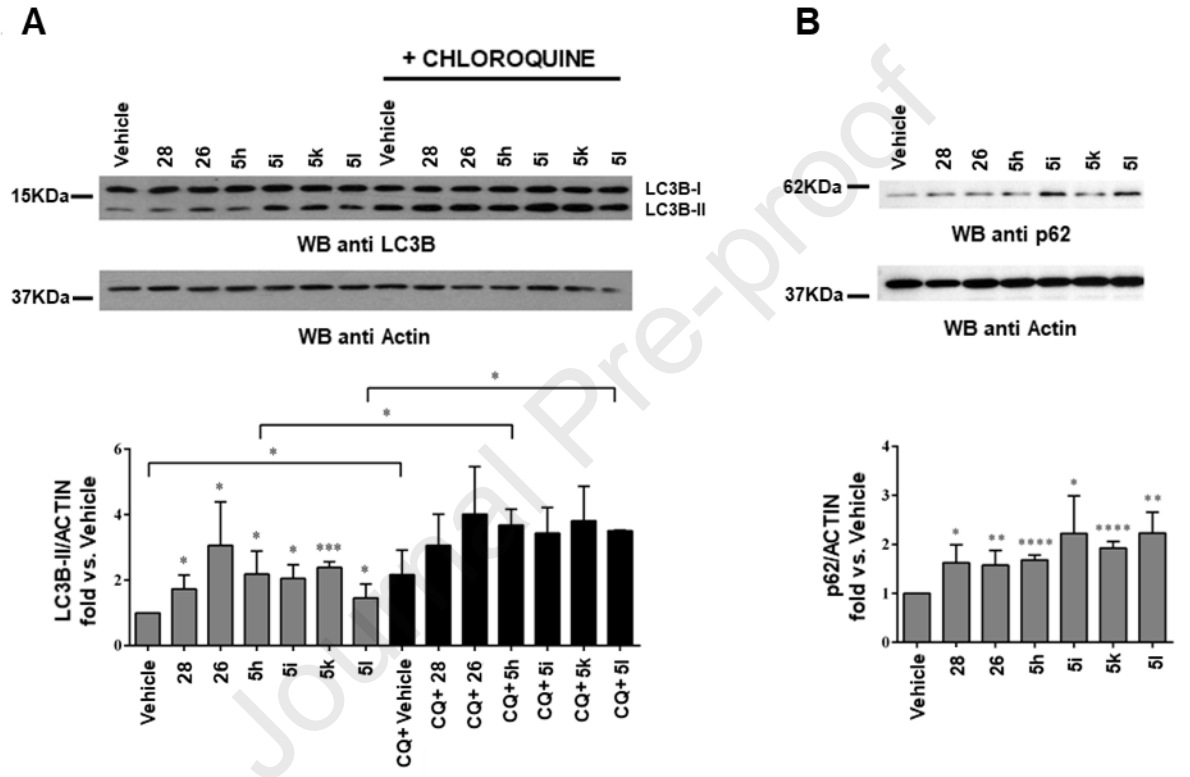

Figure 14. Immunoblot analysis of LC3B-II (A) and p62 (B) levels in HL-60 cells treated with compounds **5h**, **5i**, **5k**, **5l** and reference compounds **26** and **28** (10 μM) or DMSO (vehicle), in presence or absence of 40 μM chloroquine (CQ) for 1 h and 45 min. Control immunoblot with an anti-actin antibody of the same filters are shown. The histograms show the quantification by densitometric analysis of LC3B-II and p62 amount relative to actin. Data are presented as mean values ± SD taking the vehicle sample as 1 (n = 4). Two way Anova and unpaired T-test * $p \leq 0.05$, ** $p \leq 0.01$, ***$p \leq 0.001$, ****$p \leq 0.0001$.

To unveil the detailed mechanistic effect of the two compounds **5i** and **5k** on autophagic flux, immunofluorescence assays were also performed under both the basal and stimulated autophagy conditions in human cervical carcinoma HeLa cells.

A lysotracker staining assay on living HeLa cells was performed to check the effect of the compounds on the lysosomal pH (Figure 15). Hela cells were treated with the two compounds (**5i** and **5k** at 10 μM) or with known autophagy inhibitor, BafilomycinA1 (BafA1, 300 nM) for 3 h and then incubated with 75 nM Lysotracker red. Cells were imaged with a spinning disc microscope equipped with a stage incubator (37 °C, 5% CO_2). However, the two compounds did not markedly alter lysosomal pH and lysotracker staining is bright and visible in the treated cells. As expected, BafA1 treated cells did not show any punctate staining. **5k** induced general cell morphological changes (roundish cells) that impair a clear visualisation of the lysotracker positive compartment while **5i** treatment induced enlargement of the lysotracker positive compartment.

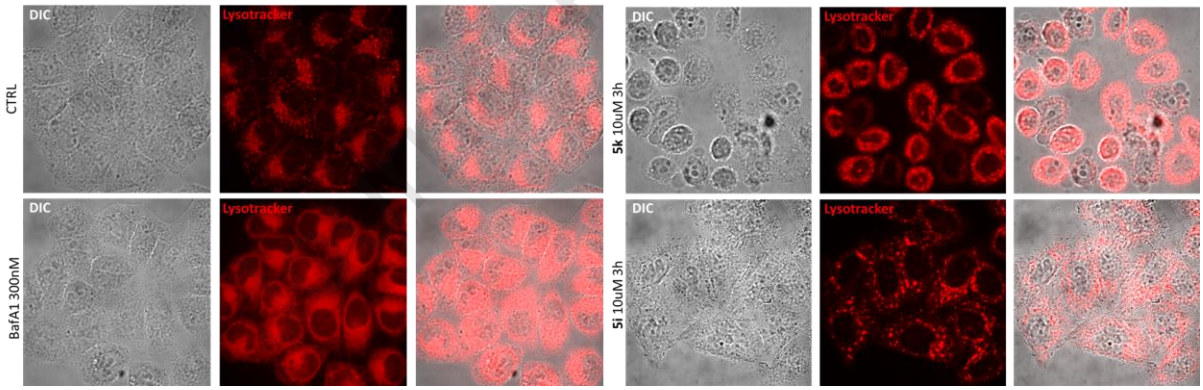

Figure 15. Hela cells were treated with the two compounds (**5i** and **5k** at 10 μM) or with BafA1 (300 nM) for 3 h and then incubated with 75 nM Lysotracker red, followed by capturing the image with a spinning disc microscope equipped with a stage incubator (37 °C, 5% CO_2).

Following on from this, an immunofluorescence study on fixed HeLa cells was performed to measure the effect of the two compounds on autophagy and autophagosome-lysosome fusion. The cells, treated with 1 and 10 μM of **5k** and **5i** in the growth medium, displayed a clear increase in the number of autophagosomes compared to the untreated cells (Figure 16). 1 μM

of **5i** and **5k** inhibited the autophagosome-lysosome fusion as there was no colocalisation between LC3 and LAMP1. 10 μM of **5i** and **5k** inhibited autophagosome degradation (as Baf1 does) as there was colocalisation between LC3 and LAMP1.

Cells treated with **5i** in Hanks' Balanced Salt Solution (HBSS) displayed a clear increase in the number of autophagosomes compared to untreated cells both at 1 and at 10 μM (Figure 17). At both the tested concentrations, **5i** inhibited the autophagosome-lysosome fusion as there was no colocalisation between LC3 and LAMP1. Cells treated with **5k** in HBSS displayed a clear increase in the number of autophagosomes compared to untreated cells only at 10 μM. Only at this concentration, **5k** inhibits autophagosome-lysosome fusion as there is no colocalisation between LC3 and LAMP1. The combined treatment (HBSS+**5k** and HBSS+**5i**) at 10 μM highlight an impaired fusion between autophagosomes and lysosomes (colocalisation that, as expected, is present in BafA1 cells). Autophagy flux is apparently normal in cells treated with 1 μM of HBSS+**5k** but still impaired in cells treated with HBSS+**5i** at the same concentrations, suggesting a higher potency of **5i** compared to **5k**.

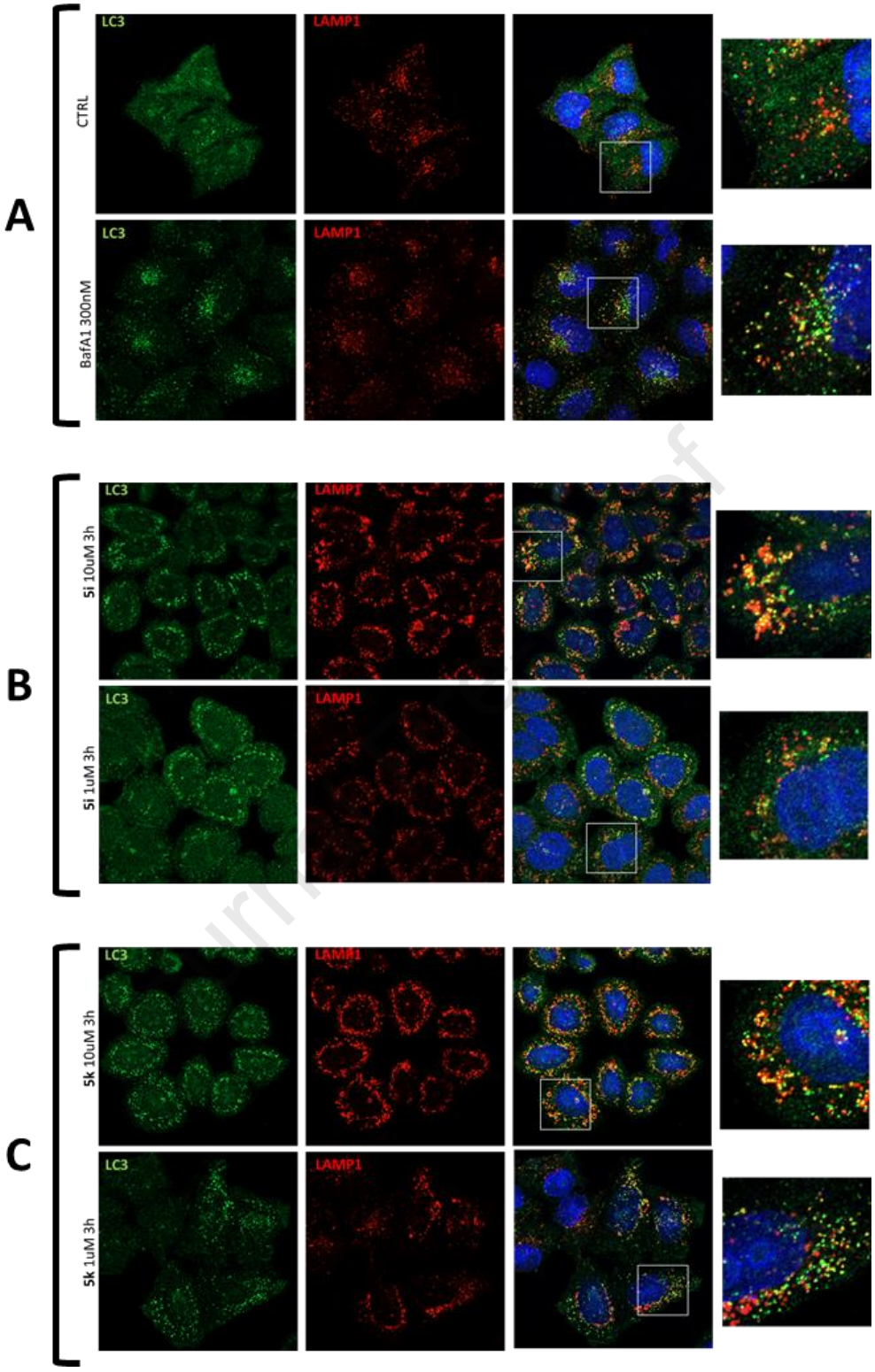

Figure 16. Hela cells were treated (**A**) in the growth medium with BafA1 (300 nM) (**B**) **5i** (**C**) **5k** at 1 and 10 μM for 3 h. Cells were then fixed in ice-cold methanol and processed for immunofluorescence with an anti-LC3 antibody (Novusbio 2220) to stain the autophagosomes and an anti-LAMP1 antibody (HybridomaBank H4A3) and imaged by laser scanning confocal microscopy (LSCM)

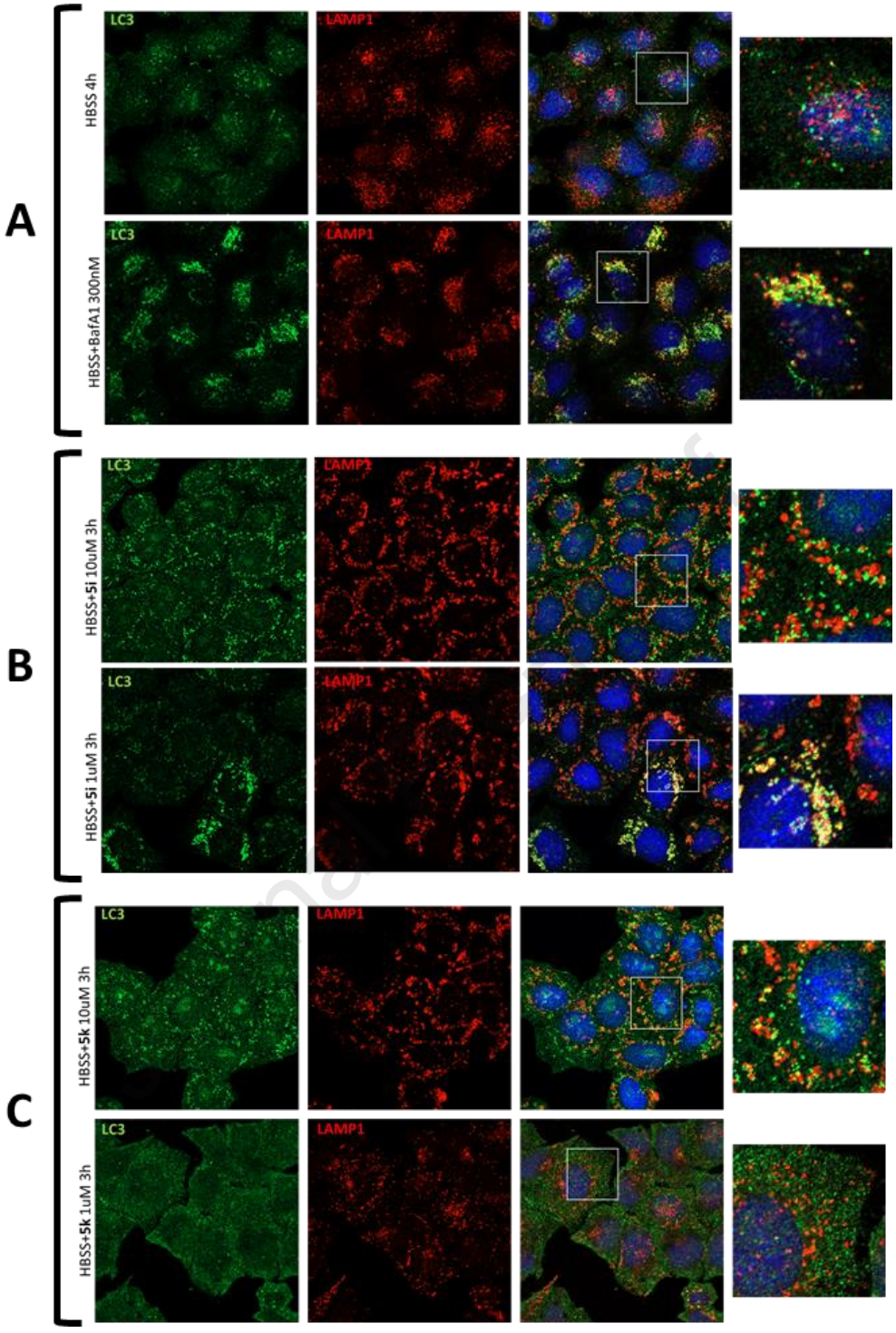

Figure 17. Hela cells were treated (**A**) in HBSS medium with BafA1 (300 nM) (**B**) **5i** (**C**) **5k** at 1 and 10 μM for 3 h. Cells were then fixed in ice-cold methanol and processed for immunofluorescence with an anti-LC3 antibody (Novusbio 2220) to stain the autophagosomes and an anti-LAMP1 antibody (HybridomaBank H4A3) and imaged by LSCM.

Cells treated with **5i** and **5k** (10 μM) displayed a clear fragmentation of the Golgi complex (Figure 18). 10 μM of **5k** induced cell rounding and general reassembly of the actin

cytoskeleton, whereas **5i** induced an increase in actin stress fibres compared to untreated and BafA1-treated cells. Cells treated with 1 μM **5k** showed normal morphology of the Golgi complex and the actin cytoskeleton, whereas **5i** showed Golgi fragmentation and actin stress fibres.

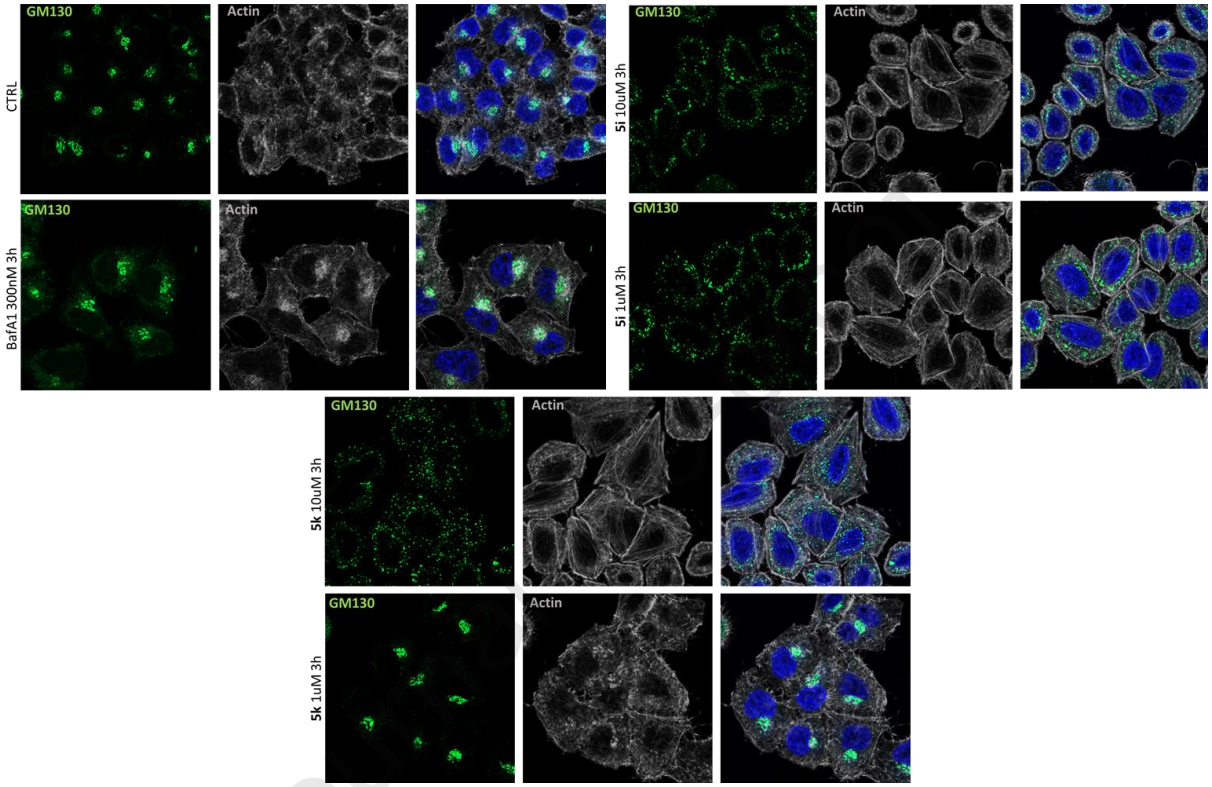

Figure 18. Hela cells were treated with the compounds **5i** and **5k** (at 10 μM and 1 μM) and with BafA1 (300nM) for 3 h in the growth medium. Cells were then fixed in 4% PFA and processed for immunofluorescence with an anti-GM130 antibody to stain the Golgi complex and an AF647-Phalloidin (LifeTechnologies) to stain the actin cytoskeleton and imaged by LSCM.

In conclusion, both the compounds **5i** and **5k** were able to impair autophagy flux by blocking the autophagosome-lysosome fusion and behaved as late-stage autophagy inhibitors.

2.9. Selected analogues inhibit Erk1/2 and NF-κB basal activation in the HL-60 cell line

The aberrant activation of Ras/RAF/MEK/ERK (MAPK) and NF-κB signalling drive carcinogenesis by promoting survival, proliferation, migration and resistance to apoptosis and

chemotherapy of cancer cells [68,69]. Moreover, mounting evidence indicates that aberrant activation of these signalling pathways contributes to the high basal activity of autophagy found in cancer cells [69,70]. Accordingly, a combination of autophagy inhibitors with NF-κB inhibitors or with MAPK inhibitors has emerged as a successful approach to overcome drug resistance, especially of RAS-mutated cancer where the treatment with MAPK inhibitors resulted in the further elevation of autophagic flux leading to drug tolerance [14,71].

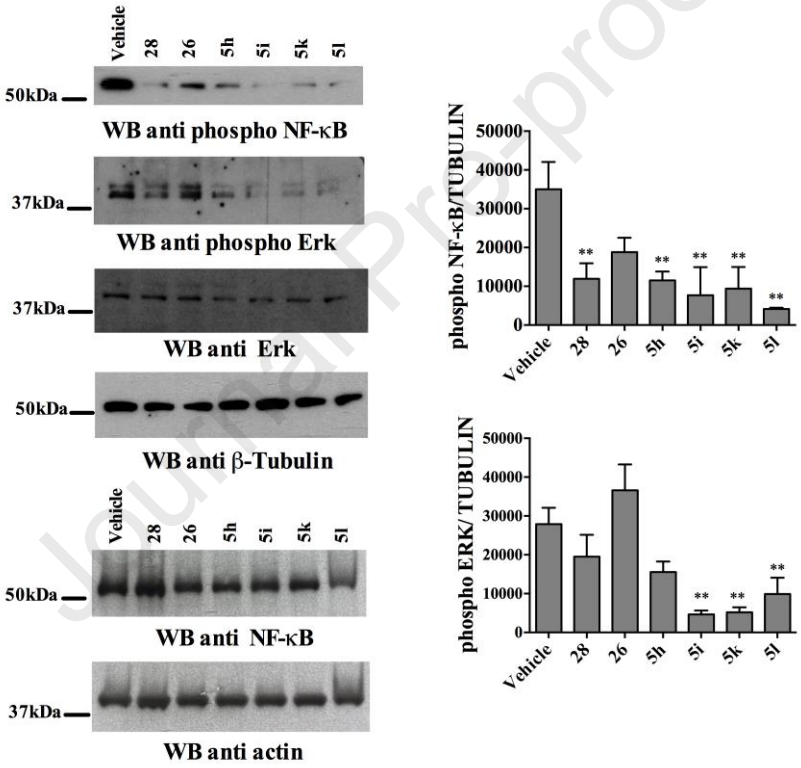

Figure 19. Immunoblot analysis of phosphorylated NF-κB and phosphorylated Erk1/2 in HL-60 cells treated with **5h**, **5i**, **5k**, **5l** and reference compounds **26** and **28** (10 μM) or DMSO (vehicle) for 2 h. Control immunoblot with anti-β-tubulin, anti-actin, anti-NFkB and anti-ERK antibody are shown. The histograms show the quantification by densitometric analysis of the levels of phospho-NF-κB or phospho-Erk1/2 relative to β-tubulin. Data are presented as mean values ± SD (n = 2). One way Anova ** $p \leq 0.01$ vs. vehicle.

Since our data demonstrate that **5h**, **5i**, **5k**, **5l** and the two reference compounds **26** and **28** act as autophagy inhibitors and promote apoptosis in HL-60 cells, an N-ras mutated acute

myelocytic leukaemia cell line, we decided to address whether these compounds affect NF-κB and Erk1/2 basal activation. Results showed (Figure 19) that all these compounds significantly reduced the constitutive phosphorylation of NF-κB when compared with the vehicle-treated sample. Interestingly, the two lead compounds, **5i** and **5k**, also efficiently abrogated Erk1/2 activation in HL-60 cells suggesting that, by targeting both autophagy and MAPK/NF-κB signalling, they could be effective against Ras-mutated cancer [70].

2.10. Physico-chemical and preliminary pharmacokinetic investigation of selected analogues

We also sought to assess the drug-like properties of the selected analogues **5h**, **5i**, and **5k**. The aqueous solubility at pH = 3 and pH = 7.4 and the chemical stability (at pH = 3) of the compounds were measured by HPLC methods (Table 6).

Table 6. Solubility and chemical stability of the selected analogues.

Cmpds	Solubility (μM)		Chemical stability (%)
	pH = 3	pH = 7.4	
5h	n.d[c]	n.d	n.d
5i	204	n.d	91
5k	271	n.d	97

[a]Solubility at 24 h; [b]Chemical stability at 36 h;
[c]n.d, not determined, not quantifiable.

As predicted, the presence of the basic amine system amended the solubility profile of the compounds in the acidic pH = 3, but none of the compounds was soluble at pH = 7.4. The solubility of **5h** at t = 0 was 99 μM but it was not stable in pH = 3 after 24 h. This may be attributed to the presence of a carbamate on the lateral chain. Interestingly, despite bearing a carbamate moiety, **5i** displayed a solubility of 204 μM at pH = 3 after 24 h and chemical stability of 91% at 36 h. **5k** demonstrated the highest solubility among the three compounds

with a value of 271 μM at pH = 3 after 24 h. The chemical stability of **5k** was almost quantitative (97% at 36 h). These results may be due to the presence of a secondary amine and ester moiety on the lateral chain that replaces the tertiary amine and the carbamate moieties of **5h** and **5i**.

*2.10.1. Preliminary in vitro metabolic studies on **5i** and **5k***

We also performed some *in vitro* studies to assess the metabolic stability of **5i** and **5k** in human liver microsomal (HLM) preparations [72]. The plot of non-metabolised compound [natural logarithm of % of recovered compound (100% at time 0 min)] as a function of incubation time exhibited a monoexponential decay relationship for both the compounds (Figure 20). The apparent decay constant (k), half-life time (t½), and intrinsic clearance (CLint) are reported in Table 7.

Table 7. Apparent decay constant (k), half-life time (t½), and intrinsic clearance (CL_{int}) values of **5i** and **5k**.

Cmpds	k (min^{-1})	t½ (min)	CL_{int}
5i	0.022	30.8	55
5k	0.0076	91.2	19

The CLint values indicate that **5i** is a preferred substrate for the xenobiotic metabolised system present in the HLM. On the contrary, **5k** with a lower CLint value indicates higher metabolic stability than **5i**. However, both the drugs can be categorised as medium clearance compounds.[73] Moreover, both compounds were not metabolised when incubated at 37 °C for 60 min with boiled microsomes or in presence of HLM but without the NADPH-GS.

Taken together these results clearly indicate that CYP(s) are responsible for the **5i** and **5k** metabolism. From *in silico* analysis with MetaSite, the hydroxylation of naphthalene moiety and the N-demethylation of *N*-methylpyperazine appear to be the two major CYP-dependent reactions towards **5i** with a similar probability score. On the contrary, **5k** seems to be metabolised only by the introduction of a hydroxyl moiety in the naphthalene system.

In conclusion, the results suggest that both compounds possess favourable pharmacokinetic properties, at least concerning their interaction with the phase I enzyme system.

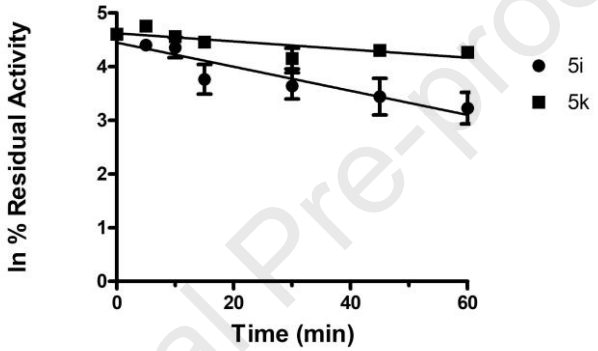

Figure 20. The plot of non-metabolized compound [natural logarithm of % of recovered compound (100% at time 0 min)] as a function of incubation time expressing a monoexponential decay relationship for both the compounds.

Conclusion

In summary, we have developed and explored the biological properties of a promising new class of multifunctional anti-tumour agents (compounds **5a-l**) endowed with both pro-apoptotic and anti-autophagic properties. The structural modifications made to the small molecules developed here were performed by an amalgamation of key features of tricyclic pro-apoptotic compounds (**26-29**) with **1a**. Using this approach, we sought to embed key anti-autophagic features while retaining the pro-apoptotic activity of the parent compounds. We assessed the ability of the new compounds to inhibit tumour cell proliferation and to induce apoptosis in a wide variety of tumour cell lines, including multidrug-resistant cell lines.

Initial examination of their pro-apoptotic effects in HL-60 cells allowed the selection of the best candidates to be further tested in various OSCC cell lines with promising results. Mutagenic safety (Ames test), and selectivity tests also allowed us to define a safety window for the best hybrids of the series. Additionally, promising pharmacokinetic properties have been determined. Finally, selected compounds (**5h**, **5i** and **5k**) were investigated, along with reference compounds **26** and **28**, for their effect on autophagic processes in SCC4, HL-60 and Hela cell lines. Quantification of LC3II/LC3I and p62 expression levels under both basal and starvation-induced conditions was evaluated using **1a** as a positive control. This revealed the CQ-like inhibitory mode of action of the tested hybrids **5i** and **5k** on autophagy and, in line with their MT-destabilisation properties, we demonstrated that the observed inhibition of autophagic flux could be amplified by a decrease in the levels of acetylated tubulin. Furthermore, immunofluorescence analysis of LC3 and LAMP1 colocalization in HeLa cells suggested that both novel compounds behave as late-stage autophagy inhibitors by impairing autophagosome-lysosome fusion. It is worth noting that although the MT binding site partially overlaps with that of colchicine, the compounds behave differently from colchicine itself, being potent inhibitors of autophagy flux. The data confirm the therapeutic potential for the two compounds **5i** and **5k**, as novel anti-cancer agents which display both anti-autophagic and potent pro-apoptotic properties.

Experimental section

General Remarks

All chemicals and reagents were purchased from commercial sources and used without any further purification, unless otherwise specified. Reaction progress was monitored by thin-layer chromatography (TLC), carried out on silica (60 F254) or alumina (60 F254, basic) gel plates with detection by UV and the products were purified by using either silica (60 M,

0.040-0.063 μm) or alumina (90, standardised) column chromatography. ^{1}H and ^{13}C NMR spectra were recorded in the indicated deuterated solvent on a Varian 300 MHz or a Bruker 400 MHz spectrometer by using the residual signal of the deuterated solvent as internal standard. Splitting patterns are indicated by s (singlet), d (doublet), dd (doublet of doublets), t (triplet), q (quartet), m (multiplet), and br (broad); chemical shifts (δ) are described in parts per million (ppm) and coupling constants (*J*) in Hertz (Hz). ESI-MS spectra were performed by an Agilent 1100 Series LC/MSD spectrometer. HRESI-MS was carried out by a Thermo Finningan LCQ Deca XP Max ion-trap mass spectrometer equipped with Xcalibur software, operated in positive ion mode. Yields refer to purified products and are not optimised. All moisture-sensitive reactions were performed under nitrogen atmosphere using oven-dried glassware and freshly distilled anhydrous solvents.

*General procedure for the synthesis of compounds **13a-b***. A solution of methanesulfonyl chloride (1.29 mmol) in dry DCM (10 mL) was added dropwise to a solution of **12a** (1.00 mmol) and dry TEA (1.50 mmol) in dry DCM (10 mL) at 0 °C. The reaction mixture was allowed to reach 25 °C and stirred for 16 h. The reaction mixture was diluted with DCM, washed with a saturated solution of $NaHCO_3$ and brine, dried over anhydrous magnesium sulfate, filtered and concentrated under reduced pressure. The resulting residue was purified by silica gel column chromatography (EtOAc/petroleum ether 7:3) to provide the title compound.

*6-Nitrobenzo[d][1,3]dioxol-5-yl methanesulfonate (**13a**)*. According with the general procedure, **13a** was obtained from **12a** in 88% yield as a yellow solid. ^{1}H NMR (300 MHz, $CDCl_3$) δ: 7.56 (s, 1H), 6.99 (s, 1H), 6.18 (s, 2H), 3.36 (s, 3H). ESI-MS *m/z* 262 $[M+H]^+$.

*7-Nitro-2,3-dihydrobenzo[b][1,4]dioxin-6-yl methanesulfonate (**13b**).* According with the general procedure, **13b** was obtained was obtained from **12b** in 78% yield as a yellow solid.

^{1}H NMR (300 MHz, $CDCl_3$) δ: 7.71 (s, 1H), 7.04 (s, 1H), 4.41-4.32 (m, 4H), 3.35 (s, 3H). ESI-MS *m/z* 276 $[M+H]^+$.

*General procedure for the synthesis of compounds **14a-b***. A mixture of the nitro derivative **13a-b** (1.00 mmol) and tin (II) chloride (5.00 mmol) in ethanol (20 mL) was refluxed at 80 °C under nitrogen pressure for 12 h. The reaction mixture was allowed to cool to 25 °C and poured into ice water. A saturated solution of $NaHCO_3$ was added to the aqueous system to adjust the pH = 8, followed by the extraction with EtOAc (3 x 15 mL). The combined organic layers were washed with brine, dried over anhydrous sodium sulfate, filtered, and concentrated under reduced pressure. The residue was purified by silica gel column chromatography (petroleum ether/EtOAc 1:1) to afford the target compounds.

*6-Aminobenzo[d][1,3]dioxol-5-yl methanesulfonate (**14a**)*. According with the general procedure, **14a** was obtained from **13a** in 70% yield as a brown solid. ^{1}H NMR (300 MHz, $CDCl_3$) δ: 6.78 (s, 1H), 6.38 (s, 1H), 5.92 (s, 2H), 3.77 (brs, 2H), 3.18 (s, 3H). ESI-MS *m/z* 232 $[M+H]^+$.

*7-Amino-2,3-dihydrobenzo[b][1,4]dioxin-6-yl methanesulfonate (**14b**)*. According with the general procedure, **14b** was obtained from **13b** in 78% yield as a pale yellow solid. ^{1}H NMR (300 MHz, $CDCl_3$) δ: 6.80 (s, 1H), 6.36 (s, 1H), 4.26-4.18 (m, 4H), 3.68 (brs, 2H), 3.18 (s, 3H). ESI-MS *m/z* 246 $[M+H]^+$.

*General procedure for the synthesis of compounds **15a-b***. A solution of 2,5-dimethoxytetrahydrofuran (1.10 mmol) in acetic acid (10 mL) was added dropwise to a stirred solution of **14a-b** (1.00 mmol) in acetic acid (20 mL), and the resulting solution was refluxed at 100 °C for 30 min. Acetic acid was evaporated and the residue was diluted with EtOAc. The organic layer was washed with a saturated solution of Na_2CO_3 and brine, dried over anhydrous sodium sulfate, filtered and concentrated under reduced pressure. The residue

was purified by a silica gel column chromatography (petroleum ether/EtOAc 3:7) to afford the target compounds.

*6-(1H-Pyrrol-1-yl)benzo[d][1,3]dioxol-5-yl methanesulfonate (**15a**).* According with the general procedure, **15a** was obtained from **14a** in 60% yield as a white solid. ^{1}H NMR (300 MHz, $CDCl_3$) δ: 6.95 (s, 1H), 6.91 (t, *J* = 2.1 Hz, 2H), 6.87 (s, 1H), 6.33 (t, *J* = 2.1 Hz, 2H), 6.09 (s, 2H), 2.52 (s, 3H). ESI-MS *m/z* 282 $[M+H]^+$.

*7-(1H-Pyrrol-1-yl)-2,3-dihydrobenzo[b][1,4]dioxin-6-yl methanesulfonate (**15b**).* According with the general procedure, **15b** was obtained from **14b** in 60% yield as a white solid. ^{1}H NMR (300 MHz, $CDCl_3$) δ: 7.01 (s, 1H), 6.94 (s, 1H), 6.91 (t, *J* = 2.2 Hz, 2H), 6.33 (t, *J* = 2.2 Hz, 2H), 4.32 (s, 4H), 2.52 (s, 3H). ESI-MS *m/z* 296 $[M+H]^+$.

*General procedure for the synthesis of compounds **10c-d**.* A finely ground potassium hydroxide powder (3.00 mmol) was added into a solution of **15a-b** (1.50 mmol) in methanol (10 mL) and the resulting mixture was refluxed for 2 h. The solvent was removed under reduced pressure and the residue was acidified with a solution of 2N HCl up to pH = 3. The aqueous layer was extracted with EtOAc (3 x 10 mL) and the combined organic layers were dried over anhydrous sodium sulfate, filtered, and concentrated under reduced pressure. The residue was purified by silica gel column chromatography (100% DCM) to obtain the target compounds.

*6-(1H-Pyrrol-1-yl)benzo[d][1,3]dioxol-5-ol (**10c**).* According with the general procedure, **10c** was obtained from **15a** in 70% yield as a white solid. ^{1}H NMR (300 MHz, $CDCl_3$) δ: 6.79 (t, *J* = 2.2 Hz, 2H), 6.73 (s, 1H), 6.60 (s, 1H), 6.39 (t, *J* = 2.2 Hz, 2H), 5.98 (s, 2H), 4.99 (brs, 1H). ESI-MS *m/z* 204 $[M+H]^+$.

*7-(1H-Pyrrol-1-yl)-2,3-dihydrobenzo[b][1,4]dioxin-6-ol (**10d**).* According with the general procedure, **10d** was obtained from **15b** in 82% yield as a white solid. ^{1}H NMR (300 MHz,

$CDCl_3$) δ: 6.82 (t, *J* = 2.1 Hz, 2H), 6.80 (s, 1H), 6.58 (s, 1H), 6.36 (t, *J* = 2.1 Hz, 2H), 5.11 (brs, 1H), 4.30-4.21 (m, 4H). ESI-MS *m/z* 218 $[M+H]^+$.

*2-(Benzyloxy)-4-bromo-1-nitrobenzene (**17**).* To a solution of **16** (2.00 g, 9.22 mmol) in dry DMF (10 mL), potassium carbonate (1.91 g, 11.06 mmol) was added at 25 °C and the reaction mixture was stirred for 2 h. Then a solution of benzyl bromide (1.89 g, 11.06 mmol) in dry DMF (10 ml) was added and the reaction mixture was refluxed at 85 °C for 12 h. Water (20 mL) was added to dilute the reaction mixture, followed by the extraction with EtOAc (3 x 15 mL). The combined organic layers were washed with a saturated solution of NH_4Cl, $NaHCO_3$, and brine. The washed organic phase was dried over anhydrous sodium sulfate, filtered, and concentrated under reduced pressure. The title compound was obtained in quantitative yield as a yellow solid and it was used in the next step without any further purification. ^{1}H NMR (300 MHz, $CDCl_3$) δ: 7.95 (s, 1H), 7.56 (d, *J* = 8.8 Hz, 1H), 7.48-7.27 (m, 5H), 7.00 (d, *J* = 8.9 Hz, 1H), 5.19 (s, 2H); ESI-MS *m/z* 385.6 $[M+Br]^-$.

*General procedure for the synthesis of compounds **18**, **24**.* Palladium(II) acetate (0.06 mmol) was added to a suspension of (±)-BINAP (0.09 mmol) in 1,4-dioxane (3 mL) in a sealed tube at 25 °C and the mixture was heated at 50 °C for 30 min. After that compound **17** (0.61 mmol), the appropriate piperazine (1.83 mmol), and cesium carbonate (323 mg, 0.92 mmol) were added, sequentially, and the mixture was heated at 100 °C for 12 h. The reaction mixture was filtered over a pad of Celite®; the solvent was removed under reduced pressure, and the residue was dissolved in water, and extracted with EtOAc. The combined organic layers were dried over anhydrous sodium sulfate, filtered, and concentrated under reduced pressure. The residue was purified by an alumina gel column chromatography (petroleum ether/EtOAc 5:1) to afford the target compounds.

*1-(4-(Benzyloxy)-3-nitrophenyl)piperazine (**18**).* According with general procedure, **18** was obtained from **17** in 71% yield as an orange solid. ^{1}H NMR (400 MHz, $CDCl_3$) δ: 7.43-7.24

(m, 6H), 7.05-6.99 (m, 2H), 5.14 (s, 2H), 3.07-2.98 (m, 8H), 1.66 (s, 1H); ESI-MS *m/z* 314.0 $[M+H]^+$.

*1-(4-(4-(Benzyloxy)-3-nitrophenyl)piperazin-1-yl)ethanone (**19**).* TEA (45 μL, 0.320 mmol) was added to a solution of **18** (100 mg, 0.32 mmol) in acetic anhydride (2 mL) at 25 °C and the resulting mixture was stirred for 12 h. The solvent was removed under reduced pressure, and the residue was diluted with a saturated solution of $NaHCO_3$ and extracted with DCM. The combined organic layers were dried over anhydrous sodium sulfate, filtered, and concentrated under reduced pressure to obtain the title compound in quantitative yield as an orange oil. ^{1}H NMR (400 MHz, $CDCl_3$) δ: 7.39-7.34 (m, 6H), 7.09-6.95 (m, 2H), 5.14 (s, 2H), 3.79-3.67 (m, 2H), 3.65-3.52 (m, 2H), 3.14-2.97 (m, 4H), 2.11 (s, 3H); ESI-MS *m/z* 356.0 $[M+H]^+$, 377.9 $[M+Na]^+$.

*1-(4-(4-Hydroxy-3-nitrophenyl)piperazin-1-yl)ethanone (**20**).* Thioanisole (2.3 mL, 19.99 mmol) was added dropwise to a solution of **19** (142 mg, 0.40 mmol) in TFA (3 mL) and toluene (3 mL) at 25 °C and the reaction mixture was refluexed at 70 °C for 12 h. The solvent was removed under reduced pressure and the residue was purified by silica gel column chromatography (petroleum ether/EtOAc 20:1) to afford the title compound in 85% yield as a red solid. ^{1}H NMR (400 MHz, $CDCl_3$) δ: 10.27 (s, 1H), 7.48 (d, *J* = 2.9 Hz, 1H), 7.28 (dd, *J* = 9.2, 2.9 Hz, 1H), 7.07 (d, *J* = 9.2 Hz, 1H), 3.80-3.72 (m, 2H), 3.65-3.56 (m, 2H), 3.13-3.01 (m, 4H), 2.12 (s, 3H). Spectroscopic data are in agreement with those previosuly reported [74].

*General procedure for the synthesis of compounds **21**, **22**.* Iron powder (7.68 mmol) and calcium chloride (3.24 mmol) were added into a solution of nitro derivative (**17**,**20)** (1.21 mmol) in ethanol:water (3:1, 18 mL) at 25 °C. The reaction mixture was refluxed at 90 °C for 30 min. Then the solvent was removed under reduced pressure, the residue was dissolved in a saturated solution of $NaHCO_3$, and extracted with EtOAc (3 x 10 mL). The combined organic

layers were filtered over a pad of Celite®, dried over anhydrous sodium sulfate, filtered, and concentrated under reduced pressure. The residue was purified by silica gel column chromatography ($CHCl_3$/MeOH 20:1) to afford the target compounds.

*1-(4-(3-Amino-4-hydroxyphenyl)piperazin-1-yl)ethanone (**21**).* According with general procedure, **21** was obtained from **20** in 60% yield as a red solid. ^{1}H NMR (400 MHz, DMSO) δ: 8.39 (s, 1H), 6.47 (d, *J* = 8.4 Hz, 1H), 6.24 (d, *J* = 2.6 Hz, 1H), 5.98 (dd, *J* = 8.4, 2.6 Hz, 1H), 4.39 (s, 2H), 3.55-3.43 (m, 4H), 2.90-2.72 (m, 4H), 1.98 (s, 3H); ESI-MS *m/z* 236 $[M+H]^+$, 258 $[M+Na]^+$.

*2-(Benzyloxy)-5-bromoaniline (**22**).* According with general procedure, **22** was obtained from **17** in 54% yield as a yellow solid. ^{1}H NMR (300 MHz, $CDCl_3$) δ: 7.98 (d, *J* = 2.5 Hz, 1H), 7.58 (dd, *J* = 8.9, 2.5 Hz, 1H), 7.46-7.29 (m, 5H), 7.00 (d, *J* = 9.0 Hz, 1H), 5.22 (s, 2H); ESI-MS *m/z* 278 $[M+H]^+$.

*1-(2-(Benzyloxy)-5-bromophenyl)-1H-pyrrole (**23**).* To a solution of **22** (2.75 g, 9.89 mmol) in 1,4-dioxane (45 mL), 2,5-dimethoxytetrahydrofuran (1 mL, 9.89 mmol) and HCl (6 N, 3 mL) were added and the resulting mixture was refluxed at 100 °C for 10 min. The reaction mixture was quenched with a saturated solution of $NaHCO_3$ and the aqueous layer was extracted with EtOAc (3 x 20 mL). The combined organic layers were dried over anhydrous sodium sulfate, filtered, and concentrated under reduced pressure. The residue was purified by silica gel column chromatography (petroleum ether/EtOAc 10:1) to afford the title compound in 88% yield as a yellow solid. ^{1}H NMR (300 MHz, $CDCl_3$) δ: 7.45 (d, *J* = 2.4 Hz, 1H), 7.39-7.28 (m, 6H), 7.02 (t, *J* = 2.2 Hz, 2H), 6.93 (d, *J* = 8.8 Hz, 1H), 6.31 (t, *J* = 2.1 Hz, 2H), 5.06 (s, 2H); ESI-MS *m/z* 329.0 $[M+H]^+$.

*1-(4-(Benzyloxy)-3-(1H-pyrrol-1-yl)phenyl)-4-methylpiperazine (**24**).* According with general procedure, **24** was obtained from **23** in presence of *N*-methylpiperazine (1.83 mmol) in 71% yield as an orange oil. ^{1}H NMR (300 MHz, $CDCl_3$) δ: 7.39-7.26 (m, 5H), 7.11 (t, *J* = 2.2 Hz,

2H), 7.00 (s, 1H), 6.97 (d, *J* = 2.9 Hz, 1H), 6.81 (dd, *J* = 8.9, 3.0 Hz, 1H), 6.38 (t, *J* = 2.2 Hz, 2H), 4.95 (s, 2H), 3.24-3.12 (m, 4H), 2.67-2.54 (m, 4H), 2.39 (s, 3H); ESI-MS *m/z* 348.0 $[M+H]^+$.

1-(4-(4-Hydroxy-3-(1H-pyrrol-1-yl)phenyl)piperazin-1-yl)ethanone ***(10e)***. The title compound was obtained from **21** following the synthetic procedure described for **10a** in 50% yield as a purple solid after purification by an alumina gel column chromatography ($CHCl_3$/MeOH 50:1). ^{1}H NMR (400 MHz, $CDCl_3$) δ: 7.24 (s, 1H), 6.96 (t, *J* = 10.0 Hz, 1H), 6.88 (d, *J* = 17.4 Hz, 3H), 6.37 (s, 2H), 5.18 (s, 1H), 3.77 (s, 2H), 3.62 (s, 2H), 3.18-2.95 (m, 4H), 2.12 (s, 3H); ESI-MS *m/z* 286.0 $[M+H]^+$, 308 $[M+Na]^+$.

4-(4-Methylpiperazin-1-yl)-2-(1H-pyrrol-1-yl)phenol ***(10f)***. To a solution of **24** (500 mg, 1.44 mmol) in MeOH (41 mL), a catalytic amount of 10% Pd-C was added under nitrogen atmosphere followed by a careful replacement by hydrogen atmosphere, and the resulting reaction mixture was stirred at 25 °C for 2 h. The solvent was removed the residue was diluted with EtOAc, and the catalyst was filtered over a pad of Celite®. The title compound was obtained without any purification in quantitative yield as a red solid. ^{1}H NMR (300 MHz, MeOD) δ: 7.00 (t, 2H), 6.96-6.75 (m, 3H), 6.19 (t, 2H), 3.24-3.11 (m, 4H), 2.90 (t, *J* = 5.0 Hz, 4H), 2.59-2.52 (m, 3H); ESI-MS *m/z* 258 $[M+H]^+$.

General procedure for the synthesis of compounds ***25a-d***. Potassium carbonate (1.50 mmol) was added to a solution of **10a-e** (1.00 mmol) in dry DMF (20 mL) at 25 °C and stirred for 10 min. A solution of **8a** (1.20 mmol) in dry DMF (5 mL) was added dropwise and the reaction mixture was stirred at 25 °C for 12 h. The solvent was removed under reduced pressure and the residue was diluted with DCM. The organic layer was washed with brine, dried over anhydrous sodium sulfate, and concentrated under reduced pressure. The residue was purified by silica gel column chromatography (*n*-hexane/EtOAc 9:1) to afford the target compounds.

*(±)-Methyl 2-(4-chloro-2-(1H-pyrrol-1-yl)phenoxy)-2-(naphthalen-1-yl)acetate (**25a**).* According with general procedure, **25a** was obtained starting form **10a** as a pale-yellow oil in 89% yield. ^{1}H NMR (300 MHz, $CDCl_3$) δ: 8.19 (d, *J* = 7.1 Hz, 1H), 7.90-7.84 (m, 2H), 7.61-7.50 (m, 3H), 7.44 (t, *J* = 7.9 Hz, 1H), 7.33 (d, *J* = 2.6 Hz, 1H), 7.12-7.09 (m, 3H), 6.95 (d, *J* = 8.9 Hz, 1H), 6.34 (t, *J* = 2.4 Hz, 2H), 6.06 (s, 1H), 3.67 (s, 3H). ESI-MS *m/z*: 392 $[M+H]^+$.

*(±)-Methyl 2-(4-methyl-2-(1H-pyrrol-1-yl)phenoxy)-2-(naphthalen-1-yl)acetate (**25b**).* According with general procedure, **25b** was obtained starting form **10b** as a colorless oil in 85% yield. ^{1}H NMR (300 MHz, $CDCl_3$) δ: 8.22 (d, *J* = 7.7 Hz, 1H), 7.87 (t, *J* = 8.7 Hz, 2H), 7.62 (d, *J* = 7.1 Hz, 1H), 7.59-7.48 (m, 2H), 7.44 (t, *J* = 7.7 Hz, 1H), 7.15 (s, 1H), 7.11 (t, *J* = 2.2 Hz, 2H), 6.94 (m, 2H), 6.32 (t, *J* = 2.2 Hz, 2H), 6.04 (s, 1H), 3.66 (s, 3H), 2.31 (s, 3H). ESI-MS *m/z*: 372 $[M+H]^+$.

*(±)-Methyl 2-((6-(1H-pyrrol-1-yl)benzo[d][1,3]dioxol-5-yl)oxy)-2-(naphthalen-1-yl) acetate (**25c**).* According with general procedure, **25c** was obtained starting form **10c** as colorless oil in 92% yield. ^{1}H NMR (400 MHz, $CDCl_3$) δ: 8.16 (d, *J* = 7.6 Hz, 1H), 7.85 (m, 2H), 7.55-7.48 (m, 3H), 7.42 (m, 1H), 6.98 (t, *J* = 2.2 Hz, 2H), 6.81 (s, 1H), 6.63 (s, 1H), 6.30 (t, *J* = 2.2 Hz, 2H), 5.94 (m, 2H), 5.69 (s, 1H), 3.63 (s, 3H). ESI-MS *m/z*: 402 $[M+H]^+$.

*(±)-Methyl 2-((7-(1H-pyrrol-1-yl)-2,3-dihydrobenzo[b][1,4]dioxin-6-yl)oxy)-2-(naphthalen-1-yl)acetate (**25d**).* According with general procedure, **25d** was obtained starting form **10d** as a white solid in 80% yield. ^{1}H NMR (300 MHz, $CDCl_3$) δ: 8.17 (d, *J* = 8.0 Hz, 1H), 7.88-7.83 (m, 2H), 7.59-7.41 (m, 4H), 7.02 (t, *J* = 2.1 Hz, 2H), 6.86 (s, 1H), 6.60 (s, 1H), 6.29 (t, *J* = 2.2 Hz, 2H), 5.88 (s, 1H), 4.22 (s, 4H), 3.65 (s, 3H). ESI-MS *m/z*: 416 $[M+H]^+$.

*(±)-Ethyl 2-(4-(4-acetylpiperazin-1-yl)-2-(1H-pyrrol-1-yl)phenoxy)-2-(naphthalen-1-yl)acetate (**25e**).* Sodium hydride (18 mg, 0.77 mmol) was added to a solution of **10e** (200 mg, 0.70 mmol) in dry THF (5 mL) at 25 °C and stirred for 1 h. A solution of **8b** (226 mg, 0.77 mmol) in dry THF (5 mL) was added dropwise and the reaction mixture was stirred for

another 12 h. The solvent was removed under reduced pressure; and the residue was dissolved in DCM and washed with brine, dried over anhydrous sodium sulfate, filtered, and concentrated under reduced pressure. The residue was purified by a silica gel column chromatography ($CHCl_3$/MeOH 30:1) to afford the title compound in quantitative yield as a yellow oil. ^{1}H NMR (400 MHz, $CDCl_3$) δ: 8.19 (d, *J* = 8.1 Hz, 1H), 7.85-7.77 (m, 2H), 7.57 (d, *J* = 7.0 Hz, 1H), 7.52-7.43 (m, 2H), 7.39 (t, *J* = 7.7 Hz, 1H), 7.09 (t, *J* = 2.0 Hz, 2H), 6.92 (t, *J* = 8.3 Hz, 1H), 6.87 (d, *J* = 2.7 Hz, 1H), 6.65 (dd, *J* = 8.9, 2.7 Hz, 1H), 6.29 (t, *J* = 2.0 Hz, 2H), 5.91 (s, 1H), 4.12-4.05 (m, 2H), 3.76-3.67 (m, 2H), 3.58-3.50 (m, 2H), 3.03 (dd, *J* = 10.1, 5.3 Hz, 4H), 2.09 (s, 3H), 1.08 (t, *J* = 7.1 Hz, 3H). ESI-MS *m/z*: 498 $[M+H]^+$.

*General procedure for the synthesis of compounds **7a-e***. A solution of sodium hydroxide (5% aqueous, 10 mL) was added dropwise into a solution of **25a-e** (1.00 mmol) in methanol (20 mL) at 25 °C for 2 h. The solvent was removed under reduced pressure and the residue was diluted with water. A solution of HCl (4N) was added dropwise in order to adjust the pH to 3 and the precipitate was extracted with EtOAc (3 x 10 mL). The combined organic layers were washed with brine, dried over anhydrous sodium sulfate, filtered, and concentrated under reduced pressure. The residue was purified by silica gel column chromatography (100% EtOAc) to afford the target compounds.

*(±)-2-(4-Chloro-2-(1H-pyrrol-1-yl)phenoxy)-2-(naphthalen-1-yl)acetic acid (**7a**)*. According with general procedure, **7a** was obtained from **25a** as a colorless solid in 95% yield. ^{1}H NMR (300 MHz, $CDCl_3$) δ: 8.18 (m, 1H), 7.90-7.84 (m, 2H), 7.61 (d, *J* = 7.2 Hz, 1H), 7.56-7.51 (m, 2H), 7.43 (m, 1H), 7.33 (d, *J* = 2.6 Hz, 1H), 7.10-7.07 (m,3H), 6.93 (d, *J* = 8.8 Hz, 1H), 6.34 (t, *J* = 2.2 Hz, 2H), 6.07 (s, 1H). ESI-MS *m/z*: 378 $[M+H]^+$.

*(±)-2-(4-Methyl-2-(1H-pyrrol-1-yl)phenoxy)-2-(naphthalen-1-yl)acetic acid (**7b**)*. According with general procedure, **7b** was obtained from **25b** as a white solid in 93% yield. ^{1}H NMR (300 MHz, $CDCl_3$) δ 8.17 (d, *J* = 6.0 Hz, 1H), 7.87 (m, 2H), 7.61-7.49 (m, 3H), 7.43 (t, *J* =

7.7 Hz, 1H), 7.14 (s, 1H), 7.06 (t, *J* = 2.2 Hz, 2H), 6.94-6.85 (m, 2H), 6.33 (t, *J* = 2.1 Hz, 2H), 6.04 (s, 1H), 2.29 (s, 3H). ESI-MS *m/z*: 356 $[M-H]^-$.

*(±)-2-((6-(1H-Pyrrol-1-yl)benzo[d][1,3]dioxol-5-yl)oxy)-2-(naphthalen-1-yl)acetic acid (**7c**).* According with general procedure, **7c** was obtained from **25c** as a white solid in 98% yield. ^{1}H NMR (300 MHz, $CDCl_3$) δ: 8.11 (d, *J* = 7.8 Hz, 1H), 7.86 (m, 2H), 7.56-7.40 (m, 4H), 6.94 (t, *J* = 2.2 Hz, 2H), 6.80 (s, 1H), 6.52 (s, 1H), 6.31 (t, *J* = 2.3 Hz, 2H), 5.93 (s, 2H), 5.68 (s, 1H); ESI-MS *m/z* 388 $[M+H]^+$.

*(±)-2-((7-(1H-Pyrrol-1-yl)-2,3-dihydrobenzo[b][1,4]dioxin-6-yl)oxy)-2-(naphthalen-1-yl)acetic acid (**7d**).* According with general procedure, **7d** was obtained from **25d** as a white solid in 98% yield. ^{1}H NMR (300 MHz, $CDCl_3$) δ: 8.17 (d, *J* = 8.0 Hz, 1H), 7.86 (m, 2H), 7.61-7.42 (m, 4H), 6.98 (t, *J* = 2.1 Hz, 2H), 6.87 (s, 1H), 6.53 (s, 1H), 6.30 (t, *J* = 2.2 Hz, 2H), 5.88 (s, 1H), 4.21 (s, 4H). ESI-MS *m/z* 402 $[M+H]^+$.

*(±)-2-(4-(4-Acetylpiperazin-1-yl)-2-(1H-pyrrol-1-yl)phenoxy)-2-(naphthalen-1-yl)acetic acid (**7e**).* According with general procedure, **7e** was obtained from **25e** as a brownish oil in 90% yield. ^{1}H NMR (400 MHz, MeOD) δ: 8.24-8.17 (m, 1H), 7.82 (dd, *J* = 15.1, 6.0 Hz, 2H), 7.52-7.41 (m, 3H), 7.36 (t, *J* = 7.6 Hz, 1H), 7.08-6.97 (m, 3H), 6.89 (d, *J* = 2.4 Hz, 1H), 6.74 (d, *J* = 9.0 Hz, 1H), 6.18 (s, 2H), 5.92 (s, 1H), 3.65 (dd, *J* = 15.6, 10.8 Hz, 4H), 3.11-2.98 (m, 4H), 2.09 (s, 3H). ESI-MS *m/z* 470 $[M+H]^+$.

*General procedure for the synthesis of compounds **6a-d**.* A solution of the acid **7a-d** (1.00 mmol) in dry DCM (20 mL) was added to a suspension of phosphorus pentachloride (1.20 mmol) and 1-butyl-3-methylimidazolium bromide (1.50 mmol) in dry DCM (50 mL) over a period of 2 h, and the reaction mixture was refluxed for 12 h. After cooling to room temperature, the reaction mixture was poured into crushed ice, basified with 10% NaOH solution, and extracted with DCM (3 x 10 mL). The combined organic layers were washed with brine, dried over anhydrous sodium sulfate, and concentrated under reduced pressure.

The residue was purified by silica gel column chromatography (100% DCM) and recrystallized (EtOAc/*n*-hexane) to afford the pure target compounds.

(±)-2-Chloro-6-(naphthalen-1-yl)benzo[b]pyrrolo[1,2-d][1,4]oxazepin-7(6H)-one ***(6a)***. According with general procedure, **6a** was obtained from **7a** as a colorless solid in 60% yield. ^{1}H NMR (300 MHz, $CDCl_3$) δ: 8.25 (d, *J* = 8.4 Hz, 1H), 7.89 (d, *J* = 8.0 Hz, 1H), 7.83 (d, *J* = 8.1 Hz, 1H), 7.66-7.52 (m, 2H), 7.51 (dd, *J* = 4.0, 1.8 Hz, 1H), 7.40 (d, *J* = 2.5 Hz, 1H), 7.35-7.28 (m, 2H), 7.17 (d, *J* =7.1 Hz, 1H), 6.89 (dd, *J* = 8.9, 2.4 Hz, 1H), 6.64 (d, *J* = 8.7 Hz, 1H), 6.60 (dd, *J* = 4.0, 2.7 Hz, 1H), 6.34 (s, 1H). ESI-MS *m/z* 360 $[M+H]^+$.

(±)-2-Methyl-6-(naphthalen-1-yl)benzo[b]pyrrolo[1,2-d][1,4]oxazepin-7(6H)-one ***(6b)***. According with general procedure, **6b** was obtained from **7b** as a white solid in 62% yield. ^{1}H NMR (300 MHz, $CDCl_3$) δ: 8.25 (d, *J* = 9.1 Hz, 1H), 7.89 (d, *J*= 7.9 Hz, 1H), 7.83 (d, *J*= 8.1 Hz, 1H), 7.64-7.52 (m, 2H), 7.46 (s, 1H), 7.38 (m, 1H), 7.34-7.22 (m, 3H), 6.79 (d, *J* = 8.2 Hz, 1H), 6.68 (d, *J* = 8.3 Hz, 1H), 6.56 (m, 1H), 6.25 (s, 1H), 2.33 (s, 3H); ^{13}C NMR (75 MHz, $CDCl_3$) δ: 190.1, 145.9, 135.6, 133.9, 133.6, 133.1, 132.0, 131.6, 129.9, 128.8, 127.9, 127.5, 126.7, 126.6, 126.0, 124.9, 124.5, 123.5, 122.5, 121.2, 111.9, 88.3, 21.0. ESI-MS *m/z* 340 $[M+H]^+$.

(±)-5-(Naphthalen-1-yl)-[1,3]dioxolo[4',5':4,5]benzo[1,2-b]pyrrolo[1,2-d][1,4]oxazepin-4(5H)-one ***(6c)***. According with general procedure, **6c** was obtained from **7c** as a white solid in 90% yield. ^{1}H NMR (300 MHz, $CDCl_3$) δ: 8.21 (d, *J* = 8.2 Hz, 1H), 7.90 (d, *J* = 8.2 Hz, 1H), 7.85 (d, *J* = 8.2 Hz, 1H), 7.63-7.52 (m, 2H), 7.42 (m, 1H), 7.33 (t, *J* = 7.6 Hz, 1H), 7.27-7.23 (m, 2H), 6.88 (s, 1H), 6.55 (t, *J* = 2.7 Hz, 1H), 6.24 (s, 2H), 5.93 (d, *J* = 9.1 Hz, 2H); ^{13}C NMR (75 MHz, $CDCl_3$) δ: 189.9, 146.0, 145.1, 133.9, 133.5, 131.8, 131.6, 130.0, 128.9, 127.6, 127.2, 126.8, 126.6 (2 C), 126.1, 124.9, 124.3, 120.8, 111.7, 104.5, 102.4, 102.0, 88.8. HRMS-ESI (*m/z*): $[M+Na]^+$ calculated for $[C_{23}H_{15}NO_4Na]^+$ 392.0893, found 392.0885.

*(±)-5-(Naphthalen-1-yl)-9,10-dihydro-[1,4]dioxino[2',3':4,5]benzo[1,2-b]pyrrolo[1,2-d][1,4]oxazepin-4(5H)-one (**6d**).* According with general procedure, **6d** was obtained from **7d** as a white solid in 84% yield. ^{1}H NMR (400 MHz, $CDCl_3$) δ: 8.20 (d, *J* = 8.2 Hz, 1H), 7.89 (d, *J* = 8.1 Hz, 1 H), 7.85 (d, *J* = 8.1 Hz, 1H), 7.61-7.51 (m, 2H), 7.42 (dd, *J* = 4.0, 1.7 Hz, 1H), 7.35 (t, *J* = 7.6 Hz, 1H), 7.28 (m, 2H), 6.93 (s, 1H), 6.53 (t, *J* = 4.0 Hz, 1H), 6.39 (s, 1H), 6.18 (s, 1H), 4.24-4.11 (m, 4H); ^{13}C NMR (75 MHz, $CDCl_3$) δ: 190.0, 142.4, 142.0, 140.9, 133.9, 133.5, 132.2, 131.6, 129.9, 128.8, 127.6, 127.3, 126.7, 126.5, 126.0, 124.9, 124.5, 120.8, 111.9, 111.7, 110.3, 89.1, 64.2 (2C). HRMS-ESI (*m/z*): $[M+H]^+$ calculated for $[C_{24}H_{18}NO_4]^+$ 384.1230, found 384.1236.

*(±)-2-(4-Acetylpiperazin-1-yl)-6-(naphthalen-1-yl)benzo[b]pyrrolo[1,2-d][1,4]oxazepin-7(6H)-one (**6e**).* Phosphorus pentachloride (7 mg, 0.03 mmol) was added to a solution of **7e** (14 mg, 0.03 mmol) in dry DCE (4 mL) and the resulting mixture was refluxed for 12 h. After cooling to room temperature, the reaction mixture was quenched by a dropwise addition of saturated solution of $NaHCO_3$ at 25 °C and the aqueous layer was extracted with DCM (3 x 5 mL). The combined organic layers were dried over anhydrous sodium sulfate, filtered, and concentrated under reduced pressure. The residue was purified by silica gel column chromatography ($CHCl_3$/MeOH 80:1) to afford the title compound in 20% yield as a yellow solid. ^{1}H NMR (400 MHz, $CDCl_3$) δ: 8.19 (d, *J* = 8.1 Hz, 1H), 7.83 (t, *J* = 9.5 Hz, 1H), 7.78 (d, *J* = 8.0 Hz, 1H), 7.52 (dt, *J* = 14.6, 6.9 Hz, 2H), 7.41 (s, 1H), 7.35-7.14 (m, 3H), 6.87 (s, 1H), 6.66 (s, 1H), 6.57-6.45 (m, 2H), 6.17 (s, 1H), 3.72 (s, 2H), 3.56 (s, 2H), 3.07 (s, 4H), 2.10 (s, 3H). ESI (*m/z*): 452 $[M+H]^+$

*(±)-2-(4-Methylpiperazin-1-yl)-6-(naphthalen-1-yl)benzo[b]pyrrolo[1,2-d][1,4]oxazepin-7(6H)-one (**6f**).* Compound **7f** [32] (25 mg, 0.06 mmol) was dissolved in dry DCE (10 mL) followed by the addition of phosphorus pentachloride (13 mg, 0.06 mmol). The reaction mixture was refluxed at 85 °C for 12 h then it was quenched by a dropwise addition of

saturated solution of $NaHCO_3$ at 25 °C and the aqueous layer was extracted with DCM (3 x 5 mL). The combined organic layers were dried over anhydrous sodium sulfate, filtered and concentrated under reduced pressure. The residue was purified by alumina column chromatography (petroleum ether/EtOAc 3:1) to afford the desired compound **6f** in 42% yield as a yellow solid. ^{1}H NMR (300 MHz, $CDCl_3$) δ: 8.20 (d, *J* = 8.2 Hz, 1H), 8.06 (d, *J* = 13.9 Hz, 1H), 7.91-7.69 (m, 2H), 7.57-7.16 (m, 6H), 6.88 (d, *J* = 2.8 Hz, 1H), 6.53 (m, 2H), 6.16 (s, 1H), 3.16 (q, *J* = 5.0 Hz, 4H), 2.57 (t, *J* = 5.0 Hz, 4H), 2.35 (d, *J* = 1.2 Hz, 3H). ^{13}C NMR (75 MHz, $CDCl_3$) δ: 190.4, 149.2, 133.9, 133.8, 132.3, 131.6, 129.8, 129.7, 128.7, 128.2, 127.5, 126.6, 126.3, 126.2, 125.9, 124.9, 124.6, 124.0, 121.0, 114.9, 111.8, 109.5, 54.9, 49.2, 46.0; ESI-MS *m/z* 424.1 $[M+H]^+$.

General procedure for the synthesis of compounds **5a-d**. A solution of ketones **6a-d** (1.00 mmol) in dry THF (2 mL) was added to a suspension of potassium hydride (30% wt dispersion in mineral oil, 0.147 g, 1.10 mmol) in dry THF (5 mL) at 25 °C and stirred for 1 h. After that appropriate acyl chloride (215 mg, 2.00 mmol) was slowly added and the resulting reaction mixture was stirred at 25 °C for another 12 h. The solvent was removed under reduced pressure and the residue was dissolved in EtOAc. The organic layer was washed with brine, dried over anhydrous sodium sulfate, filtered and concentrated under reduced pressure. The residue was purified by silica gel column chromatography (DCM/*n*-hexane 1:1) and recrystallized (EtOAc/*n*-hexane) to afford the target compounds.

*2-Chloro-6-(naphthalen-1-yl)benzo[b]pyrrolo[1,2-d][1,4]oxazepin-7-yl dimethylcarbamate (**5a**)*. According with general procedure, **5a** was obtained by using dimethylcarbamoyl chloride from **6a** as a colorless amorphous solid in 71% yield. ^{1}H NMR (300 MHz, $CDCl_3$) δ: 8.13 (m, 1H), 7.91 (d, *J* = 8.0 Hz, 2H), 7.59-7.43 (m, 5H), 7.20 (s, 1H), 7.10 (d, *J* = 8.3 Hz, 1H), 6.85 (d, *J* = 8.6 Hz, 1H), 6.48 (s, 2H), 2.76 (s, 3H), 2.65 (s, 3H); ^{13}C NMR (75 MHz, $CDCl_3$) δ: 154.1, 150.4, 145.9, 134.6, 134.1, 133.6, 131.4, 130.8, 130.7, 129.6, 128.2, 128.0,

127.4, 126.7, 126.5, 126.3, 126.1, 125.1, 123.6, 122.8, 121.4, 111.3, 110.4, 36.6, 36.1; HRMS-ESI (*m/z*): $[M+Na]^+$ calculated for $[C_{25}H_{19}ClN_2O_3Na]^+$ 453.0976, found 453.0963.

*2-Methyl-6-(naphthalen-1-yl)benzo[b]pyrrolo[1,2-d][1,4]oxazepin-7-yl acetate (**5b**).* According with general procedure, **5b** was obtained by using acetyl chloride from **6b** as a white amorphous solid in 47% yield. ^{1}H NMR (300 MHz, $CDCl_3$) δ: 8.14-8.10 (m, 1H), 7.93-7.89 (m, 2H), 7.57-7.43 (m, 4H), 7.26-7.23 (m, 2H), 6.94 (d, *J* = 8.5 Hz, 1H), 6.81 (d, *J* = 8.2 Hz, 1H), 6.44 (m, 2H), 2.40 (s 3H), 1.87 (s, 3H); ^{13}C NMR (75 MHz, $CDCl_3$) δ: 168.9, 149.7, 146.1, 135.7, 133.9, 133.7, 132.7, 131.3, 130.9, 129.6, 128.2, 127.6, 127.2, 127.1, 126.4, 126.1, 125.1, 123.3, 122.2, 121.5, 110.6, 110.0, 21.0, 20.6; HRMS-ESI (*m/z*): $[M+Na]^+$ calculated for $[C_{25}H_{19}NO_3Na]^+$ 404.1257, found 404.1250.

*5-(Naphthalen-1-yl)-[1,3]dioxolo[4',5':4,5]benzo[1,2-b]pyrrolo[1,2-d][1,4]oxazepin-4-yl acetate (**5c**).* According with general procedure, **5c** was obtained by using acetyl chloride from **6c** as a off-white amorphous solid in 38% yield. ^{1}H NMR (300 MHz, $CDCl_3$) δ: 8.13-8.09 (m, 1H), 7.93-7.90 (m, 2H), 7.57-7.43 (m, 4H), 7.15 (t, *J* = 2.3 Hz, 1H), 6.93 (s, 1H), 6.45-6.41 (m, 3H), 6.00 (s, 2H), 1.89 (s, 3H); ^{13}C NMR (75 MHz, $CDCl_3$) δ: 168.9, 146.2, 146.1, 146.0, 145.2, 134.2, 133.7, 131.2, 130.6, 129.7, 128.2, 127.2, 127.0, 126.9, 126.5, 126.4, 126.2, 125.0, 121.6, 110.5, 109.6, 103.7, 103.1, 102.0, 20.6; HRMS-ESI (*m/z*): $[M+H]^+$ calculated for $[C_{25}H_{18}NO_5]^+$ 412.1179, found 412.1186.

*5-(Naphthalen-1-yl)-9,10-dihydro-[1,4]dioxino[2',3':4,5]benzo[1,2-b]pyrrolo[1,2-d][1,4]oxazepin-4-yl acetate (**5d**).* According with general procedure, **5d** was obtained by using acetyl chloride from **6d** as a off-white amorphous solid in 45% yield. ^{1}H NMR (300 MHz, $CDCl_3$) δ: 8.13-8.11 (m, 1H), 7.91 (d, *J*= 8.1 Hz, 2H), 7.56-7.44 (m, 4H), 7.15 (t, *J* = 2.4 Hz, 1H), 6.95 (s, 1H), 6.48 (s, 1H), 6.42 (d, *J* = 2.3 Hz, 2H), 4.28-4.22 (m, 4H), 1.86 (s, 3H); ^{13}C NMR (100 MHz, $CDCl_3$) δ: 168.8, 146.0, 145.6, 141.8, 141.0, 133.9, 133.7, 131.2, 130.9, 129.6, 128.1, 127.2, 127.0, 126.9, 126.4 (2C), 126.1, 125.0, 121.5, 110.9, 110.8, 110.4,

109.7, 64.3 (2C), 20.5; HRMS-ESI (*m/z*): $[M+Na]^+$ calculated for $[C_{26}H_{19}NO_5Na]^+$ 448.1155, found 448.1143.

*2-(4-Acetylpiperazin-1-yl)-6-(naphthalen-1-yl)benzo[b]pyrrolo[1,2-d][1,4]oxazepin-7-yl acetate (**5e**).* TEA (17 µL, 0.12 mmol), DMAP (4 mg, 0.03 mmol), and acetic anhydride (11 µL, 0.12 mmol) were added sequentially to a solution of **6e** (27 mg, 0.06 mmol) in dry DCM (2 mL) at 0 °C and ther resulting reaction was mixture stirred at 25 °C for 12 h. Then, a saturated solution of ammonium chloride was added and the reaction mixture was extracted with DCM (3 x 5 mL). The combined organic layers were dried over anhydrous sodium sulfate, filtered, and concentrated under reduced pressure. The residue was purified by a silica gel column chromatograpghy (100% $CHCl_3$) to afford the title compound in 30% yield as a yellow amorphous solid. ^{1}H NMR (400 MHz, $CDCl_3$) δ: 8.06 (d, *J* = 8.5 Hz, 1H), 7.87 (d, *J* = 7.7 Hz, 2H), 7.53-7.38 (m, 4H), 7.19 (s, 1H), 6.92 (s, 1H), 6.80 (d, *J* = 8.8 Hz, 1H), 6.66 (dd, *J* = 8.8, 2.4 Hz, 1H), 6.41 (s, 2H), 3.83-3.74 (m, 2H), 3.67-3.58 (m, 2H), 3.23-3.11 (m, 4H), 2.13 (s, 3H), 1.83 (s, 3H). ESI-MS *m/z* 494.4 $[M+H]^+$.

*2-(4-Methylpiperazin-1-yl)-6-(naphthalen-1-yl)benzo[b]pyrrolo[1,2-d][1,4]oxazepin-7-yl acetate (**5f**).* To a solution of **6f** (20 mg, 0.047 mmol) in dry THF (1 mL), sodium bis(trimethylsilyl)amide (1 M solution in THF, 142 µL, 0.142 mmol) was added dropwise with cooling at -78 °C and the resulting mixture was stirred for 45 min. After that, acetyl chloride (17 µL, 0.240 mmol) was added and the mixture was allowed to reach 25 °C and stirred for another 12 h. Subsequently, a saturated solution of $NaHCO_3$ was added dropwise and the mixture was extracted with EtOAc. The combined organic layers were dried over anhydrous sodium sulfate, filtered, and concentrated under reduced pressure. The residue was purified by alumina column chromatography (*n*-hexane/EtOAc/DCM/MeOH 20:2:0.1:0.2) to afford the title compound in 23% yield as a brown amorphous solid. ^{1}H NMR (300 MHz, $CDCl_3$) δ: 8.13-8.01 (m, 1H), 7.88 (d, *J* = 7.9 Hz, 2H), 7.56-7.35 (m, 4H), 7.22 (t, *J* = 2.3 Hz,

1H), 6.91 (d, *J* = 2.8 Hz, 1H), 6.79 (d, *J* = 8.9 Hz, 1H), 6.67 (dd, *J* = 8.9, 2.8 Hz, 1H), 6.45-6.35 (m, 2H), 3.22 (t, *J* = 5.1 Hz, 4H), 2.59 (t, *J* = 5.0 Hz, 4H), 2.36 (s, 3H), 1.84 (s, 3H); ^{13}C NMR (75 MHz, $CDCl_3$) δ: 168.9, 146.3, 133.8, 133.7, 133.6, 131.2, 130.8, 129.8, 129.7, 129.6, 128.2, 127.5, 127.0, 126.4 (2C), 126.1, 125.0, 123.2, 123.1, 121.4, 111.6, 110.9, 110.2, 54.0, 48.0, 29.7, 20.5. ESI-MS *m/z* 466.1 $[M+H]^+$. HRMS-ESI (*m/z*): $[M+H]^+$ calculated for $[C_{29}H_{28}N_3O_3]^+$ 466.2125 found 466.2121.

*2-(4-Methylpiperazin-1-yl)-6-(naphthalen-1-yl)benzo[b]pyrrolo[1,2-d][1,4]oxazepin-7-yl diethylcarbamate (**5g**).* To a solution of **6f** (10 mg, 0.02 mmol) in dry THF (1 mL), sodium bis(trimethylsilyl)amide (1 M solution in THF, 71 µL, 0.07 mmol) was added at -78 °C and the mixture was stirred for 30 min. A solution of 4-nitrophenyl chloroformate (24 mg, 0.12 mmol) in dry THF (1 mL) was prepared at 0 °C in a separate flask and transferred slowly to the reaction mixture at -78 °C. Then the reaction mixture was allowed to reach 25 °C and stirred for another 3 h. Formation of the activated carbonate intermediate was confirmed by TLC on silica gel and ESI-MS *m/z* analysis (589.1 $[M + H]^+$). After that, diethylamine (7 µL, 0.07 mmol) and TEA (8 µL, 0.05 mmol) were added and the resulting mixture was stirred for another 1 h. After cooling at 0 °C, water was added slowly, and the mixture was rapidly extracted with EtOAc (3 x 5 mL). The combined organic layers were dried over anhydrous sodium sulfate, filtered, and concentrated under reduced pressure at 20 °C. The residue was purified by alumina column chromatography (petroleum ether/EtOAc 1:1) to afford the title compound in 33% yield as a yellow oil. ^{1}H NMR (300 MHz, $CDCl_3$) δ: 8.17-8.05 (m, 1H), 7.91-7.80 (m, 2H), 7.60-7.35 (m, 4H), 7.20 (t, *J* = 2.3 Hz, 1H), 6.92 (d, *J* = 2.8 Hz, 1H), 6.81 (d, *J* = 8.9 Hz, 1H), 6.66 (dd, *J* = 8.9, 2.9 Hz, 1H), 6.42 (d, *J* = 2.4 Hz, 2H), 3.21 (t, *J* = 5.0 Hz, 4H), 3.08 (d, *J* = 7.2 Hz, 2H), 2.93 (d, *J* = 7.4 Hz, 2H), 2.60 (t, *J* = 5.0 Hz, 4H), 2.37 (s, 3H), 0.88 (t, *J* = 7.4 Hz, 3H), 0.64 (t, *J* = 6.9 Hz, 3H); ^{13}C NMR (75 MHz, $CDCl_3$) δ: 153.4, 149.2, 146.2, 145.4, 134.3, 133.6, 133.5, 131.5, 131.4, 129.7, 129.2, 128.4, 128.0, 127.3,

126.7, 126.2, 125.9, 125.0, 122.6, 121.1, 114.5, 110.6, 109.6, 55.0, 49.4, 46.0, 42.0, 41.5, 14.1, 13.6; ESI-MS *m/z* 523.2 $[M+H]^+$. HRMS-ESI (*m/z*): $[M+H]^+$ calculated for $[C_{32}H_{35}N_4O_3]^+$ 523.2704, found 523.2691.

*(±)-5-(Quinolin-5-yl)naphtho[2,3-b]pyrrolo[1,2-d][1,4]oxazepin-4-yl(5-(diethylamino)pentan-2-yl) carbamate (**5h**)*. The title compound was obtained from **6g**[32] by following the procedure described for the synthesis of **5g** in presence of *N*,*N*-diethylpentane-1,4-diamine. The crude was purified by using a silica gel column chromatography (EtOAc/MeOH/TEA 20:1:0.1) to obtain the title compound in 30% yield as a light green oil. ^{1}H NMR (300 MHz, $CDCl_3$) δ: 8.93 (s, 1H), 8.53 (d, *J* = 8.4 Hz, 1H), 8.14 (d, *J* = 8.1 Hz, 1H), 7.83 (s, 2H), 7.71-7.55 (m, 3H), 7.49-7.33 (m, 4H), 7.26 (d, *J* = 8.1 Hz, 1H), 6.50 (d, *J* = 11.3 Hz, 2H), 6.07 (s, 1H), 3.46 (s, 1H), 2.34 (dd, *J* = 21.5, 15.4 Hz, 6H), 1.28 (d, *J* = 25.5 Hz, 4H), 0.97-0.75 (m, 9H); ^{13}C NMR (75 MHz, $CDCl_3$) δ: 153.2, 150.7, 150.4, 148.3, 144.1, 135.0, 132.6, 132.0, 131.2, 130.6, 128.7, 127.9, 127.7, 127.4, 127.1, 126.7, 126.2, 122.2, 121.3, 120.8, 118.9, 111.1, 110.4, 52.4, 46.7, 46.2, 34.5, 22.4, 20.5, 10.7. ESI-MS *m/z* 561.6 $[M+H]^+$. HRMS-ESI (*m/z*): $[M+H]^+$ calculated for $[C_{35}H_{37}N_4O_3]^+$ 561.2860, found 561.2845.

*5-(Quinolin-5-yl)naphtho[2,3-b]pyrrolo[1,2-d][1,4]oxazepin-4-yl 4-methylpiperazine-1-carboxylate (**5i**)*. The title compound was obtained from **6g** [32] by following the same procedure as described in the synthesis of **5g** in presence of *N*-methylpiperazine. The crude was purified by using a silica gel column chromatography (DCM/MeOH 10:1) to obtain the title compound in 56% yield as a light green oil. ^{1}H NMR (300 MHz, $CDCl_3$) δ: 8.95 (d, *J* = 3.8 Hz, 1H), 8.51 (d, *J* = 8.4 Hz, 1H), 8.17 (d, *J* = 8.3 Hz, 1H), 7.83 (d, *J* = 4.9 Hz, 2H), 7.75-7.57 (m, 3H), 7.52-7.22 (m, 5H), 6.49 (t, *J* = 8.1 Hz, 2H), 3.24 (s, 4H), 2.15 (d, *J* = 5.9 Hz, 4H), 1.87 (s, 3H); ^{13}C NMR (75 MHz, $CDCl_3$) δ: 152.5, 150.7, 150.5, 148.3, 143.9, 135.2, 135.0, 132.5, 132.1, 131.3, 131.1, 130.8, 128.8, 127.8, 127.6, 127.4, 127.1, 126.7, 126.3,

126.2, 122.4, 121.3, 120.8, 118.9, 111.2, 110.6, 54.3, 45.9, 44.3, 43.8. ESI-MS *m/z* 503.3 $[M+H]^+$. HRMS-ESI (*m/z*): $[M+H]^+$ calculated for $[C_{31}H_{27}N_4O_3]^+$ 503.2078, found 503.2070.

*1-tert-Butyl 4-(5-(quinolin-5-yl)naphtho[2,3-b]pyrrolo[1,2-d][1,4]oxazepin-4-yl) piperidine-1,4-dicarboxylate (**5j**).* To a solution of **6g** [32] (20 mg, 0.05 mmol) in dry THF (1 mL), sodium bis(trimethylsilyl)amide (1 M solution in THF, 160 µL, 0.16 mmol) was added dropwise when cooling at -78 °C and stirred for 45 min. In a separate flask, thionyl chloride (58 µL, 0.78 mmol) was added dropwise to a solution of 4-(*tert*-butoxycarbonyl)piperazine-1-carboxylic acid (40 mg, 0.39 mmol) in dry DCM (1 ml) at 0 °C and stirred at 25 °C for 10 min; the formation of *tert*-butyl 4-(chlorocarbonyl)piperidine-1-carboxylate was confirmed by ESI-MS *m/z* analysis. The solvent from the later flask was removed under reduced pressure at 20 °C, the residue was solubilized in dry THF at 25 °C, and the solution was cooled to 0 °C. This cold solution was transferred dropwise to the former flask at -78 °C. The reaction mixture was stirred at 25 °C for 12 h. Subsequently a saturated solution of $NaHCO_3$ was added and the resulting mixture was extracted with EtOAc (3 x 5 mL). The combined organic layers were dried over anhydrous sodium sulfate, filtered, and concentrated under reduced pressure at 25 °C. The residue was purified by alumina column chromatography (*n*-hexane/EtOAc/DCM/MeOH 20:2:0.1:0.2) to afford the title compound in 64% yield as a white amorphous solid. ^{1}H NMR (300 MHz, $CDCl_3$) δ: 8.97 (dd, *J* = 4.2, 1.7 Hz, 1H), 8.53-8.39 (m, 1H), 8.22-8.09 (m, 1H), 7.86 (d, *J* = 5.8 Hz, 2H), 7.72-7.60 (m, 2H), 7.53-7.32 (m, 6H), 6.51-6.35 (m, 2H), 3.72 (d, *J* = 23.0 Hz, 2H), 2.64 (t, *J* = 12.4 Hz, 2H), 2.35-2.17 (m, 1H), 1.59 (s, 4H), 1.40 (s, 9H). ^{13}C NMR (75 MHz, $CDCl_3$) δ: 172.3, 154.5, 150.8, 148.4, 134.8, 134.5, 132.5, 132.2, 131.31, 131.2, 130.8, 128.6, 127.7, 127.5, 127.2, 126.9, 126.7, 126.4, 122.6, 121.5, 121.0, 119.1, 111.2, 110.6, 79.7, 42.8, 40.7, 28.4. ESI-MS *m/z* 588.0 $[M+H]^+$. HRMS-ESI (*m/z*): $[M+H]^+$ calculated for $[C_{36}H_{34}N_3O_5]^+$ 588.2493, found 588.2481.

*5-(Quinolin-5-yl)naphtho[2,3-b]pyrrolo[1,2-d][1,4]oxazepin-4-yl piperidine-4-carboxylate (**5k**)*. To a cold solution of compound **5j** (20 mg, 0.003 mmol) in dry DCM (4 mL) at 0 °C, TFA (340 µL, 4.44 mmol) was added dropwise. The reaction mixture was stirred at 25 °C for 30 min. Subsequently, a saturated solution of $NaHCO_3$ was added dropwise at 0 °C and the resulting mixture was extracted with DCM (3 x 5 mL). The combined organic layers were dried over anhydrous sodium sulfate, filtered, and concentrated under reduced pressure at 25 °C. The residue was purified by silica gel column chromatography (DCM/MeOH 10:1) to afford the title compound in 96% yield as a light brown amorphous solid. ^{1}H NMR (300 MHz, CD_3OD) δ: 8.89 (dd, *J* = 4.3, 1.7 Hz, 1H), 8.48 (m, 1H), 8.12 (m, 1H), 8.01 (s, 1H), 7.92 (d, *J* = 8.1 Hz, 1H), 7.77 (dd, *J* = 8.6, 7.1 Hz, 1H), 7.65 (d, *J* = 8.0 Hz, 1H), 7.59-7.36 (m, 5H), 7.32 (s, 1H), 6.51-6.43 (m, 2H), 2.76 (m, 2H), 2.50-2.32 (m, 3H), 1.51 (dd, *J* = 13.4, 3.6 Hz, 2H), 1.30-1.18 (m, 2H); ^{13}C NMR (75 MHz, $CDCl_3$) δ: 172.4, 150.8, 148.3, 144.0, 134.9, 134.5, 132.5, 132.2, 131.3, 131.1, 130.9, 128.7, 127.7, 127.5, 127.2, 126.9, 126.7, 126.4 (2C), 122.6, 121.5, 121.0, 119.1, 111.2, 110.7, 44.8, 40.5, 29.7, 27.9. ESI-MS *m/z* 488.0 $[M+H]^+$. HRMS-ESI (*m/z*): $[M+H]^+$ calculated for $[C_{31}H_{26}N_3O_3]^+$ 488.1969, found 488.1963.

*5-(Quinolin-5-yl)naphtho[2,3-b]pyrrolo[1,2-d][1,4]oxazepin-4-yl nicotinate (**5l**)*. The title compound was synthesized from **6g** [32] by following the same procedure as described for **5f** in the presence of nicotinoyl chloride. The residue was purified by an alumina column chromatography (*n*-hexane/EtOAc/DCM/MeOH 20:2:0.1:0.2) to afford the title compound in 31% yield as a white amorphous solid. ^{1}H NMR (300 MHz, $CDCl_3$) δ: 9.02 (s, 1H), 8.96 (dd, *J* = 4.2, 1.7 Hz, 1H), 8.71 (dd, *J* = 4.9, 1.8 Hz, 1H), 8.59 (d, *J* = 8.6 Hz, 1H), 8.13-8.04 (m, 2H), 7.88 (d, *J* = 7.9 Hz, 2H), 7.68-7.55 (m, 3H), 7.55-7.39 (m, 4H), 7.36-7.27 (m, 2H), 6.50 (d, *J* = 2.4 Hz, 2H); ^{13}C NMR (75 MHz, $CDCl_3$) δ: 163.3, 154.1, 151.1, 150.7, 148.3, 144.6, 137.4, 134.9, 134.7, 132.4, 132.2, 131.4, 131.2, 130.6, 129.7, 128.8, 127.6, 127.5, 127.2,

126.7, 126.6, 126.5 (2C), 124.6, 123.4, 122.8, 121.5, 121.0, 119.2, 111.3, 111.0. ESI-MS *m/z* 482.1 $[M+H]^+$. HRMS-ESI (*m/z*): $[M+H]^+$ calculated for $[C_{31}H_{20}N_3O_3]^+$ 482.1499, found 482.1487.

Computational studies

Molecular Docking. The crystal structure of tubulin in complex with one of our previously developed compounds **26** was downloaded from the Protein Data Bank (PDB ID: 6GJ4) and accurately prepared by means of Protein Preparation Wizard protocol implemented in Maestro suite (Maestro, version 10.1, Schrödinger, LLC, New York, NY, 2015) in order to obtain an appropriate starting complex for the subsequent computational analyses. Compound **26** was extracted from the PDB crystal structure and prepared as the other compounds as following described [49]. The compounds used in the molecular docking calculation were drawn through the building panel in Maestro. The obtained molecules were treated by means of MacroModel (Schrödinger Release 2015-4: MacroModel, Schrödinger, LLC, New York, NY, 2015) for retrieving the lower energy conformers to use as input in molecular docking experiments. The calculation was performed using the Optimized Potentials for Liquid Simulations-all atom (OPLS-AA) force field 2005 and the Generalized-Born/Surface-Area (GB/SA) model to simulate the solvent effects. No cutoff for non-bonded interactions was used. Polak-Ribiere conjugate gradient (PRCG) method was employed with 2500 maximum iterations and 0.001 gradient convergence threshold for performing the molecular energy minimizations. MCMM (Monte Carlo Multiple Minimum) was employed as torsional sampling method for the conformational searches, performing automatic setup with 21 kJ/mol (5.02 kcal/mol) in the energy window for saving structure and 0.5 Å was used as cutoff distance for redundant conformers. The lower energies conformers were treated by LigPrep

application (Schrödinger Release 2015-4: LigPrep, Schrödinger, LLC, New York, NY, 2015), generating the most plausible ionization state at cellular pH value (7.4 ± 0.2). Once prepared the ligands and the protein, the compounds were docked employing the program Glide (Schrödinger Release 2015-4: Glide, Schrödinger, LLC, New York, NY, 2015) applying Glide standard precision (SP) scoring function to evaluate the affinity of the compounds through a visual inspection to retrieve compounds with an appropriate binding mode according to the key interactions found for the active **26**. Energy grid was prepared using default value of protein atom scaling factor (1.0 Å) within a cubic box centered on the crystallized ligand **26**. After grid generation the ligands were docked into the enzyme. The number of poses entered to post-docking minimization was set to 50. Glide SP score was evaluated.

Biological Assays

Cell Lines. SCC4 cells were purchased from Sigma-Aldrich. SCC4 cells were maintained in Dulbecco's Modified Eagles (DMEM) GlutaMAX^{TM} (Thermo Fisher Scientific; cat no. 61965026) supplemented with 10% (v/v) Foetal Bovine Serum (FBS, Sigma-Aldrich; cat no. 10270106) and 1% (v/v) penicillin-streptomycin (Sigma-Aldrich; cat no. 15140122). Earle's Balanced Salt Solution (EBSS) (Sigma-Aldrich; cat no. E2888) was stored at 4 °C and incubated at 37 °C for 2 h before the treatment.

Ca9.22 gingival squamous cell carcinoma cells (Health Science Research Resources Bank, Osaka, Japan) were cultured in minimum essential media (MEM) with 10% (v/v) FBS, penicillin/streptomycin (100 U/mL penicillin, 0.1 mg/mL streptomycin) and L-glutamine (2 mM). Cells were cultured at 37 ^{o}C, in a humidified atmosphere, containing 5% CO_2.

TR146 keratinizing squamous cell carcinoma of buccal mucosal origin cells (HPA Cultures, UK) were cultured in high glucose Dulbecco Modified Eagle's Medium (DMEM) with 10% (v/v) FBS and penicillin/streptomycin (100 U/mL penicillin, 0.1 mg/mL streptomycin).

Esophageal squamous cell carcinoma cell line KYSE-520 was purchased from the Leibniz Institute DSMZ German Collection of Microorganisms and Cell Cultures GmbH (Braunschweig, Germany). Cells were grown in RPMI 1640 medium with 10% FBS (Gibco), 2 mM L-glutamine (Gibco) and 100 units/mL penicillin-streptomycin (Gibco) at 37 ºC, in a humidified atmosphere containing 5% CO_2.

Esophageal adenocarcinoma EAC cell lines were obtained from Public Health England. OE33, FLO-1, SKGT4, OE19 and MFD-1 were maintained in RPMI (ThermoFisher Cat. No 11875093) supplemented with 10% FBS (ThermoFisher Cat. No 10500064), 1% sodium pyruvate (ThermoFisher Cat. No 11360070) and 1% penicillin/streptomycin (ThermoFisher Cat. No 15140122) at 37 °C in a humidified atmosphere containing 5% CO_2. All lines were routinely examined for mycoplasma contamination.

Human promyelocytic leukaemia cells HL-60 (CCL-240, American Type Culture Collection) were cultured in RPMI 1640 medium with 10% FBS (Gibco), 2 mM L-glutamine (Gibco) and 100 units/mL penicillin-streptomycin (Gibco) at 37 °C, in a humidified atmosphere containing 5% CO_2.

Leukemic Eμ-TCL1 cells were prepared from the spleen of Eμ-TCL1 mice using 70 micron cell strainer filters (Fisher Scientific) followed by red blood cell lysis using RBC lysis buffer (0.155 M NH_4Cl, 1 mM $KHCO_3$, 0.1 mM EDTA, pH 7.4). Cells were resuspended in RPMI 1640 medium with 10% fetal bovine serum (FBS) (Gibco), 2 mM L-glutamine (Gibco) and 100 units/ml penicillin-streptomycin (Gibco) at 37°C, in a humidified atmosphere containing 5% CO_2.

Mouse immortalised fibroblasts NIH3T3 were purchased from American Type Culture Collection. Cells were propagated in DMEM supplemented with 10% fetal calf serum, 1% L-glutamine-penicillin-streptomycin solution, and 1% MEM non-essential amino acid solution, and incubated at 37 °C in a humidified atmosphere containing 5% CO_2.

Human oral epithelial primary cells were obtained by scraping the palate using sterile swabs. The swabs were then washed in PBS with 5% antibiotics (500 U/mL penicillin and 500 μg/mL streptomycin) and centrifuged for 10 min at 800 g for cell washing and pelleting before plating them in a 24 multiwell plate at a density of $1.5x10^4$ for each well. Cells were cultured without NIH3T3 feeder layer in DMEM-High glucose supplemented with 15% of calf serum, 1% antibiotic–antimycotic solution and maintained in a humid atmosphere with temperature at 37 °C and of 5% CO_2, and used for cytotoxicity test after 24 h of incubation [75].

Human non-small lung cell carcinoma A549 cells were obtained from ATCC. Cells were propagated in RPMI 1640 supplemented with 10% fetal calf serum, 2 mM L-glutamine, 1 mM Sodium Pyruvate, 40 μg/mL gentamicin, 100 UI/mL penicillin and 200 μg/mL streptomycin. Human cervix carcinoma HeLaS3 cells were obtained from ATCC, whereas its tubulin β3 overexepressing counterpart HeLaβ3 [76] was kindly gifted by Prof. Richard Ludueña. Cells were propagated in DMEM supplemented with 10% foetal calf serum, 2 mM L-glutamine, 1 mM sodium pyruvate, 40 μg/mL gentamicin, 100 UI/mL penicillin and 200 μg/mL streptomycin. Human ovarian carcinoma A2780 and its P-gp overexpressing counterpart A2780AD[77] were a gift from Dr. Steven Williams (Fox Chase Cancer Center, Philadelphia, PA). Cells were propagated in RPMI 1640 supplemented with 10% foetal calf serum, 2 mM L-glutamine, 1 mM sodium pyruvate, 40 μg/mL gentamicin, 100 UI/mL penicillin and 200 μg/mL streptomycin. All these cell lines were incubated at 37 °C in a humidified atmosphere containing 5% CO_2.

Cytotoxicity Assays

Both NIH3T3 and human oral epithelial primary cells were suspended in complete medium at a density of 1.5×10^4/mL, seeded in a 24 well round multidish, and incubated at 37 °C in an atmosphere of 5% CO_2. After 24 h of culture, the culture medium was removed, and the test samples were solubilized in DMSO. Then it was diluted with complete medium and added to each well in order to evaluate the cytotoxic effect of increasing concentrations of the compounds. Each concentration was tested in six replicates. Complete medium was used as negative control. Cell viability and proliferation was evaluated by Neutral Red uptake after 24 h of incubation with both 3T3 and human oral epithelial primary cell as follows. First, the following solutions were prepared in order to determine the percentage of viable cells:

1. Neutral Red (NR) stock solution: 0.33 g NR dye powder in 100 mL sterile H_2O.
2. NR medium: 1.0 mL NR stock solution + 99.0 routine culture medium pre-warmed to 37 °C
3. NR desorb solution: 1% glacial acetic acid solution + 50% ethanol + 49% H_2O

At the end of incubation, the routine culture medium was removed from each plate and the cells were carefully rinsed with 1 mL pre-warmed D-PBS 0.1 M. Plates were then gently blotted with paper towels. 1.0 mL NR medium was added to each dish and further incubated at 37 °C, 95% humidity, and 5% CO_2 for 3 h. The cells were checked during incubation for NR crystal formation. After incubation, the NR medium was removed, and the cells were carefully rinsed with 1 mL pre-warmed D-PBS 0.1 M. PBS was decanted and blotted from the dishes and exactly 1 mL NR desorb solution was added to each sample. Plates were placed on a shaker for 20–45 min to extract NR from the cells and form a homogeneous solution. During this step the samples were covered to protect them from light. Five min after

removal from the shaker, absorbance was read at 540 nm with a UV/visible spectrophotometer (Varian Cary 1E).

Cell viability assays

Cell viability for A549, A2780, A2780AD, HeLa, HeLaβ3, OE33, FLO-1, SKGT4, OE19 and MFD-1 was monitored by means of the MTT assay.[78] Briefly, cells were seeded at different concentrations depending on the cell line. After 24 h the tested compounds were added at different concentrations and podophyllotoxin was used again as the reference compound. MTT was added after 48 h incubation of cells with compounds. The MTT reaction was then stopped after 2 h and colorimetric changes were evaluated in an Appliskan (ThermoFisher) plate reader the following day. Data obtained were plotted in SigmaPlot 13.0 (Systat Software, Inc) and were fitted to a four parameter logistic curve.

Ames test

The TA100 and TA98 strains of Salmonella typhimurium were utilized for mutagenicity assay in absence and presence of metabolic activation, i.e., with and without S9 fraction. The tester strains were selected because they are sensitive and detect a large proportion of known bacterial mutagens and are most commonly used routinely within the pharmaceutical industry.[79] The following specific positive controls were used, respectively, with and without S9 fraction: 2-nitrofluorene (2-NF) 2 µg/mL + 4-nitroquinoline-N-oxide (4-NQO) 0.1 µg/mL, and 2-aminoanthracene (2-AA) 5 µg/mL. Approximately, 10^7 bacteria were exposed to 6 concentrations of each test sample ranging from 0.3 to 60 µM, as well as to positive and negative controls, for 90 min in medium containing sufficient histidine to support approximately two cell divisions. After 90 min, the exposed cultures were diluted in pH indicator medium lacking histidine, and aliquoted into 48 wells of a 384-well plate. Within two days, cells which had undergone the reversion to His grew into colonies.

Metabolism by the bacterial colonies reduced the pH of the medium, changing the color of that well which can be detected visually. The number of wells containing revertant colonies were counted for each dose and compared to a zero dose control. Each dose was tested in six replicates. The material was regarded mutagenic if the number of histidine revertant colonies was twice or more than the spontaneous revertant colonies.

Alamar blue viability assay

For the IC_{50} determination on SCC4, Ca9.22 and TR146, cells were seeded in a 96-well plate at the density of 30 x 10^4 cells/well. After adhesion, cells were treated with a range of concentrations of the tested molecules and 1% EtOH as the vehicle for 48 h in triplicate. Afterwards, 10% (v/v) Alamar Blue reagent (Invitrogen) was added to each well and the plates were incubated for 3 h in 37 ºC in the dark. Fluorescence levels were read on a SPECTRAMAX Gemini Microplate Spectrofluorometer (Molecular Devices) with excitation at 544 nm, and emission at 590 nm. The IC_{50} values were determined as means of three separate experiments.

KYSE-520 cells were seeded in a 96-well plate at the density of 5 x 10^3 cells/well and allowed time to attach. Subsequently, cells were treated in triplicate with a range of concentrations of the tested molecules and 0.01% of DMSO as the vehicle for 72 h. To assess the cell viability after treatment, 10% (v/v) Alamar Blue reagent (Invitrogen) was added to each well and the plates were incubated for 3 h at 37 ºC in the dark. SPECTRAMAX Gemini Microplate Spectrofluorometer (Molecular Devices) was used to read fluorescence at 544 nm excitation and 590 nm emission wavelengths. The IC_{50} values were determined as means of three separate experiments.

Analysis of apoptosis by flow cytometry

The levels of apoptosis in SCC4, Ca9.22, TR146, and KYSE-520 cells with the tested compounds were detected by flow cytometric analysis of Annexin V/Propidium Iodide (PI)-stained cells. This double staining contains annexin V – which is a protein having high affinity to phosphatidylserine expressed on the outer membrane of apoptotic cells, and PI – a nuclear acid dye that does not permeate intact membranes, therefore only staining cells with lower plasma membrane integrity, such as late apoptotic and dead cells.

The SCC4 cell line was seeded at 150 $x10^3$ cells/well in 6 well plates. Cells were left for 24 h to adhere to the plate and then were treated with either vehicle (1% EtOH (v/v)) or with either 0.5 or 2μM of the indicated compounds. After 48h, cells were harvested, and double stained with annexin V/PI. Cells were then analyzed by flow cytometry using BD FACS Accuri software. 10,000 single cells were gated on vehicle treated cells and the percentage of cells undergoing apoptosis was determined.

Ca9.22 and TR146 cells were seeded at a density of 30 X 104 cells/mL and were left untreated (control) or treated with either vehicle (1% EtOH (v/v)) or 500 nM of compound for 48 h. After incubation cells were harvested and stained with Annexin V/Propidium Iodide (PI) and were analyzed by flow cytometry using BD FACs Accuri software. 10,000 cells were gated on vehicle treated cells.

KYSE-520 cells were seeded at the density of 1.5 x 10^5 cells/ml and treated with 3 μM and 10 μM of the tested compounds or 0.01% DMSO (v/v) as the vehicle control for 72 h. Subsequently, cells were harvested and stained with Annexin V-FITC (IQ Products) and Propidium Iodide (PI) (Invitrogen) and analyzed by flow cytometry using BD Accuri™ C6 (BD Biosciences).

The mitochondrial-dependent pro-apoptotic activity of the compounds was assessed by flow cytometry in HL-60 cells and Eμ-TCL1 splenocytes loaded with the fluorescent dye

Tetramethylrhodamine Methyl Ester (TMRM) (Sigma-Aldrich). Specifically, cells were plated 1x106 cells/ml in RPMI-1640 complete medium and treated for 48h with 10μM of the tested compounds. DMSO was used as control (0.1%). After treatment, 200.000 cells/sample were washed in RPMI w/o phenol red (Invitrogen srl) and loaded with TMRM (200 nM in RPMI w/o phenol red) for 20 min at 37°C. Samples were acquired on Guava Easy Cyte cytometer (Luminex Corp., Austin, TX, USA) and analyzed with FlowJo software (TreeStar Inc., Ashland, OR, USA).

Microtubule polymerisation assay

25 μM of tubulin in GAB buffer (10 mM NaPi pH 6.7, 30 % glycerol, 1 mM EGTA, 6 mM $MgCl_2$ and 1 mM GTP) was polymerized for nearly 2 h at 37 ºC in the presence of DMSO (vehicle), 27.5 μM of podophyllotoxin (a reference ligand for the colchicine site) or tested compounds (22 μM for each). Polymerization was monitored measuring the absorbance at 350 nm in a Multiskan (ThermoFisher) plate reader.

The stoichiometry of the tubulin assembly inhibition by **5i** was determined by turbidimetry, 20 μM tubulin in GAB buffer (10 mM NaPi pH 6.7, 30 % Glycerol, 1 mM EGTA, 6 mM $MgCl_2$ and 1 mM GTP) was polymerized for nearly 2 h at 37 ºC in the presence of **5i** ranging from 0 to 22 μM or 22 μM of podophyllotoxin. Polymerisation was monitored by measuring the absorbance at 350 nm in a Multiskan (ThermoFisher) plate reader. Data is presented as absorbance values from the plateau phase vs. **5i** concentration values.

Spectrophotometry of compound 5i

Absorption spectrum of compound 20 μM 5i was obtained in absolute ethanol by spectroscopy (Merck), using a Thermo Scientific Evolution 201 UV-visible

spectrophotometer. The range of wavelengths characterised were from 240 to 550 nm. DMSO (Merck) was used as a blanck. Measurements were performed in duplicate. The Lambert-Beer equation was employed to transform absorbance into molar extinction coefficient and data were plotted in SigmaPlot 13.0 (Systat Software, Inc).

Fluorescence assays for compound 5i

Fluorescence emission of 10 μM compound **5i** was characterised in a HoribaJobin Yvon Fluoromax-2 spectrofluorometer. Compound **5i** was excited at 350 nm and its emission was recorded from 360 to 600 nm. Additionally, fluorescence emission of 10 μM of compound **5i** was recorded in the presence of 10 μM of dimeric tubulin in 10 mM NaPi buffer pH 7.0, 0.1 mM GTP, using the same conditions mentioned before. Data obtained were plotted using SigmaPlot 13.0 (Systat Software, Inc).

Binding of 5i to the colchicine site was studied by a fluorescence displacement assay

Increasing concentrations of Podophyllotoxin up to 10 μM were incubated with three different fixed concentrations of compound **5i** and tubulin (0.1, 0.5 and 1 μM) in PEDTA buffer (NaPi 10 mM pH 7.0, 1 mM EDTA, 1.5 mM $MgCl_2$, 0.1 mM GTP) for 30 min at 25 ºC. Fluorescence measurements were performed in a Varioskan Flash plate reader (Thermoscientific) with excitation and emission wavelengths of 350 nm and 450 nm, respectively. Data were plotted using SigmaPlot 13.0 (Systat Software, Inc).

Non-specific binding of 5i to MTX and BSA was studied by fluorescence.

A fixed concentration of 1 μM of compound **5i** was incubated for 20 min at 25 ºC with increasing concentrations of BSA or MTX in PEDTA buffer (NaPi 10 mM pH 7.0, 1 mM EDTA, 1.5 mM $MgCl_2$, 0.1 mM GTP) up to 40 μM and 25 μM, respectively. Fluorescence measurements were performed in a Varioskan Flash plate reader (Thermoscientific) with

excitation and emission wavelengths of 350 nm and 450 nm, respectively. Data were plotted using SigmaPlot 13.0 (Systat Software, Inc).

Western Blot

Treated and untreated SCC4 cells were suspended in lysis buffer (50 mmol/L Tris-HCl, pH 7.4, 150 mmol/L NaCl, 1% NP40, 10 mmol/L NaF, 1 mmol/L PMSF, and protease inhibitor cocktail) and the lysis reaction was carried out for 15 min at 4 °C. Samples were then centrifuged at 13,000 rpm for 30 min at 4 °C and protein concentration was quantified by Bradford assay (Bio-Rad). 50 μg of each sample were loaded on 10% and 15% of polyacrylamide gels and transferred on nitrocellulose membrane. HL-60 cells were plated $1x10^6$ cells/mL in RPMI-1640 complete medium incubated at 37 °C for 15 min and treated with 10 μM of the tested compounds in presence or absence of 40 μM chloroquine for 1 h and 45 min. DMSO (0.1%) was used as control. Cells were lysed in 1% (v/v) Triton X-100 in 20 mM Tris-HCl (pH 8), 150 mM NaCl with Protease Inhibitor Cocktail Set III (Calbiochem Merck) and 0.2 mg/mL of Na orthovanadate. Post-nuclear supernatants were resolved by SDS-PAGE and transferred to the nitrocellulose membrane. Immunoreactive signals were detected with a horseradish peroxidase-conjugated secondary antibody (Bio-Rad or GE Healthcare). Used antibodies: p-ULK1 (Ser757) (Cell signaling Technology 6888S), ULK1 (Cell signaling Technology 8054S), ATG7 (Cell signaling Technology- D12B11), SQSTM1/p62 (sc-28359), LC3 I/II (ab51520), LC3 (Cell SignalingTechnology 3868), LC3B (D11) XP (Cell SignalingTechnology), phospho-NF-kB p65 (Cell SignalingTechnology 93H1), phospho-p44/42 MAPK (ERK1/2) (Cell Signaling Technology 9101) actin (Millipore clone C4), β-tubulin (Cell Signaling Technology D2N5G), Acetyl-tubulin (Sigma T7451) anti-ERK 2 (D-2- Santa Cruz Biotecnology), anti-Actin (clone C4, Millipore), anti-NF-k Bp65 (clone D14E12, Cell Signaling Technology) and GAPDH (Cell signaling Technology D16H11), GAPDH (Calbiochem, 6C5). All the antibodies were probed according to the

manufacturer's protocol instructions. Semi-quantitative analysis was performed using ImageJ software. Western blotting was conducted as previously described.[80]

Evaluation of Lysosomal pH by Lysotracker staining.

HeLa cells (ATCC CCL-2□) were cultured in Dulbecco's modified Eagle's medium (DMEM; Thermo Fisher Scientific–Gibco) supplemented with 10% FBS (Thermo Fisher Scientific–Gibco), 2 mM L-glutamine, and penicillin/streptomycin (100 U/mL) (Thermo Fisher Scientific–Gibco). Cells were seeded in 1.5 glass-bottomed 60 mm culture dish (MatTek) and grown to subconfluence and then left untreated or treated with **5i** (10 mM) or **5k** (10 mM) or bafilomycin A1 (300 nM) for 3 h. Cells were then incubated for 30 min with 75 nM LysoTracker™ Red DND-99 (Invitrogen, #L7528). Cells were then washed three times with Phenol red-free DMEM and imaged with a Nikon Eclipse Ti Spinning disc microscope equipped with a stage incubator and with a 63X 1,4NA oil-immersion objective. Evaluation of lysosomal pH by means of Lysotracker localization and intensity was performed with the NIS AR software (Nikon).

Immunofluorescence analysis of the effect of 5i and 5k on autophagosome-lysosome fusion and on Golgi and actin cytoskeleton morphology.

Hela cells were grown on coverlips to subconfluence and left untreated (growth medium), amino acid starved (Hank Balanced Salt Solution with Ca^{2+} and Mg^{2+}, HBSS-Gibco) or treated with BafA1 (300 nM), **5i** or **5k** at 1 and 10 μM for 3 h either in growth medium or HBSS. Cells were then fixed in ice cold methanol for 5 min at -20 □C and processed for immunofluorescence as follows. Cells were incubated for 30 min in Permeabilisation/blocking buffer (0.05% saponin, 0.5% BSA, and 50 mM NH_4Cl in PBS 1X) and then incubated for 1 h with anti-LC3 (Novusbio, #2220) to label the autophagosomes and anti-LAMP1 (HybridomaBank, #H4A3) primary antibodies diluted in blocking buffer.

Coverlisps were then washed three times with PBS 1X and incubated for 30 min with AlexaFluor-conjugated species matched secondary antibodies (Invitrogen) diluted 1:400 in blocking buffer. Cells were washed three times in PBS1X, once in water, mounted with Mowiol and imaged by Zeiss LSM800 laser scanning confocal microscope equipped with 63X 1,4NA oil immersion objective. For the analysis of Golgi and actin cytoskeleton morphology Hela cells were grown on coverlips to subconfluence and left untreated (growth medium) or treated with BafA1 (300 nM), **5i** or **5k** at 1 and 10 μM for 3 h. Cells were then fixed with 4% PFA in PBS1X and incubated for 30 min in Permeabilisation/blocking buffer and then incubated for 1h with anti-GM130 (BD, #610823) diluted in blocking buffer to label the Golgi complex. Coverlisps were then washed three times with PBS 1X and incubated for 30 min with AlexaFluor-conjugated species matched secondary antibody and with AlexaFluor-Phalloidin (Invitrogen) to label actin diluted 1:400 in blocking buffer. Cells were washed three times in PBS1X, once in water, mounted with Mowiol and imaged by Zeiss LSM800 laser scanning confocal microscope equipped with 63X 1,4NA oil immersion objective.

HPLC analysis

A stock solution of 10 mM concentration in DMSO for each tested compound was prepared. From the stock solution, three separate samples of 250 mM concentration and a final volume of 1 ml were prepared by dissolving the 25 μL of the stock solution and 975 μL of: i) the standard solution; ii) the test solutions at pH = 3.0; iii) and the test solutions pH = 7.4. The standard solution was prepared by diluting the stock solution in PBS-buffer solution (MeCN/water, 3:2). The test solution at pH = 3 was prepared by the diluting the stock solution in 50 mM acetic acid. The test solution at pH = 7.4 was prepared by diluting the stock solution in 50 mM aqueous PBS-buffer. These three suspension/solutions were sealed and left under orbital shaking to achieve “pseudothermodynamic equilibrium” at 25 °C for 24

h. After that the solutions were filtered off by using PTFE filters and successively diluted (1:2) with the respective solutions used to prepare the samples. The samples were analyzed by HPLC/UV/DAD, using UV detection at 254 nm for quantitation. Solubility of the samples was calculated by comparing the areas of the sample and that of the standard:

$$S = \frac{Asmp \times FD \times Cst}{Ast}$$

S = solubility of the compound (mM); Asmp = UV area of the sample solution; FD = dilution factor (2); Cst = standard concentration (250 mM); Ast = UV area of the standard solution.

Each of the reported solubility value is the average of three independent analyses. The same sample solutions were prepared to evaluate the chemical stability of the compounds at 25 °C for 36 h and were analyzed by HPLC/UV/DAD, by using UV detection at 254 nm for quantitation. The chemical stability, by comparing the area of the peak at T = 0 and the area of the peak at 36 h. A chemical stability percentage value was calculated by following this method at pH = 3 and pH = 7.4 for each compound by applying the following formula:

$$\%_{remaining} = \frac{Ac_{24}}{Ac_{T0}} \times 100$$

Ac_{24} = area of the sample after 24 h at 25 °C; Ac_{T0} = area of the sample at T = 0.

Each of the reported solubility and chemical stability value is the average of three independent analyses.

Analysis of *in vitro* metabolic stability in human liver microsomes

5h and **5j**, dissolved in MeCN/DMSO 3:1, was incubated separately at 5 µM (final concentration in 100 mM phosphate buffer, pH 7.4) with 0.4 mg/mL HLM protein in a final volume 250 µL. The enzymatic reactions were initiated by addition of a NADPH-

regenerating system (NADPH-GS) consisting of 2 mM β-NADPH, 10 mM glucose-6-phosphate, 0.4 U/mL glucose-6-phosphate dehydrogenase. Reactions were terminated at regular time intervals (overall range 0-60 min) by adding a double volume of cold MeCN as previously reported.[81] HPLC analysis was performed on Agilent 1100 Series liquid chromatography system (Agilent Technologies, Palo Alto, CA, USA) equipped with a EC 150/4.6 nucleosil 100-3 C18 (Macherey-Nagel, Duren, Germany) and coupling with UV-VIS detector, setting at λ = 254 nm. Analysis was carried out using gradient elution of a binary solution; eluent A was MeCN with 0.1% TFA, while eluent B was an aqueous solution of TFA (0.1%). The analysis started at 10% A that rapidly increased up to 100% in 15 min and finally remaining at 100% A until 5 min. The analysis was performed at flow rate of 1 mL/min and injection volume was 20 µL. The intrinsic clearance (CLint) was calculated by the equation:

$$CLint = \frac{k \times [V]}{[P]}$$

where, k is the rate constant for the depletion of substrate (expressed in min^{-1}), V is the volume of incubation in µL and P is the amount of microsomal proteins.

$$CLint = \frac{k\ (min^{-1}) \times [V]}{[P]}$$

where k is the rate constant for the depletion of substrate, V is the volume of incubation in µL and P is the amount of microsomal proteins in the incubation medium in mg.[81]

ASSOCIATED CONTENT

Supporting Information

The Supporting Information is available free of charge at

Figure S1. Effects of compound **5a-d** on HL-60 cell line to determine % Sub G1 for 24 h at a concentration of 10 (gray) and 25 (black) μM.

Figure S2. Flow cytometric analysis of PI-stained apoptotic HL-60 cells (percent of cells in sub G_0/G_1) following treatment with the indicated concentrations of either **5e** or the reference compound **26** for 48 h. Vehicle was 1% EtOH v/v.

Figure S3. Superposition of the complexes of compound **26** (crystal structure 6GJ4) represented in green sticks, and the docked posed obtained by the re-docking procedure (yellow sticks) with tubulin (α-tubulin in magenta cartoon, β-tubulin in light teal) following our *in silico* protocol.

Author Information

Corresponding Authors

Giuseppe Campiani − orcid.org/0000-0001-5295-9529;

Email: giuseppe.campiani@unisi.it

Stefania Butini −orcid.org/0000-0002-8471-0880;

Email: butini3@unisi.it

Acknowledgements

This research was funded by the European Union's Horizon 2020 (EU) Research and Innovation Programme under the Marie Sklodowska-Curie grant agreement No.721906-TRACT (TK, SM, MG, NMcC, GO'S, RT, VK, SG, DZ, GC, SB); Tuscany strategic project POR-FSE 2014-2020, 'Medicina di Precisione e Malattie Rare'(MePreMaRe), (ACE-ESCC) (NR, GC, SB), and by "Epigenetic Hallmarks of Multiple Sclerosis" (acronym Epi-MS) (id:415, Merit Ranking Area ERC LS) in VALERE 2019 Program; V:ALERE 2020 – Progetto competitivo "CIRCE" in risposta al bando D.R. n. 138 del 17/02/2020 Program; Blueprint 282510; EPICHEMBIO CM1406; AIRC-17217; VALERE: Vanvitelli per la Ricerca; Campania Regional Government Technology Platform Lotta alle Patologie Oncologiche: iCURE; Campania Regional Government FASE2: IDEAL. MIUR, Proof of Concept POC01_00043. POR Campania FSE 2014-2020 ASSE III.

ABBREVIATIONS

2-AA, 2-aminoanthracene; 2-NF, 2-Nitrofluorene; BafA1, BafilomycinA1; BSA, bovin serum albumin; Clint, intrinsic clearance; CLL, chronic lymphocytic leukemia; COX-2, cyclooxygenase-2; DMEM, Dulbecco's Modified Eagles Medium; EBSS, Earle's Balanced Salts; FBS, Foetal Bovine Serum; GB/SA, Generalized-Born/Surface-Area; HBSS, Hanks' Balanced Salt Solution; HDACs, Histone Deacetylases; HLM, human liver microsome; LSCM, laser scanning confocal microscopy; MCMM, Monte Carlo Multiple Minimum; MEM, minimum essential media; MT, microtubule; MTAs, Microtubule-targeting agents; NR, Neutral Red; OPLS-AA, Optimized Potentials for Liquid Simulations-all atom; PDB, Protein Data Bank; PI, Propidium iodide; PRCG, Polak-Ribiere conjugate gradient ; SAR, structure-activity relationship; TEA, triethylamine; TLC, thin-layer chromatography; TMRM, tetramethylrhodamine methyl ester.

References

[1] Y. Wang, Y. Xia, Z. Lu, Metabolic features of cancer cells, Cancer Commun. 38 (2018) 65. https://doi.org/10.1186/s40880-018-0335-7.

[2] S. He, Q. Li, X. Jiang, X. Lu, F. Feng, W. Qu, Y. Chen, H. Sun, Design of Small Molecule Autophagy Modulators: A Promising Druggable Strategy, J. Med. Chem. 61 (2018) 4656–4687. https://doi.org/10.1021/acs.jmedchem.7b01019.

[3] N. Mizushima, Autophagy: process and function., Genes Dev. 21 (2007) 2861–2873. https://doi.org/10.1101/gad.1599207.

[4] A.L. Parker, M. Kavallaris, J.A. McCarroll, Microtubules and Their Role in Cellular Stress in Cancer, Front. Oncol. 4 (2014) 153. https://doi.org/10.3389/fonc.2014.00153.

[5] C. Geeraert, A. Ratier, S.G. Pfisterer, D. Perdiz, I. Cantaloube, A. Rouault, S. Pattingre, T. Proikas-Cezanne, P. Codogno, C. Poüs, Starvation-induced hyperacetylation of tubulin is required for the stimulation of autophagy by nutrient deprivation., J. Biol. Chem. 285 (2010) 24184–24194. https://doi.org/10.1074/jbc.M109.091553.

[6] A. Bánréti, M. Sass, Y. Graba, The emerging role of acetylation in the regulation of

autophagy., Autophagy. 9 (2013) 819–829. https://doi.org/10.4161/auto.23908.

[7] M. Mauthe, I. Orhon, C. Rocchi, X. Zhou, M. Luhr, K.-J. Hijlkema, R.P. Coppes, N. Engedal, M. Mari, F. Reggiori, Chloroquine inhibits autophagic flux by decreasing autophagosome-lysosome fusion, Autophagy. 14 (2018) 1435–1455. https://doi.org/10.1080/15548627.2018.1474314.

[8] M. Pérez-Hernández, A. Arias, D. Martínez-García, R. Pérez-Tomás, R. Quesada, V. Soto-Cerrato, Targeting Autophagy for Cancer Treatment and Tumor Chemosensitization, Cancers . 11 (2019). https://doi.org/10.3390/cancers11101599.

[9] X. Qiao, X. Wang, Y. Shang, Y. Li, S. Chen, Azithromycin enhances anticancer activity of TRAIL by inhibiting autophagy and up-regulating the protein levels of DR4/5 in colon cancer cells in vitro and in vivo, Cancer Commun. 38 (2018) 43. https://doi.org/10.1186/s40880-018-0309-9.

[10] D.H. Morris, C.K. Yip, Y. Shi, B.T. Chait, Q.J. Wang, Beclin 1-Vps34 complex architecture: Understanding the nuts and bolts of therapeutic targets, Front. Biol. (Beijing). 10 (2015) 398–426. https://doi.org/10.1007/s11515-015-1374-y.

[11] N.B. Haas, L.J. Appleman, M. Stein, M. Redlinger, M. Wilks, X. Xu, A. Onorati, A. Kalavacharla, T. Kim, C.J. Zhen, S. Kadri, J.P. Segal, P.A. Gimotty, L.E. Davis, R.K. Amaravadi, Autophagy Inhibition to Augment mTOR Inhibition: a Phase I/II Trial of Everolimus and Hydroxychloroquine in Patients with Previously Treated Renal Cell Carcinoma, Clin. Cancer Res. 25 (2019) 2080 LP – 2087. https://doi.org/10.1158/1078-0432.CCR-18-2204.

[12] D. Mahalingam, M. Mita, J. Sarantopoulos, L. Wood, R.K. Amaravadi, L.E. Davis, A.C. Mita, T.J. Curiel, C.M. Espitia, S.T. Nawrocki, F.J. Giles, J.S. Carew, Combined autophagy and HDAC inhibition, Autophagy. 10 (2014) 1403–1414. https://doi.org/10.4161/auto.29231.

[13] S.M. Nathwani, S. Butler, D. Fayne, N.N. McGovern, B. Sarkadi, M.J. Meegan, D.G. Lloyd, G. Campiani, M. Lawler, D.C. Williams, D.M. Zisterer, Novel microtubule-targeting agents, pyrrolo-1,5-benzoxazepines, induce apoptosis in multi-drug-resistant cancer cells, Cancer Chemother. Pharmacol. 66 (2010) 585–596. https://doi.org/10.1007/s00280-009-1200-9.

[14] C.G. Kinsey, S.A. Camolotto, A.M. Boespflug, K.P. Guillen, M. Foth, A. Truong, S.S. Schuman, J.E. Shea, M.T. Seipp, J.T. Yap, L.D. Burrell, D.H. Lum, J.R. Whisenant, G.W. Gilcrease, C.C. Cavalieri, K.M. Rehbein, S.L. Cutler, K.E. Affolter, A.L. Welm, B.E. Welm, C.L. Scaife, E.L. Snyder, M. McMahon, Protective autophagy elicited by RAF→MEK→ERK inhibition suggests a treatment strategy for RAS-driven cancers, Nat. Med. 25 (2019) 620–627. https://doi.org/10.1038/s41591-019-0367-9.

[15] H.-Y. Chen, E. White, Role of autophagy in cancer prevention., Cancer Prev. Res. (Phila). 4 (2011) 973–983. https://doi.org/10.1158/1940-6207.CAPR-10-0387.

[16] C.-S. Lee, L.C. Lee, T.L. Yuan, S. Chakka, C. Fellmann, S.W. Lowe, N.J. Caplen, F. McCormick, J. Luo, MAP kinase and autophagy pathways cooperate to maintain RAS mutant cancer cell survival, Proc. Natl. Acad. Sci. 116 (2019) 4508–4517. https://doi.org/10.1073/pnas.1817494116.

[17] D.J. Kast, R. Dominguez, The Cytoskeleton–Autophagy Connection, Curr. Biol. 27 (2017) R318–R326. https://doi.org/https://doi.org/10.1016/j.cub.2017.02.061.

[18] R. Mackeh, D. Perdiz, S. Lorin, P. Codogno, C. Poüs, Autophagy and microtubules - new story, old players, J. Cell Sci. 126 (2013) 1071–1080. https://doi.org/10.1242/jcs.115626.

[19] A.D. Tangutur, D. Kumar, K.V.K. and S. Kantevari, Microtubule Targeting Agents as Cancer Chemotherapeutics: An Overview of Molecular Hybrids as Stabilizing and Destabilizing Agents, Curr. Top. Med. Chem. 17 (2017) 2523–2537.

https://doi.org/http://dx.doi.org/10.2174/1568026617666170104145640.

[20] S. Chauhan1, Z. Ahmed, S.B. Bradfute, J. Arko-Mensah, M.A. Mandell, S. Won Choi, T. Kimura, F. Blanchet, A. Waller, M.H. Mudd, S. Jiang, L.Sklar, G.S. Timmins, N. Maphis, K. Bhaskar, V. Piguet and V. Deretic. Pharmaceutical screen identifies novel target processes for activation of autophagy with a broad translational potential. Nature Communications 6 (2015) 8620.

[21] A. Hamaï, P. Codogno, New Targets for Acetylation in Autophagy, Sci. Signal. 5 (2012) pe29 LP-pe29. https://doi.org/10.1126/scisignal.2003187.

[22] S. Di Bartolomeo, M. Corazzari, F. Nazio, S. Oliverio, G. Lisi, M. Antonioli, V. Pagliarini, S. Matteoni, C. Fuoco, L. Giunta, M. D'Amelio, R. Nardacci, A. Romagnoli, M. Piacentini, F. Cecconi, G.M. Fimia, The dynamic interaction of AMBRA1 with the dynein motor complex regulates mammalian autophagy, J. Cell Biol. 191 (2010) 155 LP – 168. https://doi.org/10.1083/jcb.201002100.

[23] R.A. Veldhoen, S.L. Banman, D.R. Hemmerling, R. Odsen, T. Simmen, A.J. Simmonds, D.A. Underhill, I.S. Goping, The chemotherapeutic agent paclitaxel inhibits autophagy through two distinct mechanisms that regulate apoptosis., Oncogene. 32 (2013) 736–746. https://doi.org/10.1038/onc.2012.92.

[24] S. Bhattacharya, A. Das, S. Datta, A. Ganguli, G. Chakrabarti, Colchicine induces autophagy and senescence in lung cancer cells at clinically admissible concentration: potential use of colchicine in combination with autophagy inhibitor in cancer therapy, Tumor Biol. 37 (2016) 10653–10664. https://doi.org/10.1007/s13277-016-4972-7.

[25] A. Kumar, B. Singh, P.R. Sharma, S.B. Bharate, A.K. Saxena, D.M. Mondhe, A novel microtubule depolymerizing colchicine analogue triggers apoptosis and autophagy in HCT-116 colon cancer cells, Cell Biochem. Funct. 34 (2016) 69–81. https://doi.org/10.1002/cbf.3166.

[26] P. Nunes, T. Ernandez, I. Roth, X. Qiao, D. Strebel, R. Bouley, A. Charollais, P. Ramadori, M. Foti, P. Meda, E. Feraille, D. Brown, U. Hasler, Hypertonic stress promotes autophagy and microtubule-dependent autophagosomal clusters, Autophagy. 9 (2013) 550–567. https://doi.org/10.4161/auto.23662.

[27] E.N. Maginn, P. V. Browne, P. Hayden, E. Vandenberghe, B. MacDonagh, P. Evans, M. Goodyer, P. Tewari, G. Campiani, S. Butini, D.C. Williams, D.M. Zisterer, M.P. Lawler, A.M. McElligott, PBOX-15, a novel microtubule targeting agent, induces apoptosis, upregulates death receptors, and potentiates TRAIL-mediated apoptosis in multiple myeloma cells, Br. J. Cancer. 104 (2011) 281–289. https://doi.org/10.1038/sj.bjc.6606035.

[28] N.K. Verma, E. Dempsey, J. Conroy, P. Olwell, A.M. Mcelligott, A.M. Davies, D. Kelleher, S. Butini, G. Campiani, D.C. Williams, D.M. Zisterer, M. Lawler, Y. Volkov, A new microtubule-targeting compound PBOX-15 inhibits T-cell migration via post-translational modifications of tubulin, J. Mol. Med. 86 (2008) 457–469. https://doi.org/10.1007/s00109-008-0312-8.

[29] D.M. Zisterer, G. Campiani, V. Nacci, D.C. Williams, Pyrrolo-1,5-benzoxazepines induce apoptosis in HL-60, Jurkat, and Hut-78 cells: A new class of apoptotic agents, J. Pharmacol. Exp. Ther. 293 (2000) 48–59.

[30] L.M. Greene, D.P. Nolan, D. Regan-Komito, G. Campiani, D.C. Williams, D.M. Zisterer, Inhibition of late-stage autophagy synergistically enhances pyrrolo-1,5-benzoxazepine-6-induced apoptotic cell death in human colon cancer cells, Int. J. Oncol. 43 (2013) 927–935. https://doi.org/10.3892/ijo.2013.1989.

[31] M. Brindisi, C. Ulivieri, G. Alfano, S. Gemma, F. de Asís Balaguer, T. Khan, A. Grillo, G. Chemi, G. Menchon, A.E. Prota, N. Olieric, D. Lucena-Agell, I. Barasoain, J.F. Diaz, A. Nebbioso, M. Conte, L. Lopresti, S. Magnano, R. Amet, P. Kinsella,

D.M. Zisterer, O. Ibrahim, J. O'Sullivan, L. Morbidelli, R. Spaccapelo, C. Baldari, S. Butini, E. Novellino, G. Campiani, L. Altucci, M.O. Steinmetz, S. Brogi, Structure-activity relationships, biological evaluation and structural studies of novel pyrrolonaphthoxazepines as antitumor agents, Eur. J. Med. Chem. 162 (2019) 290–320. https://doi.org/10.1016/j.ejmech.2018.11.004.

[32] F. Bray, J. Ferlay, I. Soerjomataram, R.L. Siegel, L.A. Torre, A. Jemal, Global cancer statistics 2018: GLOBOCAN estimates of incidence and mortality worldwide for 36 cancers in 185 countries., CA. Cancer J. Clin. 68 (2018) 394–424. https://doi.org/10.3322/caac.21492.

[33] T. Khan, N. Relitti, M. Brindisi, S. Magnano, D. Zisterer, S. Gemma, S. Butini, G. Campiani, Autophagy modulators for the treatment of oral and esophageal squamous cell carcinomas, Med. Res. Rev. 40 (2020) 1002–1060.

[34] E. Eladl, R. Tremblay-LeMay, N. Rastgoo, R. Musani, W. Chen, A. Liu, H. Chang, Role of CD47 in hematological malignancies, J. Hematol. Oncol. 13 (2020) 1–14.

[35] J. Lindsay, B.W. Teh, K. Micklethwaite, M. Slavin, Azole antifungals and new targeted therapies for hematological malignancy, Curr. Opin. Infect. Dis. 32 (2019) 538–545.

[36] S. Federico, T. Khan, N. Relitti, G. Chemi, M. Brindisi, S. Brogi, E. Novellino, D.M. Zisterer, G. Campiani, S. Gemma, S. Butini, A Jocic-type approach for a practical and scalable synthesis of pyrrolonaphthoxazepine (PNOX)-based potent proapoptotic agents, Tetrahedron Lett. 59 (2018) 4466–4470.

[37] Z. Gao, J. Zhang, H. Yang, G. Jiang, Brønsted Acid-Promoted Friedel–Crafts Alkylation/Cyclization of (7-Hydroxynaphthalenyl)pyrrole or (2-Hydroxyphenyl)pyrroles with Isatins for the Construction of Pyrrolospirooxindole Derivatives, J. Org. Chem. 83 (2018) 11407–11414.

https://doi.org/10.1021/acs.joc.8b01703.

[38] G. Campiani, V. Nacci, I. Fiorini, M.P. De Filippis, A. Garofalo, S.M. Ciani, G. Greco, E. Novellino, D.C. Williams, D.M. Zisterer, M.J. Woods, C. Mihai, C. Manzoni, T. Mennini, Synthesis, biological activity, and SARs of pyrrolobenzoxazepine derivatives, a new class of specific "peripheral-type" benzodiazepine receptor ligands, J. Med. Chem. 39 (1996) 3435–3450. https://doi.org/10.1021/jm960251b.

[39] C. Fattorusso, S. Gemma, S. Butini, P. Huleatt, B. Catalanotti, M. Persico, M. De Angelis, I. Fiorini, V. Nacci, A. Ramunno, M. Rodriquez, G. Greco, E. Novellino, A. Bergamini, S. Marini, M. Coletta, G. Maga, S. Spadari, G. Campiani, Specific Targeting Highly Conserved Residues in the HIV-1 Reverse Transcriptase Primer Grip Region. Design, Synthesis, and Biological Evaluation of Novel, Potent, and Broad Spectrum NNRTIs with Antiviral Activity, J. Med. Chem. 48 (2005) 7153–7165. https://doi.org/10.1021/jm050257d.

[40] S. Brogi, A. Ramunno, L. Savi, G. Chemi, G. Alfano, A. Pecorelli, E. Pambianchi, P. Galatello, G. Compagnoni, F. Focher, G. Biamonti, G. Valacchi, S. Butini, S. Gemma, G. Campiani, M. Brindisi, First dual AK/GSK-3beta inhibitors endowed with antioxidant properties as multifunctional, potential neuroprotective agents., Eur. J. Med. Chem. 138 (2017) 438–457. https://doi.org/10.1016/j.ejmech.2017.06.017.

[41] G. Guillaumet, M. Hretani, G. Coudert, D. Averbeck, S. Averbeck, Synthesis and photoinduced biological properties of linear dioxinocoumarins, Eur. J. Med. Chem. 25 (1990) 45–51. https://doi.org/https://doi.org/10.1016/0223-5234(90)90163-W.

[42] A.-S. Bourlot, I. Sánchez, G. Dureng, G. Guillaumet, R. Massingham, A. Monteil, E. Winslow, M.D. Pujol, J.-Y. Mérour, New substituted 1, 4-benzoxazine derivatives with potential intracellular calcium activity, J. Med. Chem. 41 (1998) 3142–3158.

[43] I. Engelbrecht, J.P. Petzer, A. Petzer, The synthesis and evaluation of sesamol and

benzodioxane derivatives as inhibitors of monoamine oxidase, Bioorg. Med. Chem. Lett. 25 (2015) 1896–1900.

[44] G. Campiani, S. Butini, C. Fattorusso, B. Catalanotti, S. Gemma, V. Nacci, E. Morelli, A. Cagnotto, I. Mereghetti, T. Mennini, M. Carli, P. Minetti, M.A. Di Cesare, D. Mastroianni, N. Scafetta, B. Galletti, M.A. Stasi, M. Castorina, L. Pacifici, M. Vertechy, S. Di Serio, O. Ghirardi, O. Tinti, P. Carminati, Pyrrolo[1,3]benzothiazepine-Based Serotonin and Dopamine Receptor Antagonists. Molecular Modeling, Further Structure−Activity Relationship Studies, and Identification of Novel Atypical Antipsychotic Agents, J. Med. Chem. 47 (2004) 143–157. https://doi.org/10.1021/jm0309811.

[45] Y. Kiso, K. Ukawa, T. Akita, Efficient removal of N-benzyloxycarbonyl group by a 'push–pull' mechanism using thioanisole–trifluoroacetic acid, exemplified by a synthesis of Met-enkephalin, J. Chem. Soc. Chem. Commun. (1980) 101–102. https://doi.org/10.1039/C39800000101.

[46] S. Butini, S. Gemma, M. Brindisi, S. Maramai, P. Minetti, D. Celona, R. Napolitano, F. Borsini, W. Cabri, F. Fezza, L. Merlini, S. Dallavalle, G. Campiani, M. Maccarrone, Identification of a novel arylpiperazine scaffold for fatty acid amide hydrolase inhibition with improved drug disposition properties, Bioorg. Med. Chem. Lett. 23 (2013) 492–495. https://doi.org/https://doi.org/10.1016/j.bmcl.2012.11.035.

[47] A.K. Ghosh, M. Brindisi, Organic Carbamates in Drug Design and Medicinal Chemistry, J. Med. Chem. 58 (2015) 2895–2940. https://doi.org/10.1021/jm501371s.

[48] M.O. Steinmetz, A.E. Prota, Microtubule-Targeting Agents: Strategies To Hijack the Cytoskeleton., Trends Cell Biol. 28 (2018) 776–792. https://doi.org/10.1016/j.tcb.2018.05.001.

[49] M. Brindisi, C. Ulivieri, G. Alfano, S. Gemma, F. de Asís Balaguer, T. Khan, A.

Grillo, G. Chemi, G. Menchon, A.E. Prota, N. Olieric, D. Lucena-Agell, I. Barasoain, J.F. Diaz, A. Nebbioso, M. Conte, L. Lopresti, S. Magnano, R. Amet, P. Kinsella, D.M. Zisterer, O. Ibrahim, J. O'Sullivan, L. Morbidelli, R. Spaccapelo, C. Baldari, S. Butini, E. Novellino, G. Campiani, L. Altucci, M.O. Steinmetz, S. Brogi, Structure-activity relationships, biological evaluation and structural studies of novel pyrrolonaphthoxazepines as antitumor agents, Eur. J. Med. Chem. 162 (2019). https://doi.org/10.1016/j.ejmech.2018.11.004.

[50] M.M. Mc Gee, S. Gemma, S. Butini, A. Ramunno, D.M. Zisterer, C. Fattorusso, B. Catalanotti, G. Kukreja, I. Fiorini, C. Pisano, C. Cucco, E. Novellino, V. Nacci, D.C. Williams, G. Campiani, Pyrrolo[1,5]benzoxa(thia)zepines as a new class of potent apoptotic agents. Biological studies and identification of an intracellular location of their drug target, J. Med. Chem. 48 (2005) 4367–4377. https://doi.org/10.1021/jm049402y.

[51] K.C. Pak, K.Y. Lam, S. Law, J.C.O. Tang, The inhibitory effect of Gleditsia sinensis on cyclooxygenase-2 expression in human esophageal squamous cell carcinoma., Int. J. Mol. Med. 23 (2009) 121–129.

[52] C. Sobolewski, C. Cerella, M. Dicato, L. Ghibelli, M. Diederich, The role of cyclooxygenase-2 in cell proliferation and cell death in human malignancies., Int. J. Cell Biol. 2010 (2010) 215158. https://doi.org/10.1155/2010/215158.

[53] K. Subbaramaiah, A.J. Dannenberg, Cyclooxygenase 2: a molecular target for cancer prevention and treatment., Trends Pharmacol. Sci. 24 (2003) 96–102. https://doi.org/10.1016/S0165-6147(02)00043-3.

[54] A.J. Dannenberg, N.K. Altorki, J.O. Boyle, C. Dang, L.R. Howe, B.B. Weksler, K. Subbaramaiah, Cyclo-oxygenase 2: a pharmacological target for the prevention of cancer., Lancet. Oncol. 2 (2001) 544–551. https://doi.org/10.1016/S1470-

2045(01)00488-0.

[55] H. Sui, S. Zhou, Y. Wang, X. Liu, L. Zhou, P. Yin, Z. Fan, Q. Li, COX-2 contributes to P-glycoprotein-mediated multidrug resistance via phosphorylation of c-Jun at Ser63/73 in colorectal cancer., Carcinogenesis. 32 (2011) 667–675. https://doi.org/10.1093/carcin/bgr016.

[56] D. Ratnasinghe, P.J. Daschner, M.R. Anver, B.H. Kasprzak, P.R. Taylor, G.C. Yeh, J.A. Tangrea, Cyclooxygenase-2, P-glycoprotein-170 and drug resistance; is chemoprevention against multidrug resistance possible?, Anticancer Res. 21 (2001) 2141–2147.

[57] G. Contino, M.D. Eldridge, M. Secrier, L. Bower, R. Fels Elliott, J. Weaver, A.G. Lynch, P.A.W. Edwards, R.C. Fitzgerald, Whole-genome sequencing of nine esophageal adenocarcinoma cell lines, F1000Research. 5 (2016) 1336. https://doi.org/10.12688/f1000research.7033.1.

[58] L.-X. Gai, W.-Q. Wang, X. Wu, X.-J. Su, F.-C. Yang, NIR absorbing reduced graphene oxide for photothermal radiotherapy for treatment of esophageal cancer., J. Photochem. Photobiol. B. 194 (2019) 188–193. https://doi.org/10.1016/j.jphotobiol.2019.03.014.

[59] E. Garcia, A. Hayden, C. Birts, E. Britton, C. Rogerson, C.W. Bleaney, A. Cowie, K. Pickard, M. Mellone, C. Choh, M. Derouet, P. Duriez, F. Noble, M.J. White, J.N. Primrose, J.C. Strefford, M. Rose-Zerilli, G.J. Thomas, Y. Ang, A.D. Sharrocks, R.C. Fitzgerald, T.J. Underwood, Author Correction: Authentication and characterisation of a new oesophageal adenocarcinoma cell line: MFD-1., Sci. Rep. 9 (2019) 318. https://doi.org/10.1038/s41598-018-37591-7.

[60] D.J. Klionsky, K. Abdelmohsen, A. Abe, M.J. Abedin, H. Abeliovich, A. Acevedo Arozena, H. Adachi, C.M. Adams, P.D. Adams, K. Adeli, *et al.* Guidelines for the use

and interpretation of assays for monitoring autophagy (3rd edition), Autophagy. 12 (2016) 1–222. https://doi.org/10.1080/15548627.2015.1100356.

[61] R. Maurya, R. Kumar, S. Saran, AMPKα promotes basal autophagy induction in Dictyostelium discoideum, J. Cell. Physiol. n/a (2019). https://doi.org/10.1002/jcp.29373.

[62] R.K. Amaravadi, J.D. Winkler, Lys05: a new lysosomal autophagy inhibitor, Autophagy. 8 (2012) 1383–1384. https://doi.org/10.4161/auto.20958.

[63] J. Kim, M. Kundu, B. Viollet, K.-L. Guan, AMPK and mTOR regulate autophagy through direct phosphorylation of Ulk1., Nat. Cell Biol. 13 (2011) 132–141. https://doi.org/10.1038/ncb2152.

[64] A.J. Meijer, P. Codogno, Autophagy: regulation by energy sensing., Curr. Biol. 21 (2011) R227-9. https://doi.org/10.1016/j.cub.2011.02.007.

[65] Y. Wu, Y. Jin, T. Sun, P. Zhu, J. Li, Q. Zhang, X. Wang, J. Jiang, G. Chen, X. Zhao, p62/SQSTM1 accumulation due to degradation inhibition and transcriptional activation plays a critical role in silica nanoparticle-induced airway inflammation via NF-κB activation., J. Nanobiotechnology. 18 (2020) 77. https://doi.org/10.1186/s12951-020-00634-1.

[66] S.R. Yoshii, N. Mizushima, Monitoring and Measuring Autophagy, Int. J. Mol. Sci. 18 (2017). https://doi.org/10.3390/ijms18091865.

[67] C. Janke, G. Montagnac, Causes and Consequences of Microtubule Acetylation., Curr. Biol. 27 (2017) R1287–R1292. https://doi.org/10.1016/j.cub.2017.10.044.

[68] D. Verzella, A. Pescatore, D. Capece, D. Vecchiotti, M.V. Ursini, G. Franzoso, E. Alesse, F. Zazzeroni, Life, death, and autophagy in cancer: NF-κB turns up everywhere, Cell Death Dis. 11 (2020) 210. https://doi.org/10.1038/s41419-020-2399-y.

[69] J. Yuan, X. Dong, J. Yap, J. Hu, The MAPK and AMPK signalings: interplay and implication in targeted cancer therapy, J. Hematol. Oncol. 13 (2020) 113. https://doi.org/10.1186/s13045-020-00949-4.

[70] T. Monkkonen, J. Debnath, Inflammatory signaling cascades and autophagy in cancer, Autophagy. 14 (2018) 190–198.

[71] K.L. Bryant, C.A. Stalnecker, D. Zeitouni, J.E. Klomp, S. Peng, A.P. Tikunov, V. Gunda, M. Pierobon, A.M. Waters, S.D. George, G. Tomar, B. Papke, G.A. Hobbs, L. Yan, T.K. Hayes, J.N. Diehl, G.D. Goode, N. V Chaika, Y. Wang, G.-F. Zhang, A.K. Witkiewicz, E.S. Knudsen, E.F. Petricoin, P.K. Singh, J.M. Macdonald, N.L. Tran, C.A. Lyssiotis, H. Ying, A.C. Kimmelman, A.D. Cox, C.J. Der, Combination of ERK and autophagy inhibition as a treatment approach for pancreatic cancer, Nat. Med. 25 (2019) 628–640. https://doi.org/10.1038/s41591-019-0368-8.

[72] G. Campiani, C. Cavella, J.D. Osko, M. Brindisi, N. Relitti, S. Brogi, A.P. Saraswati, S. Federico, G. Chemi, S. Maramai, G. Carullo, B. Jaeger, A. Carleo, R. Benedetti, F. Sarno, S. Lamponi, P. Rottoli, E. Bargagli, C. Bertucci, D. Tedesco, D. Herp, J. Senger, G. Ruberti, F. Saccoccia, S. Saponara, B. Gorelli, M. Valoti, B. Kennedy, H. Sundaramurthi, S. Butini, M. Jung, K.M. Roach, L. Altucci, P. Bradding, D.W. Christianson, S. Gemma, A. Prasse, Harnessing the Role of HDAC6 in Idiopathic Pulmonary Fibrosis: Design, Synthesis, Structural Analysis, and Biological Evaluation of Potent Inhibitors, J. Med. Chem. 64 (2021) 9960–9988. https://doi.org/10.1021/acs.jmedchem.1c00184.

[73] T. Iwatsubo, N. Hirota, T. Ooie, H. Suzuki, N. Shimada, K. Chiba, T. Ishizaki, C.E. Green, C.A. Tyson, Y. Sugiyama, Prediction of in vivo drug metabolism in the human liver from in vitro metabolism data., Pharmacol. Ther. 73 (1997) 147–171. https://doi.org/10.1016/s0163-7258(96)00184-2.

[74] E. Salahifar, D. Nematollahi, M. Bayat, A. Mahyari, H. Amiri Rudbari, Regioselective Green Electrochemical Approach to the Synthesis of Nitroacetaminophen Derivatives, Org. Lett. 17 (2015) 4666–4669. https://doi.org/10.1021/acs.orglett.5b01837.

[75] F.B. Russo, G.C. Pignatari, I.R. Fernandes, J.L.R.M. Dias, P.C.B. Beltrão-Braga, Epithelial cells from oral mucosa: How to cultivate them?, Cytotechnology. 68 (2016) 2105–2114. https://doi.org/10.1007/s10616-016-9950-9.

[76] P.A. Joe, A. Banerjee, R.F. Ludueña, The roles of cys124 and ser239 in the functional properties of human betaIII tubulin., Cell Motil. Cytoskeleton. 65 (2008) 476–486. https://doi.org/10.1002/cm.20274.

[77] R.J. Kowalski, P. Giannakakou, S.P. Gunasekera, R.E. Longley, B.W. Day, E. Hamel, The microtubule-stabilizing agent discodermolide competitively inhibits the binding of paclitaxel (Taxol) to tubulin polymers, enhances tubulin nucleation reactions more potently than paclitaxel, and inhibits the growth of paclitaxel-resistant cells., Mol. Pharmacol. 52 (1997) 613–622.

[78] T. Mosmann, Rapid colorimetric assay for cellular growth and survival: Application to proliferation and cytotoxicity assays, J. Immunol. Methods. 65 (1983) 55–63. https://doi.org/https://doi.org/10.1016/0022-1759(83)90303-4.

[79] D. Purves, C. Harvey, D. Tweats, C.E. Lumley, Genotoxicity testing: current practices and strategies used by the pharmaceutical industry., Mutagenesis. 10 (1995) 297–312. https://doi.org/10.1093/mutage/10.4.297.

[80] R. Coyle, K. Slattery, L. Ennis, M.J. O'sullivan, D.M. Zisterer, The XIAP inhibitor embelin sensitises malignant rhabdoid tumour cells to TRAIL treatment via enhanced activation of the extrinsic apoptotic pathway., Int. J. Oncol. 55 (2019) 191–202. https://doi.org/10.3892/ijo.2019.4804.

[81] A. Grillo, F. Fezza, G. Chemi, R. Colangeli, S. Brogi, D. Fazio, S. Federico, A. Papa,

N. Relitti, R. Di Maio, G. Giorgi, S. Lamponi, M. Valoti, B. Gorelli, S. Saponara, M. Benedusi, A. Pecorelli, P. Minetti, G. Valacchi, S. Butini, G. Campiani, S. Gemma, M. Maccarrone, G. Di Giovanni, Selective Fatty Acid Amide Hydrolase Inhibitors as Potential Novel Antiepileptic Agents, ACS Chem. Neurosci. 12 (2021) 1716–1736. https://doi.org/10.1021/acschemneuro.1c00192.

HIGHLIGHTS

New microtubule targeting agents were synthesized by using a hybridization approach

Compounds are characterized by potent proapoptotic and autophagy inhibition efficacy

Autophagic flux inhibition was confirmed by the expression of LC3II/LC3I and p62 proteins

5i and 5k are late-stage autophagy inhibitors impairing autophagosome-lysosome fusion

Declaration of interests

☒ The authors declare that they have no known competing financial interests or personal relationships that could have appeared to influence the work reported in this paper.

☐The authors declare the following financial interests/personal relationships which may be considered as potential competing interests: